Synthesis of Metal-Organic Frameworks through Green Synthetic Pathways and Their Applications

A THESIS

Submitted to Delhi Technological University

For award of the degree of

DOCTOR OF PHILOSOPHY

In

APPLIED CHEMISTRY

By

USHA RAJU

2K12/PhD/AC/03

DEPARTMENT OF APPLIED CHEMISTRY

DELHI TECHNOLOGICAL UNIVERSITY

DELHI - 110042 (INDIA)

May 2018

Synthesis of Metal-Organic Frameworks through Green Synthetic Pathways and Their Applications

By

USHA RAJU

DEPARTMENT OF APPLIED CHEMISTRY

Submitted

In fulfillment of requirements of the degree of

DOCTOR OF PHILOSOPHY

To

DELHI TECHNOLOGICAL UNIVERSITY

DELHI - 110042 (INDIA)

May 2018

DELHI TECHNOLOGICAL UNIVERSITY

(formerly Delhi College of Engineering)

Department of Applied Chemistry

Shahbad Daulatpur, Bawana Road Delhi- 110042, India

DECLARATION

This is to certify that the work presented in this thesis entitled "**Synthesis of Metal Organic Frameworks Through Green Synthetic Pathways and Their Applications" is original and hasee carried out by me for the degree of Doctor of Philosophy** under the supervision of **Dr. Anil Kumar**, **Assistant Professor**, Department of Applied Chemistry. this thesis is contribution of my original researcjh work. wherever research contribution of others are involved, every effort has been made to clearly indicate the same. To the best of my Knowledge this reserach work has not been submiited in part or full the award of any degree or diploma in Delhi Technological University or in any other university/instituion.

Date
Time

Ms. Usha Raju
Research Scholar
Reg. No. 2K12/Ph.D/AC/03

DELHI TECHNOLOGICAL UNIVERSITY

(formerly Delhi College of Engineering)

Shahbad Daulatpur, Bawana Road Delhi- 110042, India

CERTIFICATE

This is to certify that the thesis entitled "**Synthesis of Metal Organic Frameworks Through Green Synthetic Pathways and Their Applications"** submitted to the Delhi Technological University, Delhi-110042, in fulfillment of the requirement for the award of the degree of **Doctor of Philosophy** by the candidate **Ms. Usha Raju**, (Reg. No. 2K12/Ph.D/AC/03) under the supervision of **Dr. Anil Kumar**, **Assistant Professor**, Department of Applied Chemistry. It is further certified that the work embodied in this thesis has neither partially nor fully submitted to any other university or institution for the award of any degree or diploma.

(Dr. Anil Kumar)

Supervisor

Department of Applied Chemistry

Delhi Technological University, Delhi

(**Dr. Archna Rani**)

Head of the Department

Department of Applied Chemistry

Delhi Technological University, Delhi

Dedicated

To

My Family

ACKNOWLEDGEMENTS

This thesis is the outcome of research work journey of five years through which I have been accompanied, motivated and supported by many people. It is a great pleasure now to express my gratitude for all of them.

First of all, I would like to convey my humble & heartfelt thanks to my supervisor **Dr. Anil Kumar** for his excellent guidance, continuous support & constant motivation for completion of research work. It is great pleasure to express my gratitude for his wonderful advice, intellectual discussions, unique suggestions, constructive criticism & being an epitome of patience & support throughout tenure of my research. I am fortunate to have you as my mentor Sir.

I wish to thank my peer group members for their unconditional support and help. I enjoyed their company throughout my research work. I take this opportunity to acknowledge technical staff for their help and technical support.

I would like to express my gratitude to Prof. D. Kumar, Prof. R. C. Sharma, Dr. G. L. Verma, Prof. S. G Warkar, Dr. Ram Singh, Dr. D. Santhiya, Dr. Roli Purwar, Dr. Saurabh Mehta, Dr. Raminder Kaur, Dr. Richa Srivastava & Prof. Archna Rani, Head of the Department, Applied Chemistry, for words of encouragement and motivation all the time. My sincere thanks are due to Dr. Girish Kumar, Mechanical Engineering department who had always been a source of great inspiration for me. I am grateful to Prof. Yogesh Singh, Vice Chancellor, Prof. S. K. Garg & Prof. Anu Singh Lather, Pro Vice Chancellor Delhi Technological University for giving me this opportunity to conduct my research work. My sincere thanks are due to the Department Of Training and Technical Education, Delhi for granting me permission for PhD work.

I gratefully acknowledge love and support of my family, without which it would not have been possible to fulfill my dream.

Finally, I would like to thank Almighty God for the successful completion of my research work.

Date: **(USHA RAJU)**

Place: Delhi

TABLE OF CONTENTS

LIST OF FIGURES

LIST OF TABLES

LIST OF ABBREVIATIONS

Å	*Angstrom*
BDC	*Benzene 1, 4 - dicarboxylic acid*
BET	*Brunauer, Emmett, Teller*
BJH	*Barrett-Joyner-Halenda*
BTC	*Benzene 1, 3, 5 - tricarboxylate*
CPCB	*Central Pollution Control Board*
DEF	*N, N- diethyl formamide*
DFT	*Density functional theory*
DMF	*N, N- Dimethylformamide*
DOE	*U.S. Department of Energy*
DPA	*Dipicolinic acid*
DSC	*Differential scanning Calorimetry*
DTG	*Differential thermogravimetry*
EBT	*Eriochrome Black T*
EDLC	*Electric double layer capacitor*
EDS	*Energy dispersive X-Ray spectroscopy*
FTIR	*Fourier transform infrared spectroscopy*
In B	*Indigo blue*
IUPAC	*International Union of Pure and Applied Chemistry*
LLCT	*Ligand-to ligand charge transfer*
LMCT	*Ligand-to-metal charge transfer*
LOHC	*Liquid Organic Hydrogen Carrier*
MBioFs	*Metal-biomolecule frameworks*
mL	*Milliliter*
MLCT	*Metal-to-ligand charge transfer*
mmol	*Mill mole*
MO	*Methyl orange*
MOF	*Metal-Organic Framework*
nm	*Nanometer*

ºC	*Degree Celsius*
PCP	*Porous coordination polymer*
pH	*Power of hydrogen*
PXRD	*Powder X-Ray Diffraction*
SBU	*Secondary building units*
SEM	*Scanning electron microscopy*
TGA	*Thermo gravimetric analysis*
TMA	*Trimesic acid or benzene-1, 3, 5-tricarboxylic acid*
UV-Vis Spectroscopy	*Ultra violet-Visible Spectroscopy*

ABSTRACT

Metal-organic framework complexes in general and multi metal-citrate complexes in particular have been synthesized through green route. Hydrothermal method adopted in present research is decorated with features; a simple one pot synthesis, cost effectiveness & easy to scale up for commercial production. Efficient synthesis conditions like mild temperature & shorter duration further rules out possibility of forming byproducts which may cause damage to environment. The synthesis is environmental benign, as it eliminates use & recovery of harmful organic solvents namely N, N-dimethyl formamide & N, N- diethyl formamide, used by researchers in synthesis of metal-organic framework complexes. Multiple metal ions introduced in their frameworks to exploit unique coordination properties of different metals ions. Multi metal-citrate complexes have also been synthesized using lime juice, squeezed from fresh fruit & strained, thereby reducing time & cost involved in extraction of citric acid commercially. These complexes are bluish green well defined crystalline solids having cubic geometry with a layered structure supported by a strong network of hydrogen bonds formed by ─OH of coordinated water lying between layers. They have been characterized by Fourier Transform Infrared Spectroscopy, Scanning Electron Microscopy, Energy Dispersive Spectroscopy, UV-Vis spectroscopy & Powder X- Ray diffraction techniques. Stability of complexes has been established by Thermogravimetric analysis. Complexes exhibit mesoporous character & narrow pore size distribution as demonstrated by BJH & DFT models. Owing to good adsorption properties & mesoporous nature, these complexes exhibit exorbitant adsorption affinity for large molecules of dyes & can be used as scavengers for dye stuff removal from industrial waste discharge to replace high cost carbon adsorbents & prevent water pollution with resultant toxic, carcinogenic & mutagenic effects of dye stuff on living beings. Multi metal-citrate complexes serve as promising luminescent probe for sensing & recognition of NH_4^+, $Fe(CN)_6^{4-}$, I^-, CrO_4^{2-} & $Cr_2O_7^{2-}$ *ions through a simple & straight forward method involving conspicuous visual display of color change upon introduction of guest ions in their framework. They may be explored for applications in gas adsorption & separation and sensing, capture & catalytic degradation of harmful gases. Being fluorescent they have great potential in bio medical field for drug storage, drug delivery, medical imaging & biological sensors which require water soluble nanocrystalline fluorescent materials.*

CHAPTER 1

INTRODUCTION

1.1 Metal-Organic Frameworks

Metal-organic frameworks refers to a genre of coordination polymers with highly porous crystalline structure, made up of individual or collection of metal ions, connected to organic ligands through coordinate bonds, to form one, two or three dimensional complexes. The organic ligand may be a mono, bi, tri or tetra-dentate ligand. The label Metal-organic framework was first put forth by O. M. Yaghi in the year 1995, with the introduction of a new compound having diamond like structure with formula Cu (4,4'- bpy) $_{1.5}$ NO_3 (H_2O) $_{1.25}$ [bpy = 4, 4′ bipyridine] **[1]**. International Union of Pure and Applied Chemistry (IUPAC) recommendations describe Metal-organic framework as:

"Metal-organic framework, abbreviated as MOF, refers to the Coordination Network with organic linkers having prospective voids. Coordination networks constitute a subset of coordination polymers and MOFs refer to division of coordination networks. Prime criterion for material to be named as MOF is presence of potential voids, irrespective of extent of porosity or other properties" **[2]**.

Since the introduction of MOFs, publications reporting new MOFs have grown prolifically in past decade **[3]**. Initially, major concern was incapability of these materials to sustain internal porosity because of framework collapse upon solvent evacuation & release of guest species. Researchers thus had quest to synthesize a stable framework with permanent porosity for applications, particularly gas adsorption & separation, which was realized by use of multidentate carboxylate linkers due to their ability to chelate with metals strongly, forming metal carboxylates bearing M-O-C units called Secondary building units (SBU), there by yielding a stable and rigid structure **[4 - 6]**.

The strong metal-carboxylate bond facilitates formation of stable framework capable to maintain its architecture during solvent evacuation. Structure of resulting network is guided by the fashion carboxylate linkers are coordinated to metal ions. Yaghi *et al.* first claimed fabrication of a stable crystalline, MOF-5 having Zn_4O units linked with BDC [BDC = Benzene 1, 4 - dicarboxylic acid] **[7].** Use of multidentate carboxylate linkers thus afforded chemists with the solution for stability of MOFs. Subsequently numerous MOFs with robust structures and permanent porosity involving strong metal-carboxylate bonds have been reported by the researchers **[8]**. Though the coordination behavior of metal ions and type of ligands govern the structure and properties of MOFs, the solvent and associated ions also modify architecture of the framework. The solvent molecules get trapped during crystallization and modify pore dimensions. The thermal evacuation of the solvent results in permanent porosity which makes MOFs suitable candidates for a wide range of applications due to their more flexible structural design and great stability.

1.2 Metal-Organic Frameworks -Versatile materials

Because of their unique properties like, exceptionally large surface area, tunable structures, high porosity, variable pore dimensions, the metal-organic frameworks find a variety of applications in diverse fields such as reversible uptake and release of hydrogen for mobile applications as a clean automobile fuel **[9, 10],** gas adsorption and separation **[11]**, detection and disintegration of toxic gases **[12]**, catalysis of organic reactions due to their active metal sites **[13]**, luminescent materials for chemical sensing and explosive detection**[14]** and in bio medical field for selective capture of proteins **[15]**, dug storage **[16]**, drug delivery **[17]** , medical imaging and sensing **[18]** to name a few.

MOFs may play a lead role for storage of H_2 - a future generation fuel due to their exceptionally large surface area, suitable pore size & volume **[19]**.The specific application based MOFs can be constructed by the proper picking of basic units' namely metal cations & ligands.

1.3 Established hydrogen storage techniques

Some of the established technologies for hydrogen storage include, compressed hydrogen gas in high pressure hydrogen cylinders, liquid H_2 storage in specially designed tank, pipeline H_2 similar to natural gas network, carbon nano tubes and carbon nano fibers to name a few. These techniques make use of physical hydrogen storage where hydrogen gas is stored by compression or liquefaction under pressure. The liquefaction of hydrogen involves a great energy loss & tank must be perfectly insulated to avoid boil off. Chemical hydrogen storage makes use of Metal hydrides such as $LiAlH_4$, $NaAlH_4$, MgH_2 etc. However the use of complex metal hydrides as hydrogen carriers has limitations of poor hydrogen capacity, slow adsorption/release of gas & high cost. Most metal hydrides involve strong bonding with hydrogen and thus require high temperature for release of hydrogen. Compounds named Liquid Organic Hydrogen Carrier (LOHC) where hydrogen can be charged & discharged in a cyclic fashion in considerable amount, have been proposed to be used as fuels which may replace hydrocarbon fuels **[20]**. Imidazolium ionic liquids in combination with metal nano particles catalyst can be employed for efficient hydrogen storage under normal pressure conditions, as claimed by J. Dupont *et al.* **[21]**. D.C Elias *et al*. reported that Graphene, an atomic layer of Graphite can react with atomic hydrogen reversibly to form Graphane & release hydrogen after heating to 450 ºC **[22]**. Dillion *et al*. provided experimental evidence for storage of hydrogen in carbon nano tubes at room temperature **[23]**. Since then attempts have been made towards hydrogen storage in various nano tubes and nanostructures as summarized by George E. Froudakis **[24]**.

Chen, *et al*. have shown that carbon nano tubes doped with Lithium & Potassium exhibit high H_2 uptake at 1 atmosphere & 200 °C - 400 °C temperature for Li doped and near room temperature for K doped carbon nano tubes **[25]**. Later on R. T. Yang adopted same procedure as reported by Chen *et al.* & concluded that high H_2 uptake was due to moisture contamination, actual adsorption by alkali doped carbon nano tubes was merely 2 wt% with dry H_2 **[26].** Results reported by one group could not be reproduced by another group due to sensitive experimental conditions & measurement procedures. Rao *et al.* investigated H_2 storage on single / multi - walled nano tubes and found that maximum adsorption of 3.7 wt% was obtained **[27]**.

1.4 Metal-Organic Frameworks for mobile H_2 storage

Fast consumption of natural petroleum reserves and resulting hazardous discharge in the air raises a serious issue of concern for the mankind and deserves much attention to devise a mechanism for use of safer non polluting fuel for automobiles. Hydrogen due to its cleaner combustion products and rich energy content can replace traditional carbon fuels which cause a great threat to the environment. However, use of H_2 as vehicular fuel seems to be an uphill task due to its highly flammable nature.

H_2 a cleaner fuel can prove a boon in pollution management once challenges for its safe & economical onboard hydrogen storage are overcome. This can be achieved by synthesis of materials suitable for charging & discharging large quantities of hydrogen at appropriate rate under normal temperature & pressure conditions, which can attain the goal set by *US Department of Energy (DOE website-energy.gov).* MOFs seem to be best possible option to serve the purpose as they can be tailored to meet requirement of mobile hydrogen storage & carrier because of their matchless characteristics like, remarkable surface area, tailor made structure and porous nature. Their structures can be manipulated by introducing multiple metals with different coordination properties and appropriate choice of organic ligands with suitable functionalities for efficient uptake & storage of H_2 for mobile applications.

MOFs have an added advantage of being synthesized by simple hydrothermal or solvothermal methods in which highly porous structure can be achieved by solvent evacuation without destabilizing the framework.

The story of hydrogen storage by MOF started in the year 2003 when Yaghi *et al.* claimed H_2 storage by MOF-5 under conditions of room temperature and 20 bar pressure **[28, 29].** Lee *et al.* carried out low temperature gas sorption analysis on three dimensional micro porous MOFs as well as two dimensional layered complexes and concluded that all micro porous metal organic frameworks have a relatively high hydrogen capacity **[30]**.

Yaghi *et al.* while analyzing the behavior of MOFs towards low pressure hydrogen adsorption in contrast with their structures, found that catenated materials display remarkable capacities for hydrogen adsorption on a molar basis whereas functionalization does not have much influence on adsorption **[31]**. Space *et al.* while studying the role of polarization interactions in H_2 storage by an MOF have demonstrated through their Monte Carlo Simulations that highly ionic frameworks with narrow pores result in large H_2 capture by an MOF **[32]**. Li *et al.* have reported that hydrogen spillover process involving atomic hydrogen adsorption, to be an appropriate method to improve H_2 storage capacity of covalent organic frameworks and metal-organic frameworks under ambient conditions **[33]**. Li *et al.* have reported an efficient and fast synthesis of three dimensional MOF, HKUST-1, Cu_3 (BTC) $_2$ [BTC = Benzene 1, 3, 5 tricarboxylate] via ultrasonic technique which has comparable H_2 storage capacity with MOFs synthesized using traditional methods **[34]**. Xiao *et al.* have presented the development of a nano porous MOF employed for storage of H_2 **[35]**. According to them good MOFs are obtained by judicious choice of metal ions, counter ions, organic ligands and pH values. B. Kuchta *et al.* have claimed that chemically substituting Boron atoms in place of Carbon atoms enhances adsorption capacity of the material **[36].**

Carbon nanostructures are considered as most desired candidates for storage of H_2 reversibly, but physical adsorption of hydrogen by them involve low hydrogen adsorption energy & weak H_2 - H_2 interactions and do not fulfill criteria prescribed by *U.S. Department of Energy*.

The amount of gas adsorbed on MOF surface depends on temperature and pressure of adsorbate. Adsorption gets enhanced commonly with drop in temperature & rise of pressure. Furthermore, greater is the surface area, more is adsorption of hydrogen. Another crucial factor is high enthalpy of hydrogen adsorption. Theoretically 22-25 kJ/mol energy interactions are sufficient for adsorption and quick de-sorption.

MOFs containing unsaturated metal sites are highly suitable for adsorption of gases and removal of volatile solvent molecules bound to metal. Post synthetic modifications or super critical CO_2 drying of MOFs can enhance their hydrogen storage capacity **[37]**.

Li *et al.* studied H_2 storage properties of metal-decorated benzenes & reported that active metals from 1st to 3rd period in the periodic table exhibit strong affinity for adsorption on benzene surface and Ca being the most suitable metal for H_2 storage **[38]**. Mannuela Gaab *et al.* reported synthesis of Al-MOF (Basonite A520) carried out in a water based route with 90% yield **[39]**. While synthesizing HKUST-1 & MOF-5, Mu reported that raising temperature, longer reaction time, use of DMF in place of DEF produces MOF with lesser surface area **[40]**. Researchers have proven that, at low pressure H_2 adsorption capacity depends on binding affinity of H_2 & at higher pressure depends on surface area of material **[41, 42].** Yaghi *et al.* designed two complexes namely MOF-200 & MOF-210 having BET surface area of 4530 m^2g^{-1} & 6240 m^2g^{-1} respectively by evacuating the samples under supercritical CO_2 **[43]**.

Figure 1.1 illustrates MOFs with high gas storage ability **[44].**

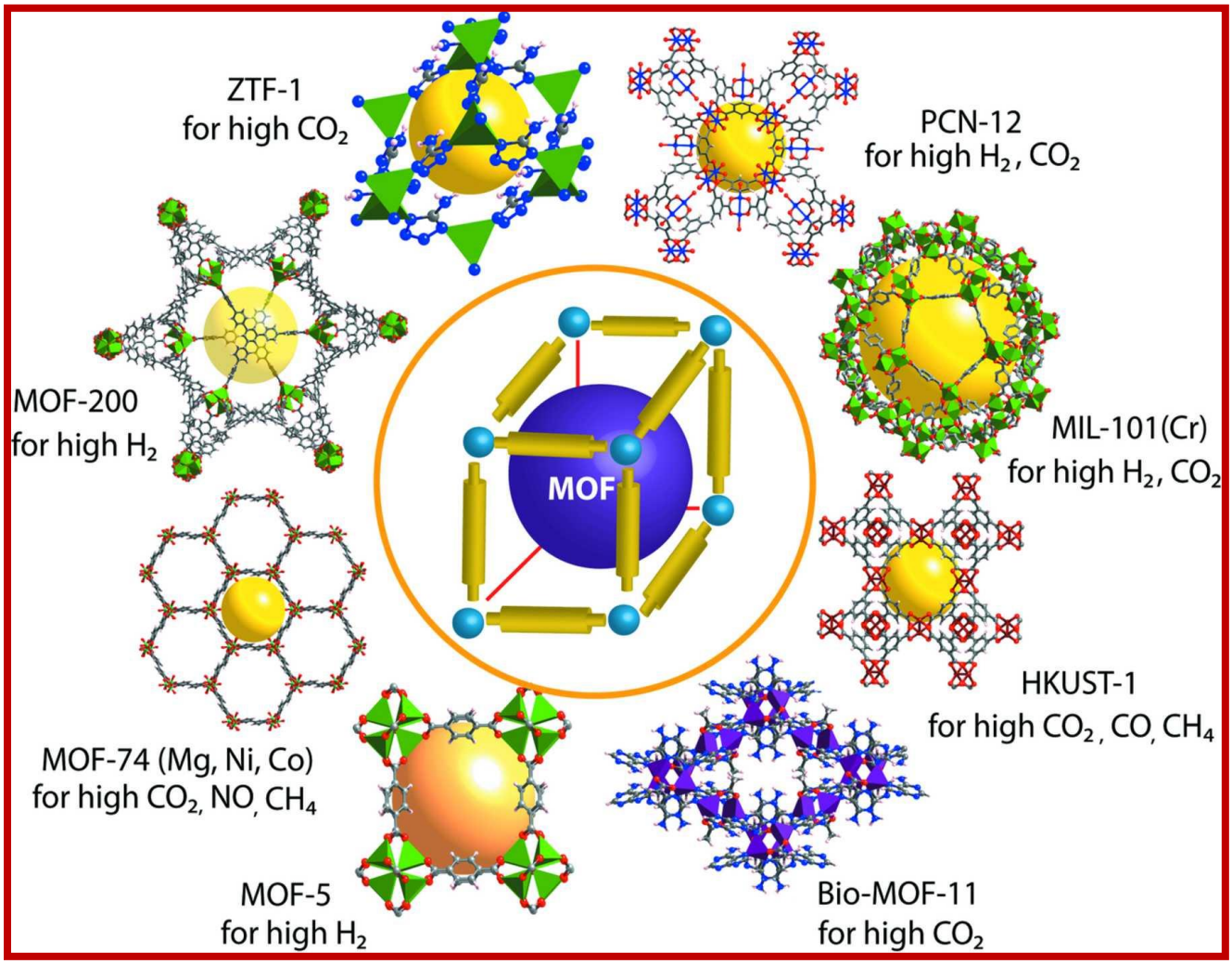

Figure 1.1 Important MOFs with high gas storage properties [44]

Due to weaker interactions between H_2 & MOFs it is still a challenging task to store of H_2 under favorable conditions. Besides having larger surface area, MOF should have high heat of H_2 adsorption **[45]**. Major chunk of MOFs with high hydrogen storage capacity at low temperatures at present, involve use of harmful organic solvents mostly DMF / DEF in their synthesis. Present research was carried out with the aim to synthesize metal-organic frameworks through green route, with active functional groups on surface to enhance H_2 interaction and consequent high hydrogen storage by them.

1.5 Metal-Organic Frameworks as adsorbents

Water, an essential commodity constitutes around 70 % of surface of earth, but unfortunately a small percentage of it is suitable for human consumption. Water is ultimate necessity of life, but access to clean; fresh & safe drinking water is a foremost worldwide concern. One major problem affecting water cycle on earth is water contamination, challenge we face today is of water pollution. Chemicals that go into water stream primarily from textile & leather industry, paper & pulp industry, paint industry & tanneries are often very difficult, if not impossible, to remove. Textile dyeing industry alone is responsible for about 20% of water pollution **[46]**.

Apart from being toxic in nature, chemical industrial waste released into water bodies, may affect quality of sunlight that penetrates to a certain depth inhibiting plant & animal metabolism. Deterioration of aesthetic & life supporting qualities of water bodies caused by industrial waste may badly affect flora & fauna, which is a matter of grave concern for mankind. Waste discharge from dyeing industry interacts with atmospheric gases and results in formation of products which are more toxic, carcinogenic & mutagenic for living beings than parent dyes **[47]**.

Leaving aside industrial dye stuff discharge into water resources, other major cause of water pollution in India includes Idol immersion in river waters. According to an assessment done by the Central Pollution Control Board (CPCB) in India, 32 tones of colors containing deadly metals; Pb, Cr, Hg, Mn *etc* is discharged into River Hooghly alone during Festivities like Dussehra **[48]**.

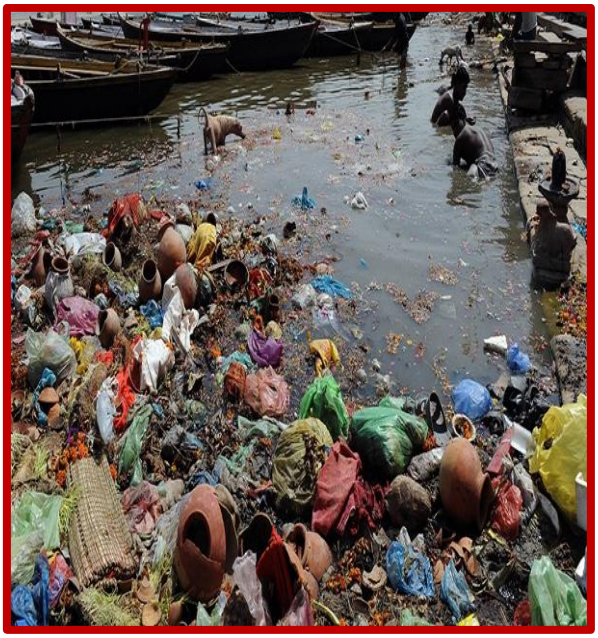

1 **2**

Figure1.2 Major sources of water pollution in India; 1 Dyeing Industry 2 Idol immersion

The phenomenon of adsorption has been exploited by the mankind since ancient times, utilizing the adsorbent properties of clay and wood charcoal for water purification **[49]**. Adsorption is one of the processes commonly used for dye removal in wastewater treatment **[50 - 52]**. The activated carbons usually employed for treatment of waste water are not only expensive, but add additional cost for their regeneration.

MOFs sometimes termed as ‘ Porous Coordination Polymers ’ (PCPs) encompass crystal structures with open space in them. These materials having extraordinary high surface area, variable pore dimensions & active functional groups, thus may serve as host for a variety of guest species.

An MOF consisting of tricarboxylate ligand coordinated to Zn (II) ions, containing large pores has recently been reported to encapsulate large guest molecules **[53]**. Pore size which is associated with transport mechanism is a crucial issue in adsorption of gases & other applications of porous materials.

A large variety of Metal-organic framework complexes have been tailored in the past for gas storage, separation & capture of small molecules by exploiting their microscopic nature. However there is still dearth of metal-organic frameworks with larger pores in their structure to be employed as scavengers for organic pollutant, particularly organic dye stuff discharge from textile industry, paper & pulp industry, tanneries *etc*.

1.6 Metal-Organic Framework as Luminescent materials

Photoluminescence in complexes arises from phenomena like, transfer of charge; from ligand → metal (LMCT), metal → ligand (MLCT), ligand → ligand (LLCT) and metal attached with antenna ligands **[54]**. The luminescent characteristics of complexes can be modified by judicious choice of metal species and appropriate choice of ligands. Specific application based luminescent materials can be tailored by selection of ligands bearing suitable functionalities, high porosity and appropriate particle size.

Because of their porous nature the multi metal-citrate complexes act as host for different types of ionic species and luminescence resulting from guest ion or transfer of charge between metal and ligand **[55]**.

Luminescent MOFs have key advantages over other luminescent probe materials as MOFs have well defined crystalline structure which is finely established by XRD, thereby providing exact knowledge of atomic positions and interactions that may be involved in detection of an analyte **[56]**.

Luminescence of MOFs can be exploited for host of applications; biomolecule sensor **[57]**, transport of drug **[58]**, chemical sensing & explosive detection **[59]**, fluorescent thermometers **[60]** and biomedical imaging **[61].** Fluorescence-based detection of explosive molecules with luminescent MOF sensors was first reported by Li *et al.* **[62].** Biomolecule recognition & sensing applications of MOFs have been explored by Lin *et al.* **[63]**. Though luminescent properties of lanthanide based MOFs have widely been exploited in various fields, yet controlling size & morphology of luminescent lanthanide MOFs to nanoscale is a challenging task, as variation in particle size gives rise to unique optical properties. It is even more challenging to apply different metal cations and ligands to produce lanthanide based luminescent materials for practical applications **[64, 65]**.

Figure1.3 Reveals various applications of luminescent Metal-organic framework complexes.

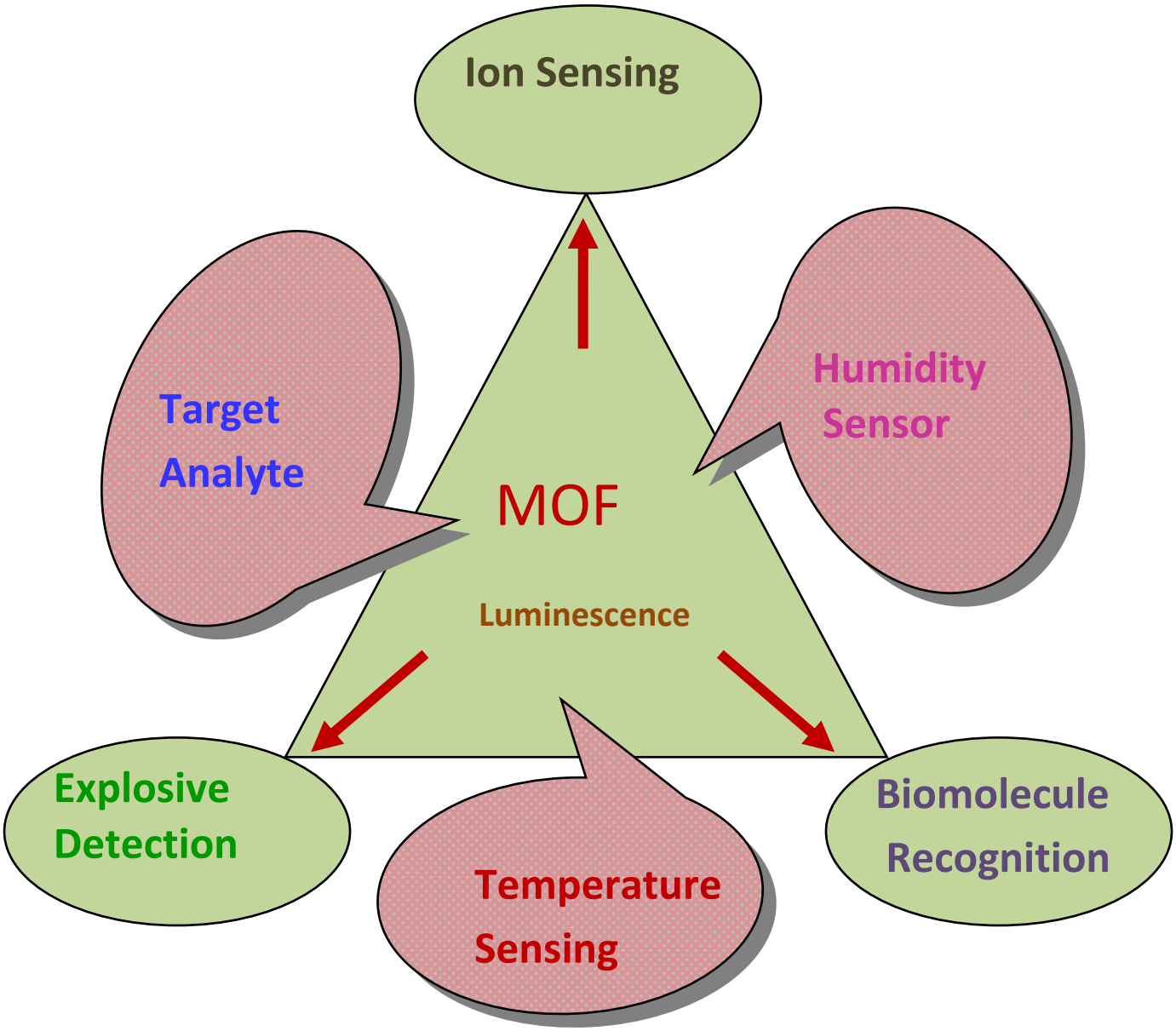

Figure 1.3 Applications of luminescent Metal-organic framework complexes

1.7 Multi Metal-Organic Framework complexes

The architecture of an MOF can be varied by introducing multiple metals with different coordination properties and appropriate choice of organic ligands with suitable functionalities. Yaghi group has designed complexes containing multiple metal atoms in a pre decided sequence. They have established that making such complexes bearing multiple hetero metal atoms in their structure is "notoriously tough". However these complexes deserve special attention for selectivity in catalysis or "cascading reactions" **[66, 67]**. Wang *et al.* have designed multi-metal MOF-74 with 2 - 10 hetero metal atoms **[68]**. Li *et al.* have reported much better catalytic activity of MOFs containing multiple hetero atoms, especially in heterogeneous catalysis **[69]**.

1.8 Structure of Metal-Organic Frameworks

A noteworthy feature of MOF chemistry is ability of their primary molecular building blocks namely metal atoms or their clusters and organic linkers to maintain their structural integrity throughout the synthesis and form specific secondary building units (SBU) which further undergo self assembly to form final MOF architecture. Some of remarkable research highlights for MOFs and their structure are discussed here.

MOF-5: First reported in 1999, consists of ZnO_4 tetrahedra aggregating to form (Zn_4O) O_{12} octahedral SBU connected by 1, 4-benzenedicarboxylic acid struts between the nodes, forming Zn_4 O $(BDC)_3$ having three dimensional cubic network structure **[7]**.

MIL-101: Ligand 1, 4-benzenedicarboxylic acid coordinates with Cr_3O inorganic building block resulting in mesoporous material with extraordinary large surface area & large pore volume **[70]**.

HKUST-1: The highly porous MOF $[Cu_3$ (TMA) $_2(H_2O)_3]$ consists of Cu_2 located at six vertices of an octahedron in SBU **[71]**.

MOF-2: Zinc based MOF-2, Zn (BDC).DMF H_2O, has a layered structure **[72].**

MOF-3: The tri nuclear SBU in $Zn_3(BDC)_3\ 6CH_3OH$ is octahedral and linked with benzene di carboxylate linker to form porous three dimensional structure having poly trigonal prismatic topology **[72]**.

Catenation in the form of interpenetration and interweaving usually caused by long linkers is generally considered as one of the most undesirable features in synthesis of porous network and a threat to structural stability and porosity of open frameworks. Yaghi group has however been successful in achieving highly porous structures with great degree of interpenetration / interweaving and permanent porosity **[73, 74]**.

Figure 1.4 depicts structures of some prominent MOFs (a) MOF-5 **[7]** (b) HKUST-1**[71]** (c) MOF-2 **[72]** (d) MOF-3 **[72].**

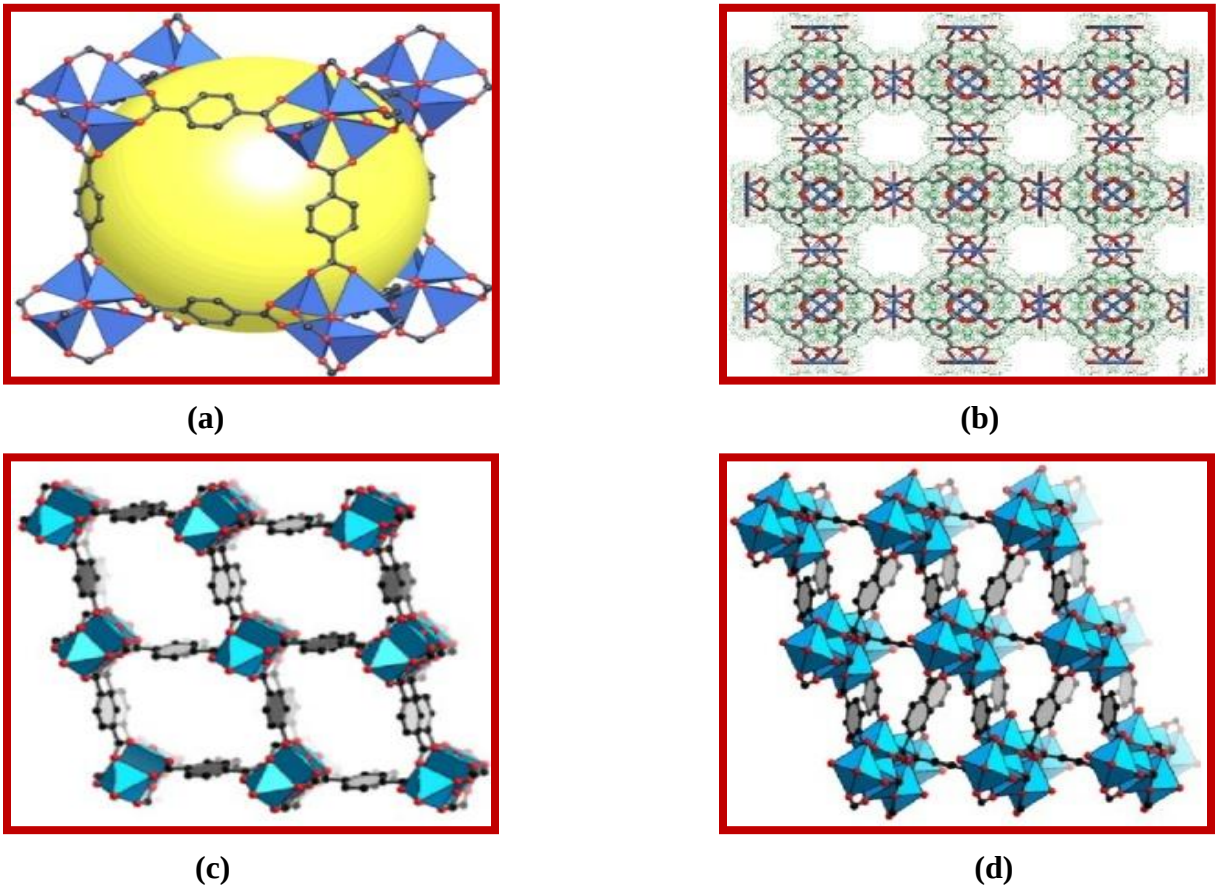

(a) **(b)**

(c) **(d)**

Figure 1.4 Structures of Metal-Organic Frameworks (a) MOF-5 [7] (b) HKUST-1 [71] (c) MOF-2 [72] (d) MOF-3 [72]

1.9 Synthesis of Metal-Organic Framework complexes

Metal-organic frameworks hold an edge over other porous materials because of their simple and convenient synthesis by hydrothermal or solvothermal methods. However, solvothermal method has been the most favorite method, adopted by a large community of researchers for synthesis of transition metals complexes with organic ligands, involves use of harmful organic solvents namely DMF & DEF. Salifoglou *et al.* reported first synthesis of anionic Iron-citrate complex containing iron coordinated to two citrate linkers and charge balanced by NH_4^+ counter ions in aqueous medium. The complex contains an extensive array of hydrogen interactions in its network **[75]**. Synthesis of many MOFs through a water based route has been reported by researchers in the past **[76 - 78].** Li *et al.* synthesized two dimensional mixed ligands-metal co-ordination complexes by bridging oxalate and 4, 4'- bipyridine ligands with different metals through hydrothermal route **[79]**. Alkaline earth metals based MOFs have also been synthesized by hydrothermal method **[80]**. Hydrothermal synthesis of metal-organic framework, $Co_3(BTC)_2.12H_2O$ containing an array of hydrogen bonding with water coordinated to metal has been reported **[81]**. Researchers have reported the electrochemical synthesis, mechano-chemical synthesis, microwave assisted synthesis and ultrasound synthesis of metal-organic frameworks **[82 - 85]**. These materials have fascinated the researchers to such an extent that metal-biomolecule frameworks (MBioFs) and even edible metal organic framework materials have been tailored from natural products **[86, 87].** Yaghi *et al.* have claimed creation of popular MOFs namely; MOF-5, MOF-74, MOF-177, MOF-199 under normal temperature conditions and extended the method for synthesis of IRMOF-0 with cubic geometry **[88]**.

Figure 1.5 illustrates metal-organic framework synthesis through different routes and comparison of MOFs synthesized using different synthetic routes **[44].**

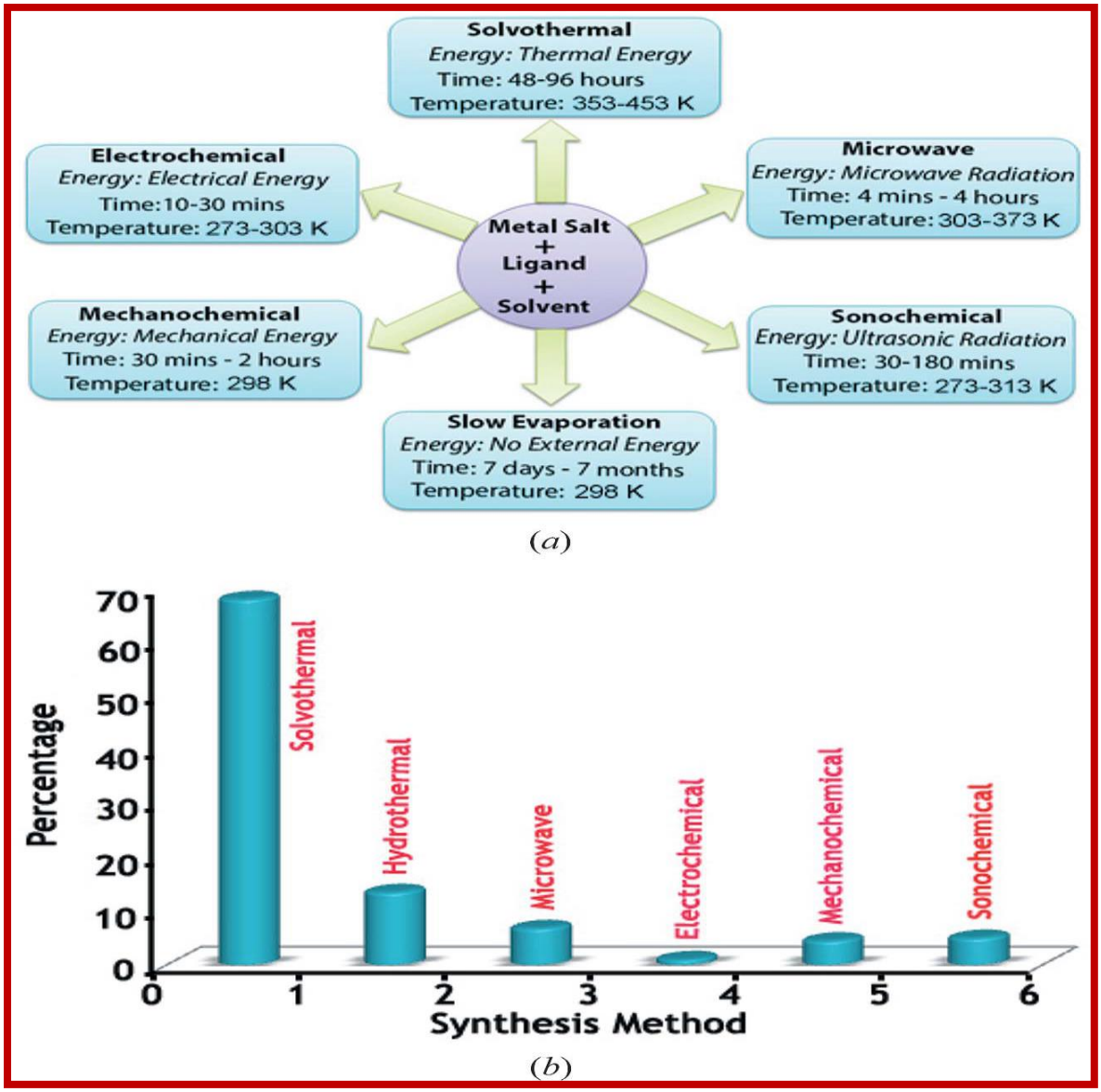

Figure 1.5 (a) Metal-organic framework synthesis through various routes (b) Comparative study of MOFs synthesized through different routes [44]

1.10 Twelve guiding principles for green route to synthesis

Proposed by P. Anastas and J. Warner green synthesis is based on twelve principles **[89]:**

1.10.1 Waste prevention: The amount of waste generated may be reduced by changing design and methodology or appropriate use of materials or products for cost reduction and environment benefits.

1.10.2 Atom economy: Atom economy refers to efficacy of conversion of reactants into desired products. The higher is the atom economy in a process, the greener the process will be.

1.10.3 Less hazardous chemical syntheses: A chemical process should be designed in a way which generates minimum or no toxic chemical products which may be dangerous for human health or cause damage to the environment.

1.10.4 Designing safer chemicals: The researchers and the chemical companies must think about the toxicity and consequent adverse effects of products before they are designed and to minimize toxicity whenever possible through rational chemical design.

1.10.5 Safer solvents and auxiliaries: Green process should either avoid the use of solvents and other auxiliaries, if possible, or should be safe if necessary.

1.10.6 Use of energy efficient technology: The researcher should design, construct and execute the project in a way which minimizes the use of energy. One should adopt energy-efficient technologies for designing a product.

1.10.7 Use of renewable feed stocks: The raw materials or feedstock used in a chemical synthesis should be renewable rather than depleting resources which take much longer to be replenished, and are being consumed at a faster rate by the mankind.

1.10.8 Reduce derivatives: The strategy should be made to simplify the process in order to reduce the number of steps, as all these steps will lead to the use of additional chemicals and their recovery.

1.10.9 Catalysis: A catalyst increases the rate of a chemical reaction by providing an alternate path of low activation energy. The use of a safe catalyst thus helps in making a process more economical in terms of time and energy.

1.10.10 Design for degradation: During synthesis the methodology should lead to the formation of products which are biodegradable and do not harm the environment in any way.

1.10.11 No generation of hazardous environment pollutants: The process should be designed in such a way which allows the real time monitoring of all the steps to control the generation of hazardous by products.

1.10.12 Safer chemistry for accident prevention: The process should involve the use of inherently safer chemical reaction process, design and operation to avoid accidents, fires, hazards and explosions.

REFERENCES

1. O. M. Yaghi, H. Li, Hydrothermal synthesis of a metal-organic framework containing large rectangular channels, *J. Am. Chem. Soc*., **1995**, 117(41), 10401-10402.

2. S. R. Batten, N. R. Champness, X. M. Chen, J. Garcia-Martinez, S. Kitagawa, L. Ohrstrom, M. O'Keeffe, M. P. Suh, J. Reedijk, Terminology of metal–organic frameworks and coordination polymers (**IUPAC Recommendations 2013**), *Pure Appl. Chem*., **2013**, 85(8), 1715-1724.

3. H. C. Zhou, J. R. Long, O. M. Yaghi, Introduction to metal-organic frameworks, *Chem. Rev*., **2012**, 112(2), 673-674.

4. H. Li, M. Eddaoudi, T. L. Groy, O. M. Yaghi, Establishing micro porosity in open metal organic frameworks: Gas sorption isotherms for Zn (BDC), (BDC) =1, 4-Benzenedicarboxylate), *J. Am. Chem. Soc*., **1998**, 120(33), 8571-8572.

5. M. Eddaoudi, H. Li, T. M. Reineke, M. Fehr, D. Kelley, T. L. Groy, O. M. Yaghi, Design and synthesis of metal-carboxylate frameworks with permanent micro porosity, *Top. Catal.*, **1999**, 9(1), 105-111.

6. M. Eddaoudi, D. B. Moler, H. Li, B. Chen, T. M. Reineke, M. O'Keeffe, O. M. Yaghi, Modular chemistry: secondary building units as a basis for the design of highly porous and robust metal-organic carboxylate frameworks, *Acc. Chem. Res.*, **2001**, 34(4), 319-330.

7. H. Li, M. Eddaoudi, M. O'Keeffe, O. M. Yaghi, Design and synthesis of an exceptionally stable and highly porous metal-organic framework, *Nature*, **1999**, 402(6759), 276-279.

8. A. Schoedel, O. M. Yaghi, Porosity in metal-organic compounds, Chapter 9 in Macro cyclic and supramolecular chemistry: How Izatt–Christensen award winners shaped the field, R. M. Izatt. (Ed.), 1st edition, John Wiley & Sons Ltd., United Kingdom **2016**.

9. J. L. C. Rowsell, E. C. Spencer, J. Eckert, J. A. K. Howard, O. M. Yaghi, Gas adsorption sites in a large-pore metal-organic framework, *Science*, **2005**, 309(5739), 1351-1354.

10. D. Sun, S. Ma, Y. Ke, D. J. Collins, H. C. Zhou, An interweaving MOF with high hydrogen uptake, *J. Am. Chem. Soc.*, **2006**, 128(12), 3896-3897.

11. S. Keskin, Molecular simulation study of CH_4/H_2 mixture separations using metal-organic framework membranes and composites, *J. Phys. Chem.*, C, **2010**, 114(30), 13047-13054.

12. E. Barea, C. Montoro, J. A. R. Navarro, Toxic gas removal- metal-organic frameworks for the capture and degradation of toxic gases and vapours, *Chem. Soc. Rev.*, **2014**, 43(16), 5419-5430.

13. S. Loera-Serna, E. Ortiz, Catalytic applications of metal-organic frameworks, Chapter 4 in Advanced catalytic materials- Photocatalysis and other current trend, L. E. Norena, J. A. Wang. (Eds.), InTech **2016**.

14. S. Halder, P. Ghosh, C. Rizzoli, P. Banerjee, P. Roy, Nitro aromatics explosives detection by a luminescent Cd (II) based metal organic framework, *Polyhedron*, **2017**, 123, 217-225.

15. Y. Chen, Z. Xiong, L. Peng, Y. Gan, Y. Zhao, J. Shen, J. Qian, L. Zhang, W. Zhang, Facile preparation of core-shell magnetic metal-organic framework nanoparticles for the selective capture of phosphopeptides, *ACS Appl. Mater. Interfaces*, **2015**, 7(30), 16338-16347.

16. I. Erucar, S. Keskin, Efficient storage of drug and cosmetic molecules in biocompatible metal-organic frameworks: A molecular simulation study, *Ind. Eng. Chem. Res*., **2016**, 55(7), 1929-1939.

17. C.Y. Sun, C. Qin, C. G. Wang, Z. M. Su, S. Wang, X. L. Wang, G. S. Yang, K. Z. Shao, Y. Q. Lan, E. B. Wang, Chiral nanoporous metal-organic frameworks with high porosity as materials for drug delivery, *Adv. Mater.*, **2011**, 23(47), 5629-5632.

18. A. M. Morawski, G. A. Lanza, S. A. Wickline, Targeted contrast agents for magnetic resonance imaging and ultrasound, *Curr. Opin. Biotechnol*., **2005**, 16(1), 89-92.

19. N. L. Rosi, M. Eddaoudi, J. Kim, M. O'Keeffe, O. M. Yaghi, Advances in the chemistry of metal-organic frameworks, *Cryst. Eng. Comm*., **2005**, 4(68), 401-404.

20. D. Teichmann, W. Arlt, P. Wsasserscheid, R. Freymann, A future energy supply based on liquid organic hydrogen carriers (LOHC), *Energy Environ. Sci.*, **2011**, 4(8), 2767-2773.

21. M. P. Stracke, G. Ebeling, R. Cataluna, J. Dupont, Hydrogen-storage materials based on Imidazolium ionic liquids, *Energy Fuels*, **2007**, 21(3), 1695-1698.

22. D. C. Elias, R. R. Nair, T. M. Mohiuddin, S. V. Morozov, P. Blake, M. P. Halsall, A. C. Ferrari, D. W. Boukhvalov, M. I. Katsnelson, A. K. Geim, K. S. Novoselov, Control of graphene's properties by reversible hydrogenation: evidence for graphane, *Science*, **2009**, 323(5914), 610-613.

23. A. C. Dillion, K. M. Jones, T. A. Bekkedahl, C. H. Kiang, D. S. Bethune, M. J. Heben, Storage of hydrogen in single-walled carbon nanotubes, *Nature*, **1997**, 386(6623), 377-379.

24. G. E. Froudakis, Hydrogen storage in nanotubes & nanostructures, *Mater. Today*, **2011**, 14, 324-328.

25. P. Chen, X. Wu, J. Li, K. L. Tan, High H2 uptake by alkali-doped carbon nanotubes under ambient pressure and moderate temperatures, *Science*, **1999**, 285(5424), 91-93.

26. R. T. Yang, Hydrogen storage by alkali-doped carbon nanotubes–revisited, *Carbon*, **2000**, 38(4), 623-626.

27. G. Gundiah, A. Govindaraj, N. Rajalakshmi, K. S. Dhathathreyan, C. N. R. Rao, Hydrogen storage in carbon nanotubes & related materials, *J. Mater. Chem.*, **2003**, 13(2), 209-213.

28. Volume 89 Issue 2, p. 8, News of The Week, Chemical & Engineering News, USA

Issue Date: January 10, **2011**.

29. N. L. Rosi, J. Eckert, M. Eddaoudi, D. T. Vodak, J. Kim, M. O'Keeffe, O. M. Yaghi, Hydrogen storage in microporous metal-organic frameworks, *Science*, **2003**, 300(5622), 1127-1129.

30. J. Y. Lee, J. Li, J. Jagiello, Gas sorption properties of microporous metal organic frameworks, *J. Solid State Chem.*, **2005**, 178(8), 2527-2532.

31. J. L. C. Rowsell, O. M. Yaghi, Effects of functionalization, catenation, and variation of the metal oxide and organic linking units on the low-pressure hydrogen adsorption properties of metal-organic frameworks, *J. Am. Chem. Soc.*, **2006**, 128(4), 1304-1315.

32. J. L. Belof, A. C. Stern, M. Eddaoudi, B. Space, On the mechanism of hydrogen storage in a metal-organic framework material, *J. Am. Chem. Soc.*, **2007**, 129(49), 15202-15210.

33. Y. Li, R. T. Yang, Hydrogen storage in metal-organic and covalent-organic frameworks by spillover, *AIChE Journal*, **2008**, 54(1), 269-279.

34. Z. Q. Li, L. G. Qiu, T. Xu, Y. Wu, W. Wang, Z. Y. Wu, X. Jiang, Ultrasonic synthesis of the microporous metal-organic framework $Cu_3(BTC)_2$ at ambient temperature and pressure: An efficient and environmentally friendly method, *Mater. Lett*., **2009**, 63(1), 78-80.

35. B. Xiao, Q. Yuan, Nanoporous metal organic framework materials for hydrogen storage, *Particuology*, **2009**, 7(2), 129-140.

36. B. Kuchta, L. Firlej, R. Cepel, P. Pfeifer, C. Wexler, Structural and energetic factors in designing a nanoporous sorbent for hydrogen storage, *Colloids Surf. A Physicochem. Eng. Asp.*, **2010**, 357, 61-66.

37. Z. Xiang, D. Cao, X. Shao, W. Wang, J. Zhang, W. Wu, Facile preparation of high-capacity hydrogen storage metal-organic frameworks: A combination of microwave-assisted solvothermal synthesis and supercritical activation, *Chem. Eng. Sci*., **2010**, 65(10), 3140-3146.

38. P. Li, S. H. Deng, G. H. Liu, L. Zhang, J. Huang, J. Y. Yu, Stability and hydrogen storage properties of various metal-decorated benzene complexes, *J. Power Sources*, **2012**, 211, 27-32.

39. M. Gaab, N. Trukhan, S. Maurer, R. Gummaraju, U. Muller, The progression of Al-based metal-organic frameworks - From academic research to industrial production and applications, *Microporous Mesoporous Mater*., **2012**, 157, 131-136.

40. B. Mu, Synthesis and gas adsorption study of porous metal-organic framework materials, Ph. D Thesis, Georgia Institute of Technology, Atlanta, Georgia, United States **2011**.

41. B. Panella, M. Hirscher, H. Putter, U. Muller, Hydrogen adsorption in metal-organic frameworks: Cu-MOFs and Zn-MOFs compared, *Adv. Funct. Mater*., **2006**, 16(4), 520-524.

42. H. Frost, T. Duren, R. Q. Snurr, Effects of surface area, free volume, and heat of adsorption on hydrogen uptake in MOFs. *J. Phys. Chem. B.*, **2006**, 110(19), 9565-9570.

43. O. M. Yaghi, J. Kim, N. Ko, S. B. Choi, H. Furukawa, Open metal organic frameworks with exceptional surface area and high gas storage capacity, *US 8841471 B2*, **2014**.

44. C. Dey, T. Kundu, B. P. Biswal, A. Mallick, R. Banerjee, Crystalline metal-organic frameworks (MOFs): synthesis, structure and function, *Acta Cryst*., **2014**, B70, 3-10.

45. L. Zou, H. C. Zhou, Hydrogen storage in metal-organic frameworks, in Nanostructured materials for next-generation energy storage and conversion, Y. P. Chen, S. Bashir, J. Liu (Eds.), Springer, Berlin, Heidelberg **2017**.

46. A. Scott, Cutting out textile pollution, Cleaning up one of the world's dirtiest industries will require new technology and more, *Chem. Eng. News*, **2015**, 93(41), 18-19.

47. Z. Carmen, S. Daniela, Textile organic dyes – Characteristics, polluting effects and separation/elimination procedures from industrial effluents – A critical overview, In Organic pollutants ten years after the Stockholm Convention - Environmental and analytical update, T. Puzyn (Ed.), InTech Croatia **2012**.

48. M. R. Senapati, Puja immersions: water bodies polluted beyond repair, The Pioneer, Bhubaneswar, 15 October **2016**.

49. F. Rodriguez-Reinoso, J. Rouquerol, K. K. Unger, K. Sing (Eds.), Characterization of porous solids III, Volume 87, Ist Ed., Elsevier, Amsterdam **1994**.

50. H. M. Freeman, Standard handbook of hazardous waste treatment and disposal, 2nd Ed., McGraw-Hill, New York **1989**.

51. T. G. Danis, T. A. Albanis, D. E. Petrakis, P. J. Pomonis, Removal of chlorinated phenols from aqueous solutions by adsorption on alumina pillared clays and mesoporous alumina aluminum phosphates, *Water Res*., **1998**, 32(2), 295-302.

52. A. Dabrowski, Adsorption – from theory to practice, *Adv. Colloid Interface Sci*., **2001**, 93(1-3), 135-224.

53. P. Z. Li, J. Su, J. Liang, J. Liu, Y. Zhang, H. Chen, Y. Zhao, A highly porous metal-organic framework for large organic molecule capture and chromatographic separation, *Chem. Commun*., **2017**, 53(24), 3434-3437.

54. X. Zhang, W. Wang, Z. Hu, G. Wang, K. Uvdal, Coordination polymers for energy transfer: Preparations, properties, sensing applications, and perspectives, *Coord. Chem. Rev*., **2015**, 284, 206-235.

55. W. P. Lustig, F. Wang, S. J. Teat, Z. Hu, Q. Gong, J. Li, Chromophore-based luminescent metal-organic frameworks as lighting phosphors, *Inorg. Chem.,* **2016**, 55(15), 7250-7256.

56. W. P. Lustig, S. Mukherjee, N. D. Rudd, A. V. Desai, J. Li, S. K. Ghosh, Metal-organic frameworks: functional luminescent and photonic materials for sensing applications, *Chem. Soc. Rev*., **2017**, 46, 3242-3285.

57. X. Zhu, H. Zheng, X. Wei, Z. Lin, L. Guo, B. Qiu, G. Chen, Metal-organic framework (MOF): a novel sensing platform for biomolecule, *Chem. Commun*., **2013**, 49, 1276-1278.

58. M. Ibrahim, R. Sabouni, G. A. Husseini, Anti-cancer drug delivery using metal organic frameworks (MOFs), *Curr Med Chem*., **2017**, 24(2), 193-214.

59. Z. Hu, B. J. Deibert, J. Li, Luminiscent metal-organic frameworks for chemical sensing and explosive detection, *Chem. Soc. Rev*., **2014**, 43(16), 5815-5840.

60. D. Zhao, X. Rao, J. Yu, Y. Cui, Y. Yang, G. Qian, Design and synthesis of an MOF thermometer with high sensitivity in the physiological temperature range, *Inorg. Chem*., **2015**, 54(23), 11193-11199.

61. J. D. Rocca, D. Liu, W. Lin, Nanoscale metal-organic frameworks for biomedical imaging and drug delivery, *Acc. Chem. Res*., **2011**, 44(10), 957-968.

62. A. Lan, K. Li, H. Wu, D. H. Olson, T. J. Emge, W. Ki, M. Hong, J. Li, A luminescent microporous metal-organic framework for the fast and reversible detection of high explosives, *Angew. Chem., Int. Ed*., **2009**, 48, 2334-2338.

63. W. J. Rieter, K. M. L. Taylor, W. Lin, Surface modification and functionalization of nanoscale metal-organic frameworks for controlled release and luminescence sensing, *J. Am. Chem. Soc*., **2007**, 129, 9852-9853.

64. D. Hu. Y. Song. L. Wang, Nanoscale luminescent lanthanide-based metal-organic frameworks: properties, synthesis, and applications, *J. Nanopart. Res*., **2015**, 17:310.

65. W. P. Lustig, S. Mukherjee, N. D. Rudd, A. V. Desai, J. Li, S. K. Ghosh, Metal-organic frameworks: functional luminescent and photonic materials for sensing applications, *Chem. Soc. Rev.*, **2017**, 46, 3242-3285.

66. P. Vairaprakash, H. Ueki, K. Tashiro, O. M. Yaghi, Synthesis of metal-organic complex arrays, *J. Am. Chem. Soc*., **2011**, 133(4), 759-761.

67. K. Sajna, A. M. Fracaroli, O. M. Yaghi, K. Tashiro, Modular synthesis of metal-organic complex arrays containing precisely designed metal sequences, *Inorg. Chem*., **2015**, 54(4), 1197-1199.

68. L. J. Wang, H. Deng, H. Furukawa, F. Gandara, K. E. Cordova, D. Peri, O. M. Yaghi, Synthesis and characterization of metal-organic framework-74 containing 2, 4, 6, 8, and 10 different metals, *Inorg Chem*., **2014**, 53(12), 5881-5883.

69. D. Sun, F. Sun, X. Deng, Z. Li, Mixed-metal strategy on metal-organic frameworks (MOFs) for functionalities expansion: Co Substitution induces aerobic oxidation of cyclohexene over inactive Ni-MOF-74, *Inorg. Chem*., **2015**, 54(17), 8639-8643.

70. G. Ferey, C. Mellot-Draznieks, C. Serre, F. Millange, J. Dutour, S. Surble, I. Margiolaki, A chromium terephthalate-based solid with unusually large pore volumes and surface area, *Science*, **2005**, 309, 2040-2042.

71. S. S. Y. Chui, S. M. F. Lo, J. P. H. Charmant, A. G. Orpen, I. D. Williams, A chemically functionalizable nanoporous material $[Cu_3(TMA)_2(H_2O)_3]N$, *Science*, **1999**, 283(5405), 1148-1150.

72. A. Schoedel, O. M. Yaghi, Reticular chemistry of metal-organic frameworks composed of Copper and Zinc metal oxide secondary building units as nodes, in The chemistry of metal-organic frameworks: Synthesis, characterization, and applications, S. Kaskel. (Ed.), 1st Ed., Wiley-VCH Verlag GmbH & Co. KGaA, Germany **2016**.

73. T. M. Reineke, M. Eddaoudi, D. Moler, M. O'Keeffe, O. M. Yaghi, Large free volume in maximally interpenetrating networks: the role of secondary building units exemplified by $Tb_2(ADB)_3[(CH_3)_2SO]_4$, $16[(CH_3)_2SO]$, *J. Am. Chem. Soc*., **2000**, 122, 4843-4844.

74. B. Chen, M. Eddaoudi, S. T. Hyde, M. O'Keeffe, O. M. Yaghi, Interwoven MOF on a periodic minimal surface with extra-large pores, *Science*, **2001**, 291(5506), 1021-1023.

75. M. Matzapetakis, C. P. Raptopoulou, A. Tsohos, V. Papaefthymiou, N. Moon, A. Salifoglou, Synthesis, spectroscopic and structural characterization of the first mononuclear, water soluble iron-citrate complex, $(NH_4)_5Fe(C_6H_4O_7)_2\ 2H_2O$, *J. Am. Chem. Soc.*, **1998**, 120(50), 13266-13267.

76. C. Gabriel, C. P. Raptopoulou, A. Terzis, V. Tangoulis, C. Mateescu, A. Salifoglou, pH-Specific synthesis and spectroscopic, structural, and magnetic studies of a chromium(III)-citrate species. Aqueous solution speciation of the binary chromium (III)-citrate system, *Inorg. Chem*., **2007**, 46(8), 2998-3009.

77. Y. Qi, F. Luo, Y. Che, J. Zheng, Hydrothermal synthesis of metal-organic frameworks based on aromatic polycarboxylate and flexible bis (imidazole) ligands, *Cryst. Growth Des.*, **2008**, 8(2), 606-611.

78. E. Y. Choi, K. Park, C. M. Yang, H. Kim, J. H. Son, S. W. Lee, Y. H. Lee, D. Min, Y.U. Kwon, Benzene-templated hydrothermal synthesis of metal-organic frameworks with selective sorption properties, *Chem. Eur. J*., **2004**, 10, 5535-5540.

79. J. Y. Lu, M. A. Lawandy, J. Li, T. Yuen, C. L. Lin, A new type of two-dimensional metal coordination systems: hydrothermal synthesis and properties of the first oxalate-bpy mixed-ligand framework [M(ox)(bpy)] (M = Fe(II), Co(II), Ni(II), Zn(II); ox) $C_2O_4^{2-}$; bpy) 4,4′-bipyridine), *Inorg. Chem*., **1999**, 38, 2695-2704.

80. D. Saha, T. Maity, S. Koner, Alkaline earth metal-based metal-organic framework: hydrothermal synthesis, X-ray structure and heterogeneously catalyzed Claisen–Schmidt reaction, *Dalton Trans*., **2014**, 43, 13006-13017.

81. J. L. Crane, K. E. Anderson, S. G. Conway, Hydrothermal synthesis and characterization of a metal-organic framework by thermo gravimetric analysis, powder x-ray diffraction, and infrared spectroscopy: an integrative inorganic chemistry experiment, *J. Chem. Educ*., **2015**, 92(2), 373-377.

82. U. Mueller, H. Putter, M. Hesse, M. Schubert, H. Wessel, J. Huff, M. Guzmann, Method for electrochemical production of a crystalline porous metal organic skeleton material, *US20110105776 A1*, **2011**.

83. A. Pichon, A. Lazuen-Garay, S. L. James, Solvent-free synthesis of a microporous metal-organic framework, *Cryst. Eng. Comm*., **2006**, 8, 211-214.

84. J. Klinowski, F. A. Paz, P. Silva, J. Rocha, Microwave-assisted synthesis of metal-organic frameworks, *Dalton Trans*., **2011**, 40, 321-330.

85. N. A. Khan, S. H. Jhung, Facile syntheses of metal-organic framework Cu_3 $(BTC)_2$ $(H_2O)_3$ under ultrasound, *Bull. Korean Chem. Soc*., **2009**, 30(12), 2921-2927.

86. I. Imaz, M. Rubio-Martinez, J. An, I. Sole-Font, N. L. Rosi, D. Maspoch, Metal-biomolecule frameworks (MBioFs), *Chem. Commun.*, **2011**, 47, 7287-7302.

87. R. A. Smaldone, R. S. Forgan, H. Furukawa, J. J. Gassensmith, A. M. Z. Slawin, O. M. Yaghi, J. F. Stoddart, Metal-organic frameworks from edible natural products, *Angew. Chem. Int. Ed*., **2010**, 49(46), 8630-8634.

88. D. J. Tranchemontagne, J. R. Hunt, O. M. Yaghi, Room temperature synthesis of metal-organic frameworks: MOF-5, MOF-74, MOF-177, MOF-199, and IRMOF-0, *Tetrahedron*, **2008**, 64(36), 8553-8557.

89. P. T. Anastas, J. C. Warner, Green chemistry: Theory and practice, Oxford University Press, New York **1998**.

CHAPTER 2

SCOPE OF THE RESEARCH

In view of continuous depletion of petroleum reserves & ever rising threat of environmental pollution, hydrogen - A future generation fuel may prove boon for mobile applications once challenges for its onboard storage are overcome. Metal-organic framework materials can function as facilitator for hydrogen storage and supply for mobile applications as an automobile fuel. Storage of hydrogen under normal temperature conditions till now is a great challenging task owing to weak interactions of H_2 with metal-organic frameworks. Solvothermal, the most prevalent technique employed for synthesis of MOFs, though has merits of fast crystal growth, phase purity & larger surface area of product, yet suffers from serious impediment of use and recovery of harmful & expensive organic solvents mostly *N, N*- dimethyl formamide and *N, N*-diethyl formamide. Thus there arises a need for environmental friendly method to be devised for synthesis of MOFs.

Present research was carried out with the motivation to synthesize MOFs with active functional groups on surface to enhance hydrogen interaction & hydrogen storage capacity, through green route, completely eliminating role of harmful organic solvents namely, DMF & DEF.

Citric acid, a naturally occurring complexing agent and its environment friendly nature, employed to provide active functional groups on MOF surface to enhance H_2 interaction & hydrogen storage capacity, further compliments green route to synthesis. An excellent chelating agent, citric acid can easily co-ordinate with different metal ions to form a variety of one, two and three dimensional complexes under mild conditions.

Citric acid linker facilitates the optimization of pore size, inclusion of open metal sites and attractive sites for improving hydrogen storage in multi metal-organic frameworks.

Lime juice squeezed from fresh fruit, used as a source of citric acid further reduces time & cost involved in extraction of citric acid commercially.

The aim of present research was to synthesize metal-organic frameworks as metal-citrate complexes through green synthetic pathways adopting a water based route, completely eliminating the role of harmful organic solvents namely DMF and DEF commonly employed in the synthesis of MOFs. Multiple metal ions in different combinations introduced in the framework to exploit different coordination properties of transition metal ions and to obtain metal ions with coordinative unstauration or vacant sites, after removal of solvent guest molecules in multi metal-citrate complexes. The multi metal-citrate complexes have potential applications in storage of hydrogen, separation of gases, capture of organic dye molecules, sensors for fatal ionic species in industrial waste discharge and bio medical applications due to their photo luminescent properties.

The broad objectives of the present research are summarized as under:

Objective

Synthesis of Metal-organic frameworks through green synthetic pathways and their applications

Specific objectives

- Green synthesis of Multi metal-citrate complexes using citric acid linker.
- Green synthesis of Multi metal-citrate complexes using lime juice, a source of citric acid.
- Characterization of multi metal-citrate complexes by Fourier Transform Infrared Spectroscopy, Scanning Electron Microscopy, UV-Vis spectroscopy, Energy Dispersive Spectroscopy and Powder X- Ray diffraction techniques.
- Introduction of multiple metal ions in the framework.
- Study of stability of these complexes through Thermogravimetric analysis.
- Applications of Multi metal-citrate complexes.

CHAPTER 3

EXPERIMENTAL SECTION

3.1 Materials

Materials used in synthesis and characterization of multi metal-citrate complexes, Copper II sulfate pentahydrate ($CuSO_4.5H_2O$), Iron II sulfate heptahydrate ($FeSO_4.7H_2O$), Nickel II sulfate hexahydrate ($NiSO_4.6H_2O$), Zinc II sulfate heptahydrate ($ZnSO_4.7H_2O$), Citric acid monohydrate (2-hydroxypropane-1, 2, 3-tricarboxylic acid, $C_6H_8O_7.\ H_2O$), oxalic acid dihydrate (Ethanedioic acid, $C_2H_2O_4{\cdot}2H_2O$), sodium hydroxide pellets (NaOH), and Phenolphthalein indicator were commercially available analytical grade and used as obtained without further purification. Lime juice used was squeezed from fresh fruit and strained to discard pulp. Water used was double distilled water. All the reactions were carried out in the air.

3.2 Characterization and measurements

Powder X-ray diffraction patterns were recorded with a Bruker D8 ADVANCE X-ray powder diffractometer operated at 40 KV & 40 mA with monochromated CuKα radiation (λ = 1.5406 Å). Fourier transform infrared spectra were recorded in wavenumber range 4000 - 400 cm^{-1} by using a Nicolet 380 FTIR spectrometer adopting KBr pellet technique. Scanning electron microscopy to observe microscopic morphology of crystals and energy dispersive X-ray spectroscopy to identify the relative elemental composition was performed with HITACHI S-3700N electron microscope with a "built-in" Energy Dispersive X-Ray Analyzer. Absorption spectra were recorded with Shimadzu UV-1800 at room temperature. Fluorescence spectra were recorded on JobinYyon HoribaFluorolog-3 spectrofluorometer.

Thermogravimetric analysis of complexes was carried out in PerkinElmer thermogravimetric analyzer TGA4000 with a scanning rate of 10 $^oC\ min^{-1}$.

Nitrogen physisorption measurements to determine specific surface area of multi metal-citrate complexes were performed using N_2 adsorbate (Molecular Weight.: 28.013u, Liquid Density: 0.806 g cc^{-1}, Eff. mol. diameter (D): 3.54 Å, Cross Section: 16.200 $Å^2$, Temperature 77.350K) using a Quanta chrome Instrument version 3.0, Autosorb iQ., Automated gas sorption analyzer, having cell type 6mm w/o rod. All the samples were pretreated for outgas at temperature 300 °C before adsorption measurements. The BET plot is displayed automatically by ASiQwin software. Collected adsorption data were treated by BET-isotherm in the range $0.05 < P/P_o < 0.3$.

3.3 Outline of Research

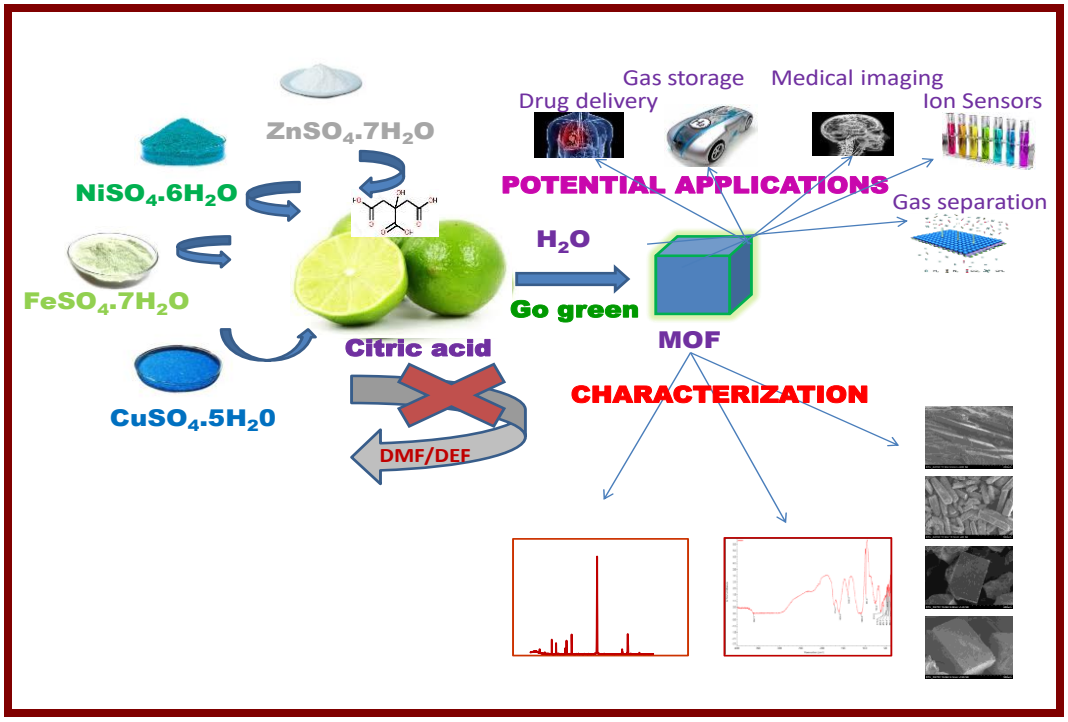

3.4 Green Synthesis of Multi Metal-Citrate Complexes 1-4 using Citric Acid

Synthesis of complex 1

Multi Metal-Citrate complex **1** was synthesized by stirring a solution of 10 mmol each of $NiSO_4.6H_2O$ (2.63 g, 10.0 mmol) and $ZnSO_4.7H_2O$ (2.88 g, 10.0 mmol) with 20 mmol of Citric acid monohydrate in 20 mL of double distilled water. The reaction mixture was initially heated to a temperature of 30 - 40 ºC for 30 minutes & solution was stirred continuously for four hours. The resultant solution was having pH in the range 3 - 4. Upon cooling bluish green needle shaped crystalline product was obtained in 54% yield after 48 hours.

Synthesis of complex 2

Complex **2** was prepared by complexation of Citric acid monohydrate with $CuSO_4.5H_2O$ (2.49 g, 10 mmol) & $FeSO_4.\ 7H_2O$ (2.78 g, 10 mmol) in a molar ratio of 2:1:1 using 20 mL double distilled water as a solvent on the same lines as complex **1**. Upon cooling yellowish green cubical crystals were obtained in 52% yield.

Synthesis of complex 3

Complex **3** was synthesized by the complexation of Citric acid monohydrate with $CuSO_4.5H_2O$ (2.49 g, 10 mmol), $FeSO_4.\ 7H_2O$ (2.78 g, 10 mmol) and $NiSO_4.6H_2O$ (2.63 g, 10.0 mmol) in a molar ratio of 2:1:1:1 and dark green cubical crystals were obtained in 62% yield.

Synthesis of complex 4

The complex **4** was synthesized by taking a solution of 10 mmol each of $CuSO_4.5H_2O$ (2.49 g, 10.0 mmol), $FeSO_4.\ 7H_2O$ (2.78 g, 10.0 mmol), $NiSO_4.6H_2O$ (2.63 g, 10.0 mmol) & $ZnSO_4.7H_2O$ (2.88 g, 10.0 mmol) with 20 mmol of Citric acid in 20 mL of double distilled water adopting procedure as complex **1**, dark green crystals were separated out in 59% yield. The complexes 1-4 were washed with ice cold distilled water and dried in air.

3.5 Green Synthesis of Multi Metal-Citrate Complexes I-IV using Lime Juice

Synthesis of complex I

Multi metal-citrate complex **I** was synthesized by dissolving 10.0 mmol each of $NiSO_4.6H_2O$ (2.63 g, 10.0 mmol) and $ZnSO_4.7H_2O$ (2.88 g, 10.0 mmol) in 20 mL of double distilled water. Lime juice was squeezed from fresh fruit and strained. 20 mL of fresh lime juice was added to the solution of $NiSO_4.6H_2O$ and $ZnSO_4.7H_2O$. The resultant mixture was heated to 30 - 40 ºC under stirring for 30 minutes and stirring continued for four hours. The mixture solution was in the pH range 3 - 4. The resultant solution was allowed to cool in air and kept undisturbed. The bluish green crystals of the complex **I** separated out in 58% yield after 48 hours and subsequently re-crystallized from distilled water.

Synthesis of complex II

Complex **II** was synthesized by dissolving 10 mmol each of $CuSO_4.5H_2O$ (2.49 g, 10 mmol) and $FeSO_4.7H_2O$ (2.78 g, 10 mmol) in 20 mL of double distilled water. Lime juice was squeezed from fresh fruit and strained.

20 mL of fresh lime juice was poured in the reaction mixture. The resultant solution was heated to 30 - 40 ºC under stirring for 30 minutes and stirring continued for four hours. The same procedure was followed as reported for complex **I.** Yellow green crystals in 42% yield were obtained after the solution being kept undisturbed for ten days.

Synthesis of complex III

Complex **III** was synthesized by dissolving 10 mmol each of $CuSO_4.5H_2O$ (2.49 g, 10 mmol), $FeSO_4.7H_2O$ (2.78 g, 10 mmol) and $NiSO_4.6H_2O$ (2.63 g, 10.0 mmol) in 20 mL of double distilled water. 20 mL of fresh squeezed and strained lime juice was added to the above solution. The same procedure was followed as reported for complex **I.** Dark green crystals in 60% yield were obtained after the solution being kept undisturbed for four days.

Synthesis of complex IV

Complex **IV** was synthesized by the same procedure as adopted for complexes **I**, **II** and **III** by stirring a solution of 10 mmol each of $CuSO_4.5H_2O$ (2.49 g, 10 mmol), $FeSO_4.\ 7H_2O$ (2.78 g, 10 mmol), $NiSO_4.6H_2O$ (2.63 g, 10.0 mmol) and $ZnSO_4.7H_2O$ (2.88 g, 10.0 mmol) with 20 mL of double distilled water and 20 mL of fresh squeezed and strained lime juice was added to the reaction mixture. Bluish green crystals were obtained in 54% yield after four days.

3.6 Determination of Citric Acid content in Lime Juice

The citric acid content in lime juice, squeezed from fresh lime fruit and strained was determined by titrating it against standardized sodium hydroxide solution. Fresh squeezed and strained lime juice was titrated against standardized sodium hydroxide solution using phenolphthalein indicator as per standard methods of volumetric analysis. The citric acid content in fresh squeezed lime juice was found to be 5.99% by weight and 5.97% by volume. The citric acid content in lime juice was calculated by standard procedure.

Citric acid + Sodium hydroxide → Sodium citrate + water

$C_6H_8O_{7\,(aq.)} + 3\ NaOH_{\,(aq.)} \rightarrow Na_3C_6H_5O_{7\,(aq.)} + 3\ H_2O_{\,(l)}$

Volume of lime juice taken for each titration = 0.010L

Mass of 0.010 L of lime juice = 10.25 g

Molarity of standardized NaOH solution = 0.9615M

Volume of sodium hydroxide solution used for

neutralization of citric acid in lime juice = 0.0101L

$Moles_{\,(NaOH)}$ = Molarity × Volume

= 0.9615 × 0.0101

= 0.0097mol.

Moles $_{(C6H8O7)}$ = Moles $_{(NaOH)}$ / 3

= 0.0097/3

= 0.0032 mol.

Formula mass $_{(C6H8O7)}$ = 192.06 g

Mass $_{(C6H8O7)}$ = Moles × formula mass

= 0.0032 × 192.06

= 0.6146 g

Percentage of citric acid (by mass) in fresh lime juice

Mass $_{(0.010\ L\ of\ lime\ juice)}$ = 10.25 g

Percentage $_{(C6H8O7)}$ = Mass $_{(C6H8O7)}$ / Mass $_{0.010\ L\ of\ lime\ juice}$ × 100

= 0.6146/10.25 × 100

= 5.99 %

Percentage of citric acid (by volume) in fresh lime juice

Density $_{(C6H8O7)}$ = 1.03 g m L^{-1}

Volume $_{(C6H8O7)}$ = Mass/Density

= 0.6146/1.03

= 0.5967 m L

Percentage $_{(C6H8O7)}$ = Volume $_{(C6H8O7)}$ /Volume $_{0.010\ L\ of\ lime\ juice}$ × 100

= 0.5967/10 × 100 = 5.97 %

3.7 Characterization of Multi Metal-Citrate complexes

All complexes synthesized using citric acid and lime juice have been characterized by:

- Fourier Transform Infrared Spectroscopy.
- Scanning Electron Microscopy.
- Energy Dispersive X-Ray Spectroscopy.
- Powder X- ray Diffraction Spectroscopy.
- UV-Vis Spectroscopy.
- Surface characteristics determined by BET, BJH and DFT methods.
- Stability of complexes established by Thermogravimetric analysis.
- Photo luminescent properties of complexes explored.
- Crystal structure of complexes could not be determined by single crystal X- ray diffraction probably due to overlapping of reflections.

CHAPTER 4

RESULTS AND DISCUSSION

4.1 FTIR Spectroscopy of Multi Metal-Citrate Complexes synthesized using Citric Acid

Infrared spectroscopy (IR) is a quantitative and qualitative analysis to detect functional groups associated with the sample. The material absorbs Infrared radiations and undergoes vibrational transitions which are characteristics for every functional group. The technique helps to identify the conversion, appearance or disappearance of functional groups present in sample during the course of a chemical reaction. Fourier Transform Infrared Spectroscopy of the multi metal-citrates in KBr indicates the presence of vibrationally active carboxylate group **(Figure 4.1, Figure 4.2).** Both anti-symmetric and symmetric stretching vibrations of the carboxylate groups present in the coordinated citrate ligand are revealed by the FTIR spectra of the complexes. Strong absorption bands between 1630 ─ 1600 cm^{-1} are assigned to anti- symmetric, while between 1450 ─ 1400 cm^{-1} are due to symmetric stretching vibrations of the carboxylate groups of citrate ligand. Due to acidic medium the intensities of these bands decrease **[1]**. The difference between anti-symmetric and symmetric stretching vibrations in complex **1** & **2** being greater than 200 cm^{-1}, indicates that carboxylate groups of citrate ligand in these complexes are coordinated to metal ions in a mono dentate fashion **[2]**, while a separation of 180 ─ 200 cm^{-1} in complex **3** & **4** refers to bidentate bridging bonding, the most preferred co-ordination of carboxylate groups of citrate ligand in these complexes **[3, 4]**.

A peak at 1724 cm^{-1} and 1726 cm^{-1} in complex **1** & **2** respectively, suggests that a fraction of hydrogen atoms of carboxylate group of citric acid remain bound while others are replaced by metal atoms forming multi metal-citrate complexes **[5]**.

Absence of characteristic vibrational band of carboxyl group of citric acid between 1750 – 1720 cm^{-1} reflects presence of complete deprotonated form of the citric acid in complexes **3** & **4 [6].**

In addition strong –OH stretching band in the range 3200 ─ 2500 cm^{-1} and in-plane and out-of-plane O─H bending bands of carboxylic acids at 1430 cm^{-1} and 930 cm^{-1} are absent in multi metal-citrate complexes **[7]**. Thus hydroxyl group of citrate ligand is coordinated as shown by Hedwig *et al.* through potentiometric and spectroscopic study for synthesis of Ni (II) complex with citric acid in aqueous solution in pH range 3-6 **[8]**. The characteristic vibrational bands of alcoholic hydroxyl group of citric acid at 3450, 1290, 1265, 1165, 1125, 1060, 925, 890 & 820 cm^{-1} disappear in FTIR spectrum of prepared complexes **[6]**. A broad peak between 3700 ─ 3200 cm^{-1} in all complexes is assigned to hydrogen bonding by hydroxyl group of coordinated water, lying between tetrahedral and octahedral sheets in these complexes **[7]**. A layered structure similar to one assigned to metal carboxylates by researchers in the past is thus proposed for hydrothermally synthesized multi metal-citrate complexes in the present research **[9]**. Two vibrational bands at around 760 cm^{-1} and 630 cm^{-1} confirm the presence of coordinated water molecules in the complexes **[10]**.

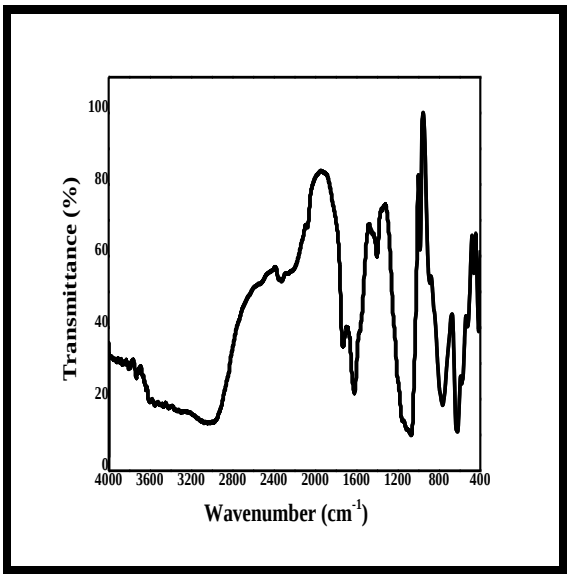

Complex 1

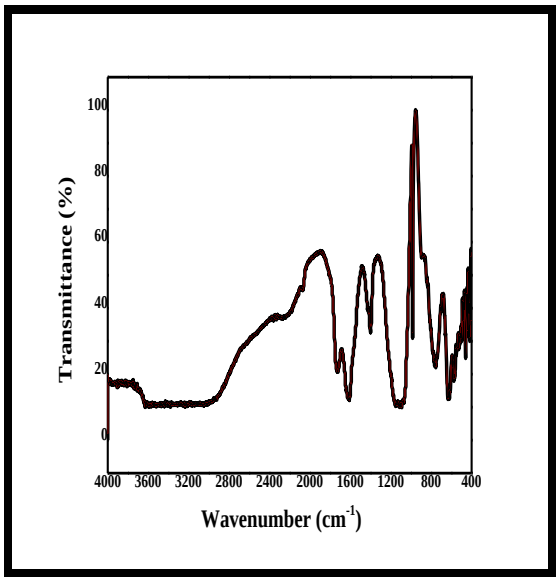

Complex 2

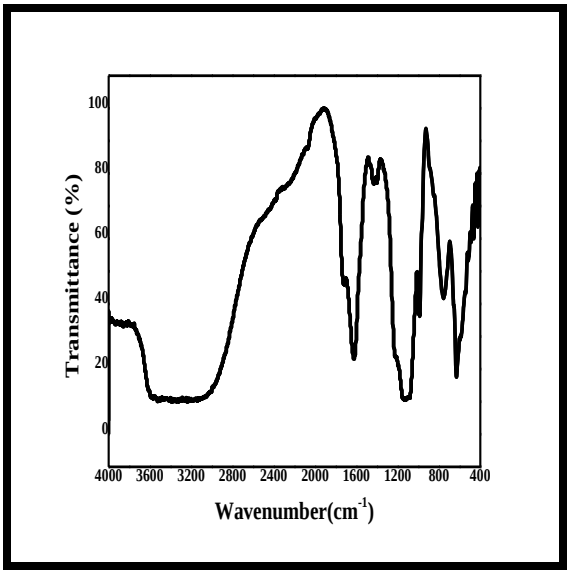

Complex 3

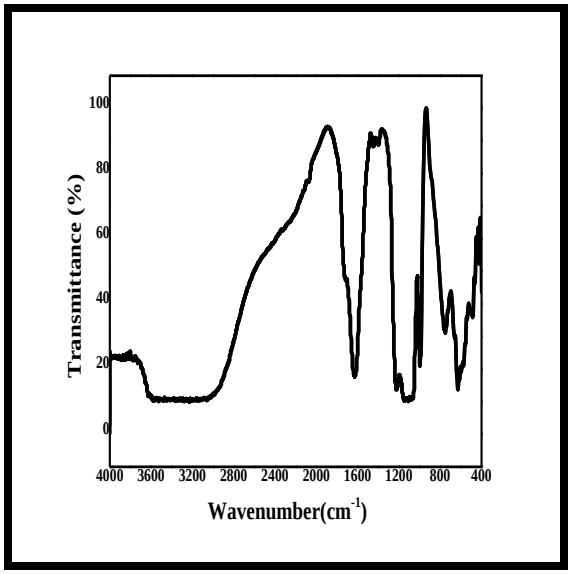

Complex 4

Figure4.1 FTIR Spectroscopy of Complex 1- 4 synthesized using Citric Acid

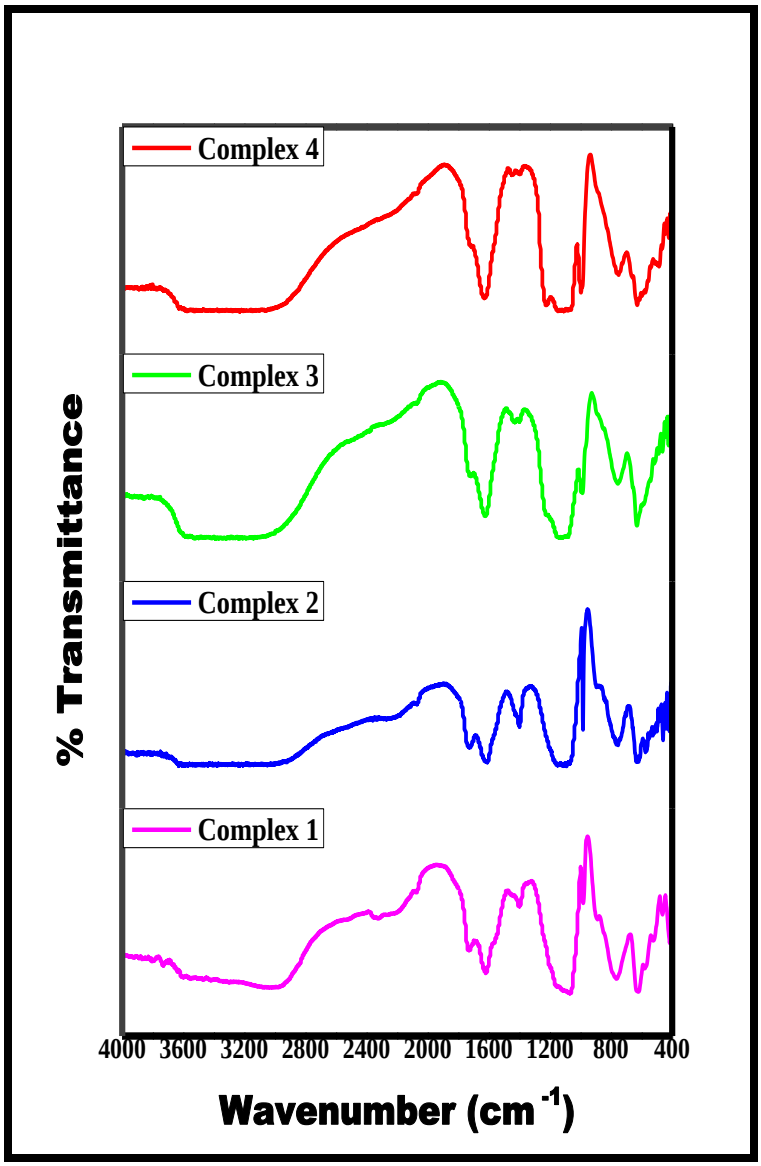

Figure4.2 FTIR combined graph for Complexes 1 - 4 synthesized using Citric Acid

4.2 FTIR Spectroscopy of Multi Metal-Citrate Complexes synthesized using Lime Juice

FTIR spectroscopy of multi metal-citrate complexes synthesized using lime juice, in KBr indicates presence of vibrationally active −COOH **(Figure 4.3, Figure 4.4)**. FTIR spectra of complexes exhibit both symmetric & anti-symmetric stretching vibrations of −COOH present in coordinated citrate ligand. A strong band in range 1630 - 1620 cm^{-1} is assigned to anti-symmetric stretching vibrations, while the one in range 1401 - 1384 cm^{-1} to symmetric stretching vibrations of −COOH of citrate ligand in complexes **[1]**. A difference greater than 200 cm^{-1} between anti-symmetric & symmetric stretching vibrations reveals mono dentate bonding of carboxylate groups of citrate linker with metal ions **[2]**. The peak at 1726 cm^{-1} in complex **1** reveals that a fraction of hydrogen atoms of −COOH of citric acid remain bound while others are replaced by metal atoms forming multi metal-citrate complexes **[5]**. A similar peak at 1726 cm^{-1} & 1724 cm^{-1} was also observed in complexes when synthesized using citric acid. A peak around 1100 cm^{-1} in complexes assigned to C ─ O coordinated to metal cations **[11]**. Weak band between 575 cm^{-1} & 573 cm^{-1} attributed to in plane vibration of O ─ C ═ O group **[12]**. A strong band at 980 cm^{-1} in multi metal-citrate complexes is assigned to C ─ C skeletal bonds of citric acid moiety **[13, 14]**. Characteristic vibrational bands of ─OH group of citric acid at 3450, 1290, 1265, 1165, 1125, 1060, 925, 890 & 820 cm^{-1} are absent in FTIR spectra of complexes **[6]**. In-plane & out-of-plane ─OH bending vibrational bands of −COOH at 1430 cm^{-1} & 930 cm^{-1} disappear in complexes **[7]**. ─OH group of citrate ligand is coordinated as shown by Hedwig *et al.* for synthesis of Ni^{2+} complex with citric acid in aqueous solution in pH range 3-6 **[8]**. Removal of proton from ─OH group of citric acid depends upon nature of metal ion bound to citric acid, with Cu bound to citric acid, tetraionised Cit^{4-} is formed at pH 4 **[15].** A broad band between 3732 cm^{-1} & 3200 cm^{-1} in multi metal-citrate complexes is observed, due to hydrogen bonding of water molecules coordinated to metal ions and lying between tetrahedral & octahedral sheets in complexes **[7]**.

Further two vibrational bands between 765 cm^{-1} ─ 750 cm^{-1} & 635 cm^{-1} ─ 615 cm^{-1} due to rocking $\rho r(H_2O)$ & wagging $\rho w(H_2O)$ vibrations confirm presence of coordinated H_2O in complexes **[10]**. Absorption band at 3154 cm^{-1} in complex **1** is assigned to symmetric ─OH stretching mode associated to tetrahedral coordinated water molecule **[16]**.

The vibrational bands observed for multi metal-citrate complexes **I - IV** appear to be quite similar and comparable to those obtained for complexes **1 - 4** synthesized using commercially available citric acid. FTIR peaks characteristics for heavy transition metals in these complexes appear beyond 400 cm^{-1}. A strong network of hydrogen bonding in these complexes is further confirmed by their thermogravimetric analysis.

Figure 4.3 and **Figure 4.4** reveal Fourier Transform Infrared spectra of multi metal-citrate complexes **I - IV** synthesized through green route using lime juice.

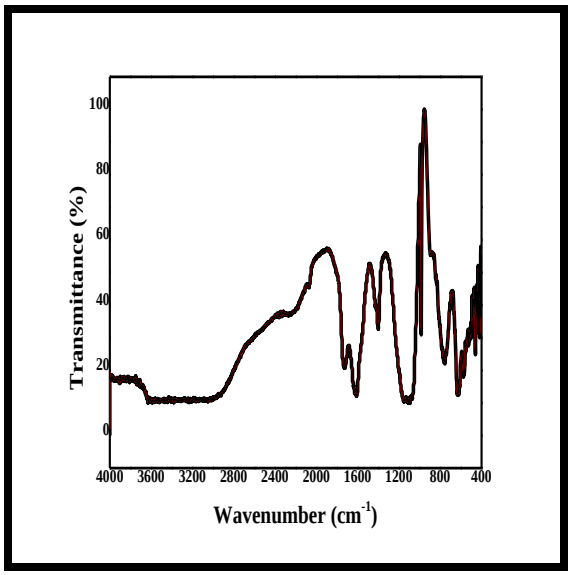

Complex I

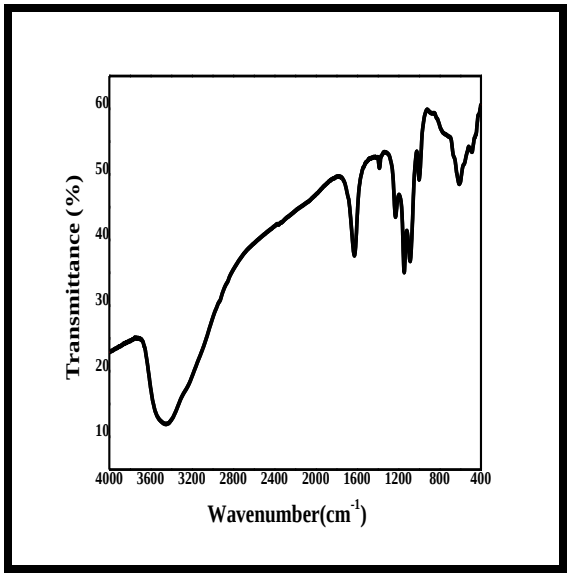

Complex II

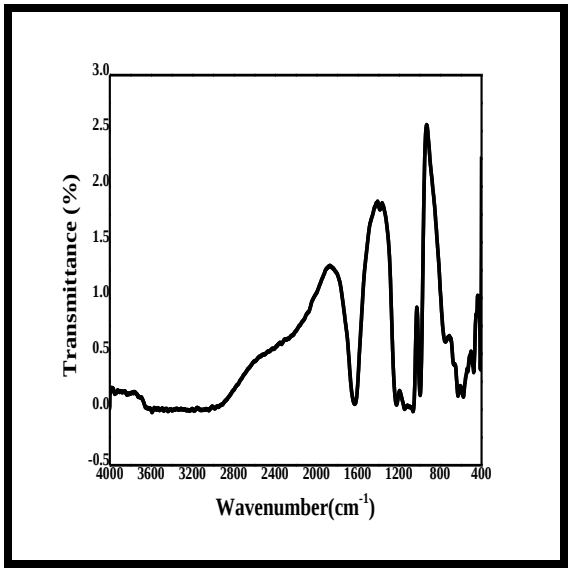

Complex III

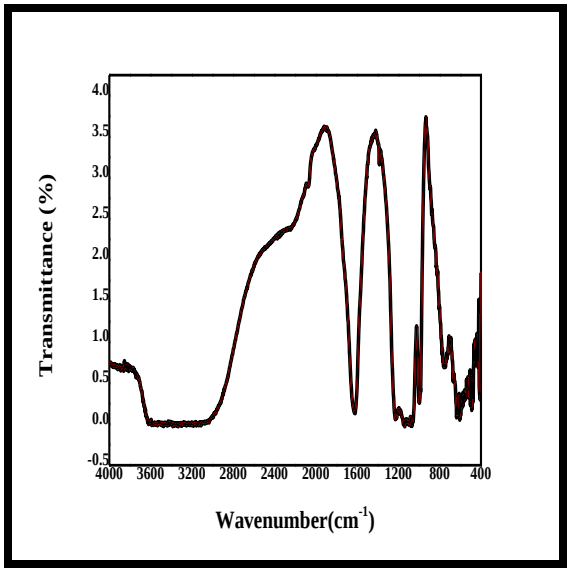

Complex IV

Figure4.3 FTIR Spectroscopy of Complex I - IV synthesized using Lime Juice

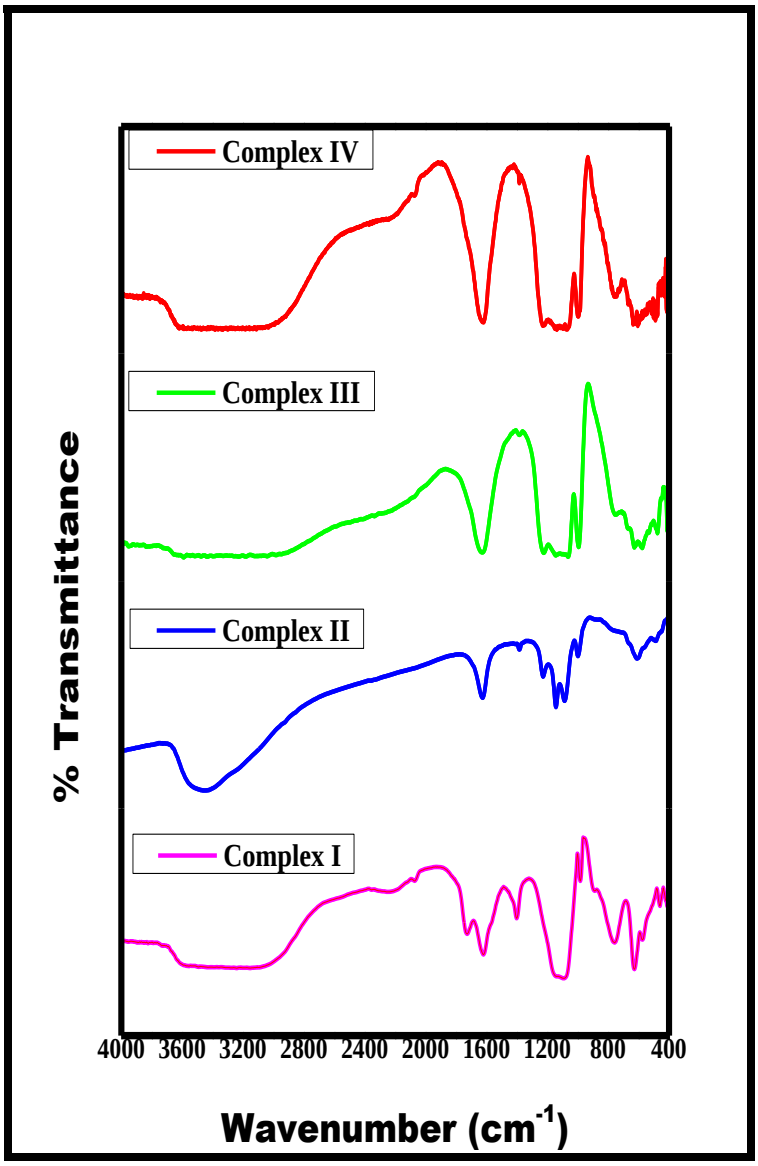

Figure4.4 FTIR combined graph for Multi Metal-Citrate complex I-IV synthesized using Lime Juice

4.3 Structure of Multi Metal-Citrate Complexes synthesized using Citric acid & Lime Juice

All multi metal-citrate complexes are colored, well defined crystalline solids, stable in air and decompose at higher temperature. Based on their Fourier transform infrared spectroscopy, a layered structure similar to one reported in the literature for metal carboxylates is proposed for multi metal-citrate complexes synthesized using citric acid as well as synthesized using lime juice in the present research **[9]**. The −COOH group of citrate ligand in complexes **1** & **2** are coordinated to metal ions in a mono dentate fashion and a fraction of the hydrogen atoms of carboxylate group of citric acid remain bound while others are replaced by metal atoms forming multi metal-citrate complexes, whereas in complex **3** & **4** citrate ligand exhibits complete deprotonated form involving co-ordination of hydroxyl group also and binds with metal ions by bidentate bridging mode, which is the most preferred co-ordination of −COOH groups of citrate ligand in these complexes. In complexes **I-IV** synthesized using lime juice, −COOH groups of citrate ligand are coordinated to metal ions in a mono dentate fashion. In complex **I** synthesized using lime juice a fraction of the hydrogen atoms of carboxylate group of citric acid remain bound while others are replaced by metal atoms forming multi metal-citrate complexes just like its counterparts **1** & **2** synthesized using citric acid. The hydrogen bonded hydroxyl group of coordinated water lying between the tetrahedral and octahedral sheets in the complexes is indicated in these complexes. The comparative Fourier transform infrared frequencies of complexes synthesized using commercially available citric acid and using fresh lime juice are depicted in **Table I.**

Figure 4.5 depicts the structure assigned to multi metal-citrate complexes synthesized using commercial citric acid and lime juice.

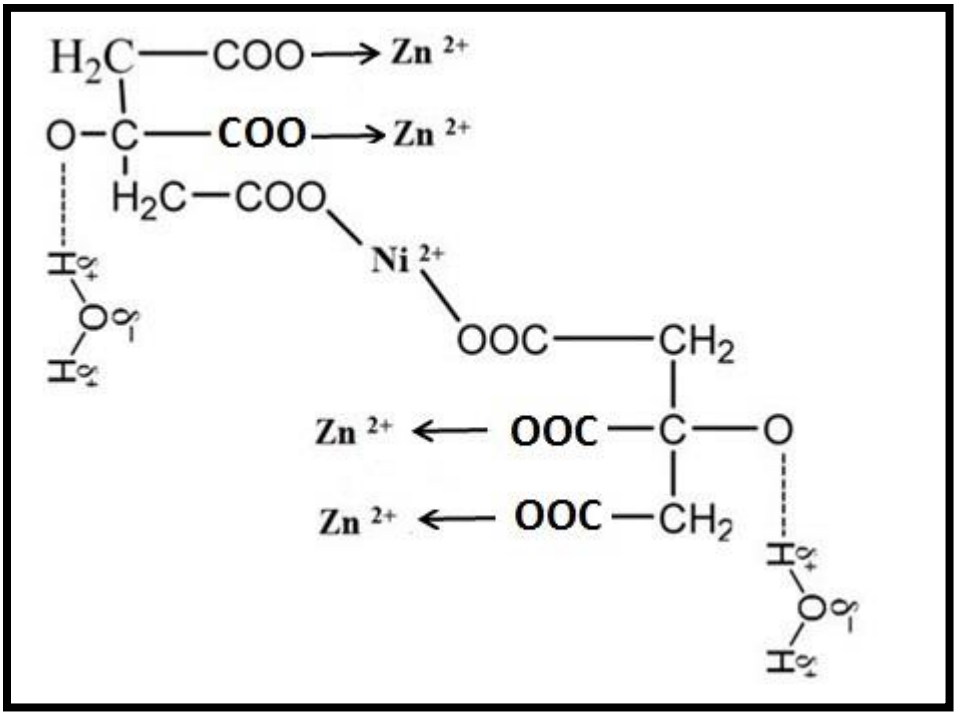

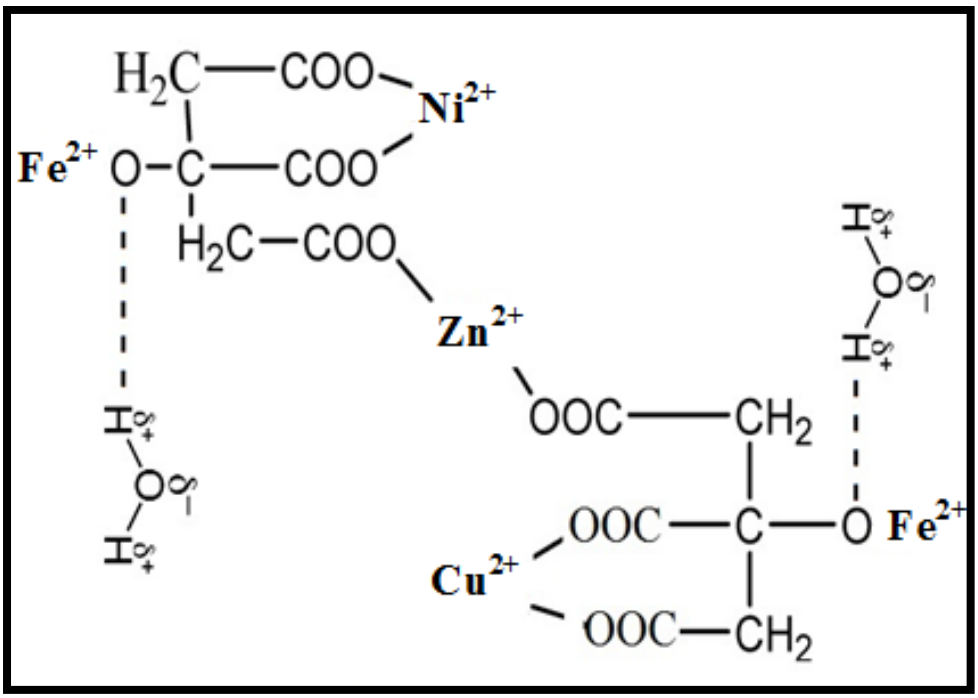

Figure 4.5 Proposed structure of Multi Metal-Citrate complexes

Table 1 Comparison of FTIR Frequencies of Multi Metal-Citrate Complexes synthesized using Citric acid 1-4 & Lime Juice I-IV

Complex 1 Peak/ Cm^{-1}	**Complex I Peak/ Cm^{-1}**	**Complex 2 Peak/ Cm^{-1}**	**Complex II Peak/ Cm^{-1}**	**Complex 3 Peak/ Cm^{-1}**	**Complex III Peak/ Cm^{-1}**	**Complex 4 Peak/ Cm^{-1}**	**Complex IV Peak/ Cm^{-1}**	**Assignment**
3732		3627	3444	3389	3590	3231	3333	ν(O-H) H_2O
3040	3154							ν (O-H)
2326								ν (C-H)
1726	1726	1724						ν (C=O)
1620	1620	1609	1622	1623	1627	1630	1619	ν_{as} (COO^{-})
1401	1401	1401	1384	1432	1380	1450	1384	ν_{s}(COO^{-})
			1228		1223	1224	1229	ν(C–O)
1068	1092	1093	1143	1120	1063	1111	1137	ν(C–O)
982	983	984	988	987	994	997	996	ν(S=O)/ν(C-C)
765	758	753	753	755	750	750	758	ρr(H_2O)
620	627	635	615	629	628	628	635	ν(Ni O)/ρw(H_2O)
	574	574			575		573	νO-C=O
		526					514	ν (Fe-O)
		486	482	483		486	489	ν (Cu-O)
		474		463	476		476	ν (Fe-O)
463	459	459	446			443	464	ν (Zn-O)
		440		439			444	ν (Cu-O)
		438		424		422	430	ν (Fe-O)

4.4 Powder X- Ray Diffraction Spectroscopy of Multi Metal-Citrate Complexes synthesized using Citric Acid and Lime Juice

X-ray diffraction method is commonly employed to study the structure of crystalline material when monochromatic X-Ray beam fall on the surface and interaction of incident rays with sample produces diffraction lines owing to constructive interference when Bragg's Law is obeyed. The diffraction pattern thus obtained provides valuable information to analyze atomic structure and microstructure of a sample. Characterization of a sample from its diffraction pattern is based upon position and relative intensities of diffraction lines. Diffraction patterns are collected as 2 θ versus absolute intensity.

X-ray diffraction studies were carried out using powder technique where sample was ground to a fine homogeneous powder. Unit cell dimensions, crystal lattice, inter planar spacing of lattice planes and miller indices of reflection planes have been calculated from crystallographic data which establish cubic nature of crystals. All reflections have been indexed for [h, k, l] values using methods reported in literature.

All Multi Metal-Citrate complexes exhibit sharp lines in their Powder X-Ray diffraction spectroscopy **(Figure 4.6 – Figure 4.13)** which reflects their highly crystalline nature of single phase. Cubic nature of complexes is substantiated by the fact that $\mathrm{Sin}^2\ \theta$ values of diffraction lines give a set of integers and satisfy equation **(1)** obtained by combining Bragg's Law with plane spacing equation for cubic system **[17]**.

$$\frac{\sin^2\theta}{(h^2+k^2+l^2)} = \frac{\sin^2\theta}{\delta} = \frac{\lambda^2}{4a^2} \qquad \textbf{(1)}$$

(θ = Bragg's diffraction angle in radian, [h k l] = Miller indices, $\delta = h^2+k^2+l^2$= an integer, λ= wave length of the CuKα radiation (0.15406 nm), a = lattice constant).

The lattice parameters of these complexes were calculated by using the formula

$$a = d\sqrt{h^2 + k^2 + l^2} \quad \textbf{(2)}$$

Where a = lattice constant, d = inter planar distance and [*h k l*] = Miller indices.

Unit cell dimensions of cubic structure assigned to multi metal-citrate complexes **1- 4** synthesized using citric acid are found to be 6 Å for complex **1** & **2** and 7 Å for complex **3** &**4**, while for complexes synthesized using lime juice the cubic cell dimensions are found to be 4 Å, 6 Å, 9 Å & 5 Å for complexes **I, II, III** & **IV** respectively. The variation in lattice constants can be attributed to difference in ionic radii of different metal ions **[18]**. The average crystallite size of the complexes was calculated using Scherrer formula **[19, 20]**.

$$\tau = \frac{K\lambda}{\beta \cos\theta} \quad \textbf{(3)}$$

Where λ is wave length of CuKα radiation (0.15406 nm), K is shape factor, a constant (0.94), β (FWHM) is broadening of diffraction line measured in radian at half of its maximum intensity, θ is Bragg's diffraction angle in radian.

The crystallite size of multi metal-citrate complexes synthesized from Citric acid and Lime Juice, calculated using Scherrer formula is shown in **Table II**.

Table 2 Crystallite size/nm calculated using Scherrer formula for Multi Metal-Citrate Complexes synthesized using Citric Acid 1–4 and using Lime Juice I–IV

Complex	2 θ/ degrees	FWHM of 100% peak, degrees	Crystallite size, nm	Lattice strain
1	48.00	0.232	39.16	0.0023
I	32.80	0.133	65.06	0.0020
2	15.20	0.124	67.54	0.0041
II	35.24	0.105	82.95	0.0014
3	31.96	0.206	41.92	0.0031
III	18.44	0.170	49.47	0.0046
4	18.44	0.214	39.31	0.0058
IV	18.56	0.146	57.61	0.0039

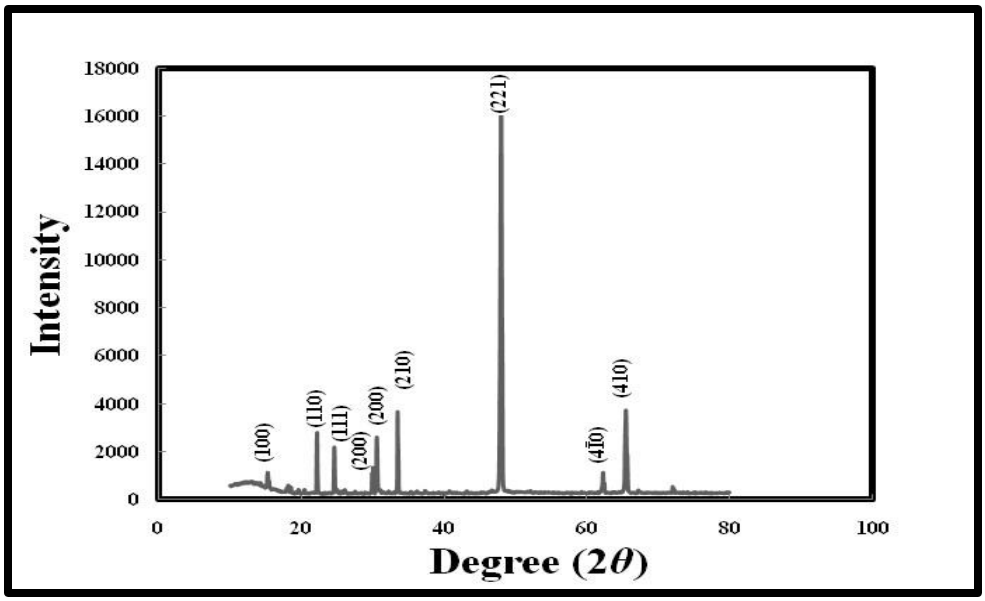

Figure4.6 Powder XRD pattern of complex 1 synthesized using Citric acid

Table 3 Indexing of Powder XRD pattern of complex 1

2θ (deg)	θ (deg)	θ (rad)	Sin θ	Sin^2 θ	Ratio	k factor	$h^2+k^2+l^2$	[hkl]	2 Sin θ (rad)	D spacing (Å)	cell parameter a (Å)	ratio $\sin^2\theta/ h^2+k^2+l^2$
15.28	7.64	0.133	0.132	0.017	1	1	1	100	0.265	5.79173	5.791738	0.01767
22.20	11.10	0.193	0.192	0.037	2.09	2.0969	2	110	0.385	3.99954	5.656207	0.01853
24.60	12.30	0.214	0.213	0.045	2.56	2.5675	3	111	0.426	3.61451	6.260521	0.01512
29.96	14.98	0.261	0.258	0.066	3.78	3.7800	4	200	0.516	2.97893	5.957861	0.01670
30.56	15.28	0.266	0.263	0.069	3.92	3.9292	4	200	0.527	2.92180	5.843603	0.01736
33.48	16.74	0.292	0.288	0.082	4.69	4.6936	5	210	0.576	2.67334	5.977774	0.01659
48.00	24.00	0.418	0.406	0.165	9.35	9.3596	9	221	0.813	1.89311	5.679345	0.01838
62.28	31.14	0.543	0.517	0.267	15.1	15.129	15	4$\bar{1}$0	1.034	1.48898	5.766810	0.01782
65.48	32.74	0.571	0.540	0.292	16.5	16.548	17	410	1.081	1.42374	5.870241	0.01720

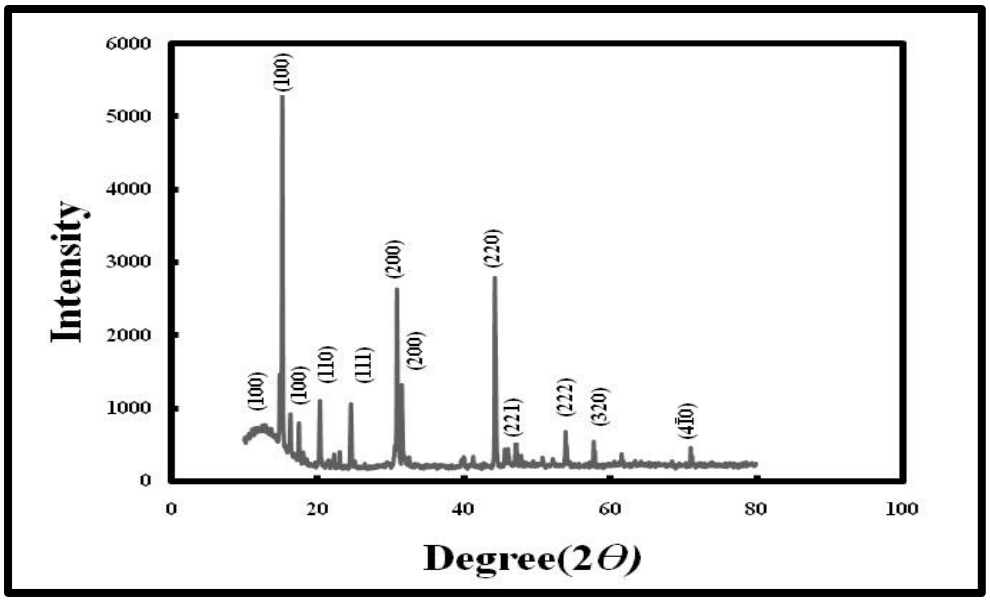

Figure4.7 Powder XRD pattern of complex 2 synthesized using Citric Acid

Table 4 Indexing of Powder XRD pattern of complex 2

2θ (deg)	*θ* (deg)	*θ* (rad)	*Sin θ*	*Sin² θ*	Ratio	*k* factor	$h^2+k^2+l^2$	*[hkl]*	2 *Sin θ* (rad)	D spacing (Å)	cell parameter a (Å)	ratio $Sin^2\theta$ / $h^2+k^2+l^2$
15.20	7.60	0.132	0.13	0.017	1	1	1	100	0.264	5.82202	5.82202493	0.01749
14.84	7.42	0.129	0.12	0.016	0.953	0.9534	1	100	0.258	5.96244	5.96244049	0.01667
16.32	8.16	0.142	0.14	0.020	1.151	1.1517	1	100	0.283	5.42490	5.42490765	0.02014
17.48	8.74	0.152	0.15	0.023	1.319	1.3199	1	100	0.303	5.06742	5.06742705	0.02308
20.36	10.18	0.177	0.17	0.031	1.785	1.7857	2	110	0.353	4.35665	6.16123782	0.01561
24.60	12.30	0.214	0.21	0.045	2.594	2.5944	3	111	0.426	3.61450	6.26051110	0.01512
30.88	15.44	0.269	0.26	0.070	4.052	4.0520	4	200	0.532	2.89224	5.78449119	0.01771
31.56	15.78	0.275	0.27	0.073	4.227	4.2278	4	200	0.543	2.83146	5.66292331	0.01848
44.28	22.14	0.386	0.37	0.142	8.119	8.1198	8	220	0.753	2.04313	5.77887082	0.01775
47.12	23.56	0.411	0.39	0.159	9.133	9.1337	9	221	0.799	1.92640	5.77920162	0.01775
53.96	26.98	0.470	0.45	0.205	11.76	11.766	12	222	0.907	1.69723	5.87938960	0.01715
57.80	28.90	0.504	0.48	0.233	13.35	13.352	13	320	0.966	1.59327	5.74462177	0.01796

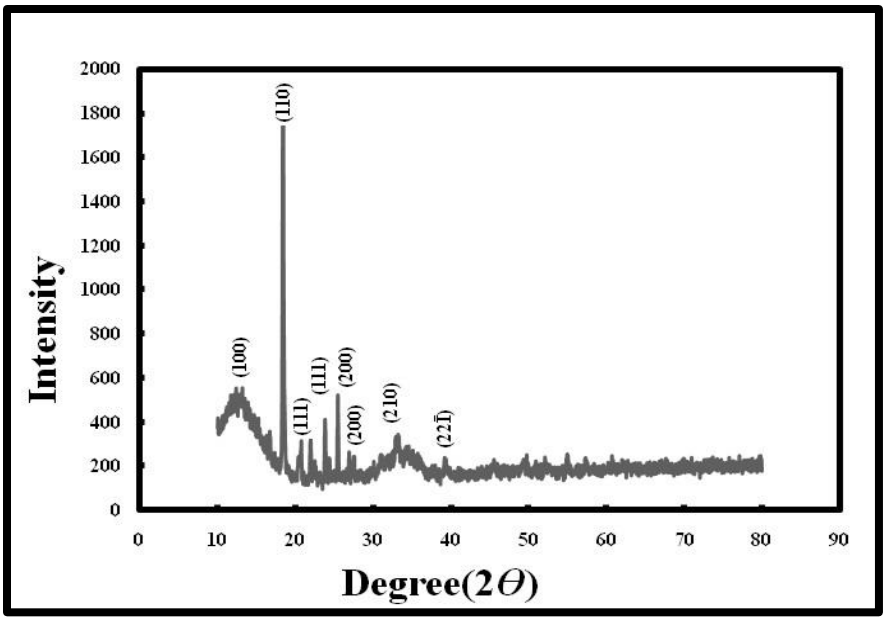

Figure4.8 Powder XRD pattern of complex 3 synthesized using Citric Acid

Table 5 Indexing of Powder XRD pattern of complex 3

2θ (deg)	*θ* (deg)	*θ* (rad)	*Sin θ*	*Sin² θ*	ratio	*k* factor	$h^2+k^2+l^2$	*[hkl]*	2 *Sin θ* (rad)	D spacing (Å)	cell parameter a (Å)	ratio $Sin^2\theta$ / $h^2+k^2+l^2$
12.40	6.20	0.108	0.107	0.0116	1	1	1	100	0.215	7.12967	7.12967216	0.0116638
18.44	9.22	0.160	0.160	0.0256	2.20	2.2010	2	110	0.320	4.80571	6.79631344	0.0128361
20.78	10.39	0.181	0.180	0.0325	2.78	2.7885	3	111	0.360	4.26953	7.39505284	0.0108417
21.98	10.99	0.191	0.190	0.0363	3.11	3.1158	3	111	0.381	4.03907	6.99588464	0.0121142
23.82	11.91	0.207	0.206	0.0425	3.65	3.6515	4	200	0.412	3.73107	7.46214544	0.0106476
25.48	12.74	0.222	0.220	0.0486	4.16	4.1694	4	200	0.441	3.49163	6.98326548	0.0121580
26.92	13.46	0.234	0.232	0.0541	4.64	4.6451	5	210	0.465	3.30803	7.39699485	0.0108360
32.94	16.47	0.287	0.283	0.0803	6.89	6.8913	7	22Ī	0.567	2.71592	7.18565489	0.0114828

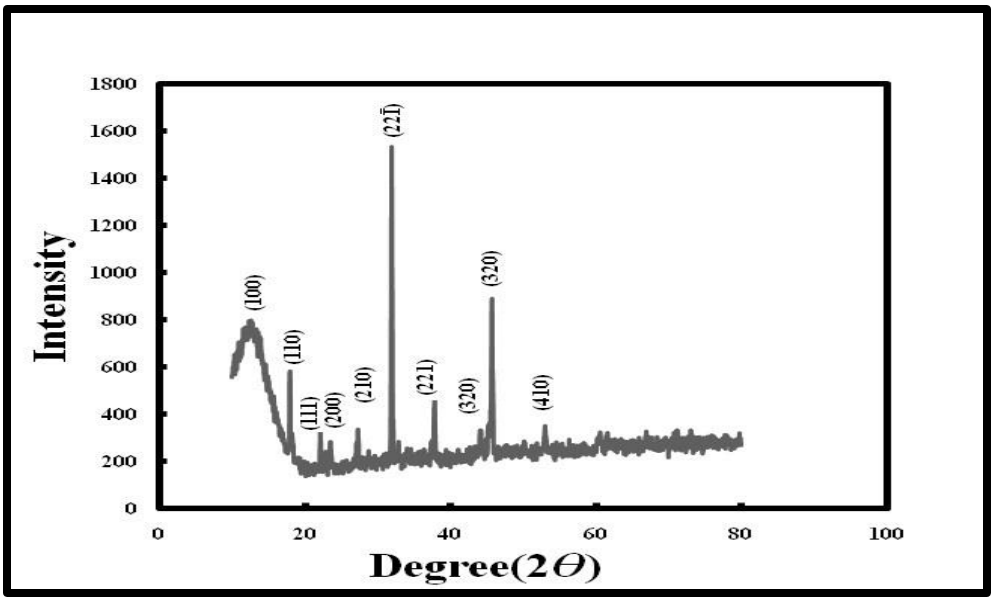

Figure4.9 Powder XRD pattern of complex 4 synthesized using Citric Acid

Table 6 Indexing of Powder XRD pattern of complex 4

2θ (deg)	*θ* (deg)	*θ* (rad)	*Sin θ*	*Sin² θ*	ratio	*k* factor	$h^2+k^2+l^2$	*[hkl]*	2 *Sin θ* (rad)	D spacing (Å)	cell parameter a (Å)	ratio $Sin^2\theta$ / $h^2+k^2+l^2$
12.36	6.18	0.107	0.107	0.0115	1	1	1	100	0.215	7.152	7.152677	0.011589
18.00	9.00	0.157	0.156	0.0244	2.111	2.1116	2	110	0.312	4.922	6.961047	0.012235
22.16	11.08	0.193	0.192	0.0369	3.186	3.1869	3	111	0.073	4.006	6.939775	0.012310
23.56	11.78	0.205	0.204	0.0416	3.596	3.5964	4	200	0.408	3.771	7.543325	0.010419
27.32	13.66	0.238	0.236	0.0557	4.812	4.8124	5	210	0.472	3.260	7.290702	0.011154
31.96	15.98	0.278	0.275	0.0757	6.539	6.5399	7	22Ī	0.550	2.796	7.399977	0.010827
37.88	18.94	0.330	0.324	0.1053	9.090	9.0906	9	221	0.649	2.372	7.116933	0.011705
45.76	22.88	0.399	0.388	0.1511	13.04	13.044	13	320	0.777	1.980	7.140586	0.011628
45.20	22.60	0.394	0.384	0.1476	12.74	12.743	13	320	0.768	2.003	7.224331	0.011360
53.04	26.52	0.462	0.446	0.1993	17.20	17.203	17	410	0.89302	1.724	7.110235	0.011727

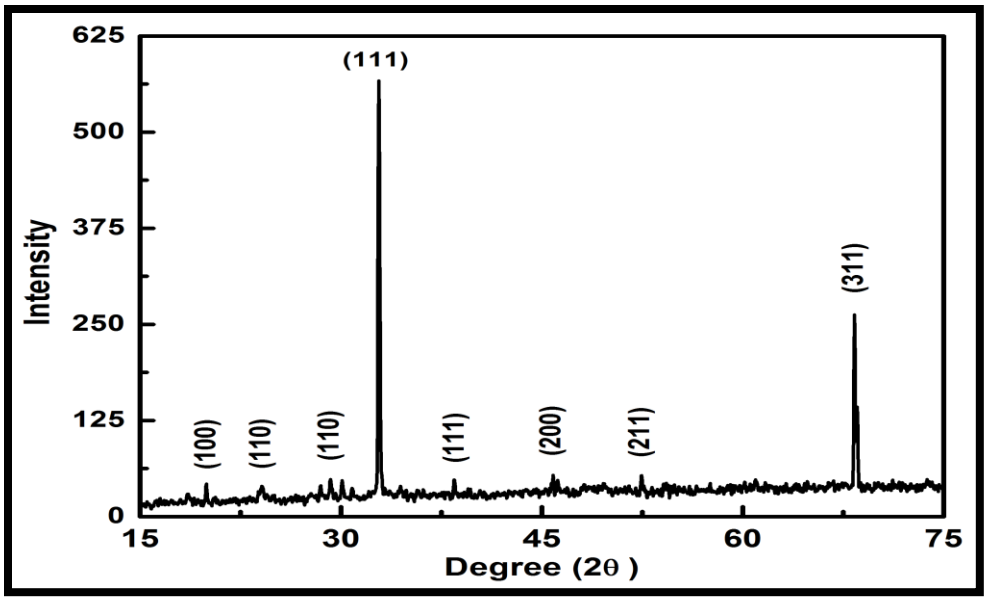

Figure4.10 Powder XRD pattern of complex I synthesized using Lime Juice

Table 7 Indexing of Powder XRD pattern of complex I

2θ (deg)	*θ* (deg)	*θ* (rad)	*Sin θ*	*Sin² θ*	ratio	*k* factor	$h^2+k^2+l^2$	*[hkl]*	2 *Sin θ* (rad)	D spacing (Å)	cell parameter a (Å)	ratio $Sin^2\theta$ / $h^2+k^2+l^2$
19.94	9.97	0.1740	0.1731	0.0299	1	1	1	100	0.34626	4.453236	4.453236432	0.02997486
28.48	14.24	0.2485	0.2459	0.0605	2.0186	2.0186	2	110	0.49196	3.134348	4.432638276	0.03025409
28.52	14.26	0.2488	0.2463	0.0606	2.0241	2.0241	2	110	0.49264	3.130043	4.42655002	0.03033737
32.80	16.40	0.2862	0.2823	0.0797	2.6594	2.6594	3	111	0.56468	2.730736	4.72977362	0.02657223
34.44	17.22	0.3005	0.2960	0.0876	2.9238	2.9238	3	111	0.59208	2.604364	4.510891996	0.02921352
38.50	19.25	0.3359	0.3296	0.1086	3.6262	3.6262	4	200	0.65938	2.338555	4.677111778	0.02717398
52.46	26.23	0.4577	0.4419	0.1953	6.5168	6.5168	6	211	0.88395	1.744440	4.272988392	0.03255707
68.32	34.16	0.5962	0.5615	0.3152	10.518	10.518	11	311	1.12301	1.373093	4.554035911	0.02866261
79.68	39.84	0.6953	0.6406	0.4104	13.692	13.692	14	321	1.28129	1.203472	4.502983346	0.02931622

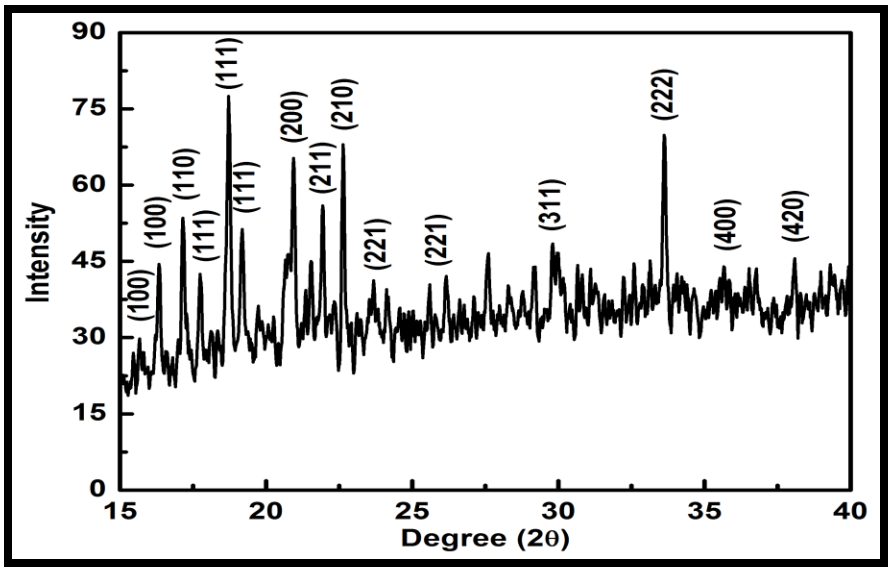

Figure4.11 Powder XRD pattern of complex II synthesized using Lime Juice

Table 8 Indexing of Powder XRD pattern of complex II

2θ (deg)	*θ* (deg)	*θ* (rad)	*Sin θ*	*Sin² θ*	Ratio	*k* factor	$h^2+k^2+l^2$	*[hkl]*	2 *Sin θ* (rad)	D spacing (Å)	cell parameters a (Å)	ratio $Sin^2\theta$ / $h^2+k^2+l^2$
13.88	6.94	0.121125	0.120	0.0146	1	1	1	100	0.24166	6.37259	6.37259566	0.014599
16.52	8.26	0.144164	0.143	0.0206	1.413	1.4136	1	100	0.28733	5.35967	5.35967801	0.020639
19.08	9.54	0.166504	0.165	0.0274	1.881	1.8814	2	110	0.33147	4.64593	6.57035065	0.013734
22.60	11.30	0.197222	0.195	0.0383	2.629	2.6298	3	111	0.39189	3.92965	6.80635552	0.012798
24.32	12.16	0.212232	0.210	0.0443	3.039	3.0390	3	111	0.42128	3.65548	6.33148524	0.014790
25.44	12.72	0.222005	0.220	0.0484	3.320	3.3207	3	111	0.44037	3.49703	6.05703714	0.016160
27.48	13.74	0.239808	0.237	0.0564	3.864	3.8640	4	200	0.47503	3.24188	6.48376396	0.014103
33.92	16.96	0.296007	0.291	0.0850	5.828	5.8282	6	211	0.58340	2.63966	6.46582514	0.014181
31.84	15.92	0.277856	0.274	0.0752	5.153	5.1533	5	210	0.54859	2.80719	6.27708444	0.015047
35.24	17.62	0.307527	0.302	0.0916	6.276	6.2760	6	211	0.60540	2.54375	6.23089167	0.015271
37.28	18.64	0.325329	0.319	0.1021	6.997	6.9971	7	22$\bar{1}$	0.63924	2.40910	6.37389018	0.014593
42.32	21.16	0.369311	0.360	0.1303	8.924	8.9248	9	221	0.72194	2.13312	6.39936000	0.014477
48.36	24.18	0.422020	0.409	0.1677	11.49	11.491	11	311	0.81920	1.87986	6.23479563	0.015252
49.60	24.80	0.432841	0.419	0.1759	12.05	12.050	12	222	0.83890	1.83572	6.35914888	0.014661
57.20	28.60	0.499164	0.478	0.2291	15.69	15.695	16	400	0.95738	1.60855	6.43420177	0.014321

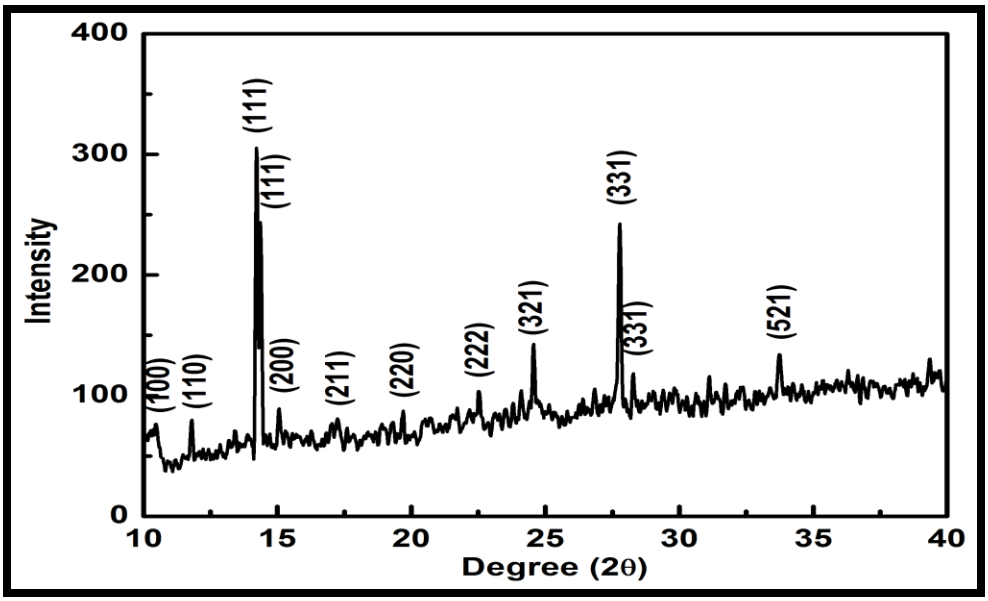

Figure4.12 Powder XRD pattern of complex III synthesized using Lime Juice

Table 9 Indexing of Powder XRD pattern of complex III

2θ (deg)	*θ* (deg)	*θ* (rad)	*Sin θ*	*Sin² θ*	Ratio	*k* factor	$h^2+k^2+l^2$	*[hkl]*	2 *Sin θ* (rad)	D spacing (Å)	cell parameter a (Å)	ratio $Sin^2\theta$ / $h^2+k^2+l^2$
10.12	5.06	0.0883	0.088	0.0077	1	1	1	100	0.1763	8.74160	8.74160488	0.007779
13.56	6.78	0.1183	0.118	0.0139	1.79	1.7916	2	110	0.2361	6.53072	9.23583875	0.006968
18.40	9.20	0.1605	0.159	0.0255	3.28	3.2860	3	111	0.3197	4.82233	8.35252223	0.008520
18.68	9.34	0.1630	0.162	0.0263	3.38	3.3858	3	111	0.3245	4.75067	8.22840997	0.008779
20.04	10.02	0.1748	0.173	0.0302	3.89	3.8916	4	200	0.3479	4.43124	8.86248001	0.007568
24.04	12.02	0.2097	0.208	0.0433	5.57	5.5751	6	211	0.4165	3.70222	9.06856326	0.007228
28.52	14.26	0.2488	0.246	0.0606	7.79	7.7997	8	220	0.4926	3.13004	8.85309997	0.007584
35.00	17.50	0.3054	0.300	0.0904	11.6	11.624	12	222	0.6014	2.56396	8.88184510	0.007535
39.04	19.52	0.3406	0.334	0.1116	14.3	14.352	14	321	0.6682	2.30744	8.63366673	0.007974
45.52	22.76	0.3972	0.386	0.1496	19.2	19.240	19	331	0.7737	1.99290	8.68688308	0.007877
45.64	22.82	0.3982	0.387	0.1504	19.3	19.336	19	331	0.7756	1.98794	8.66525882	0.007916
57.36	28.68	0.5005	0.479	0.2303	29.6	29.607	30	521	0.9598	1.60652	8.79930991	0.007677

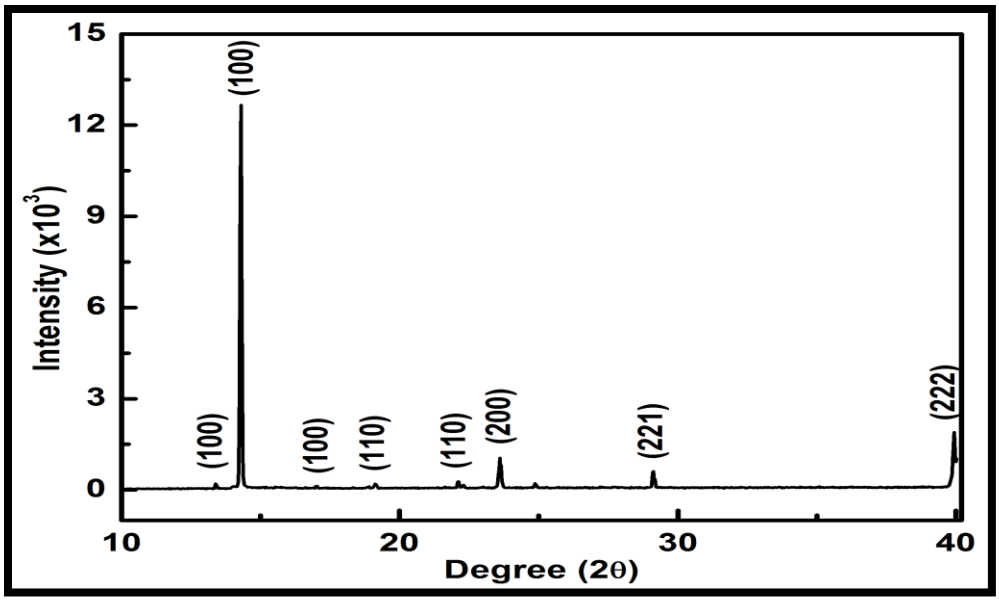

Figure4.13 Powder XRD pattern of complex IV synthesized using Lime Juice

Table 10 Indexing of Powder XRD pattern of complex IV

2θ (deg)	*θ* (deg)	*θ* (rad)	*Sin θ*	Sin^2 *θ*	ratio	*k* factor	$h^2+k^2+l^2$	*[hkl]*	2 *Sin θ* (rad)	D spacing (Å)	cell parameter a (Å)	ratio $Sin^2\theta$ / $h^2+k^2+l^2$
17.70	8.86	0.154	0.154	0.0237	1	1	1	100	0.3080	5.00582	5.0058232	0.0237224
18.60	9.28	0.161	0.161	0.0260	1.09	1.0962	1	100	0.3225	4.78111	4.7811186	0.0260046
19.40	9.70	0.169	0.168	0.0283	1.19	1.1967	1	100	0.3369	4.57595	4.5759561	0.0283887
28.10	14.06	0.245	0.242	0.0590	2.48	2.4879	2	110	0.4858	3.17365	4.4882205	0.0295094
28.00	13.98	0.243	0.241	0.0583	2.46	2.4602	2	110	0.4831	3.19144	4.5133881	0.0291812
37.20	18.58	0.324	0.318	0.1015	4.27	4.2796	4	200	0.6372	2.41974	4.8394924	0.025381
48.20	24.08	0.420	0.408	0.1664	7.01	7.0175	7	22$\bar{1}$	0.8160	1.88965	4.9995473	0.0237819
69.80	34.90	0.609	0.572	0.3273	13.7	13.799	12	222	1.1442	1.34755	4.6680794	0.0272792

4.5 Scanning Electron Microscopy (SEM) of Multi Metal-Citrate complexes

Scanning Electron Microscopy provides valuable information about surface texture and morphology, surface roughness and composition of the material surface when a beam of electrons scans the surface of a sample, interact with electrons of sample atoms and produce characteristic signals which reveal great information about the material. At low pH value metal oxides micro crystals preferably grow into thermodynamically stable morphologies, such as cube & octahedron as revealed by SEM images of complexes **[21]**. Crystalline nature of complexes is supported by their SEM images. SEM images of complexes **1-4** synthesized using citric acid and complexes **I-IV** synthesized using lime juice are depicted in **Figure 4.14**.

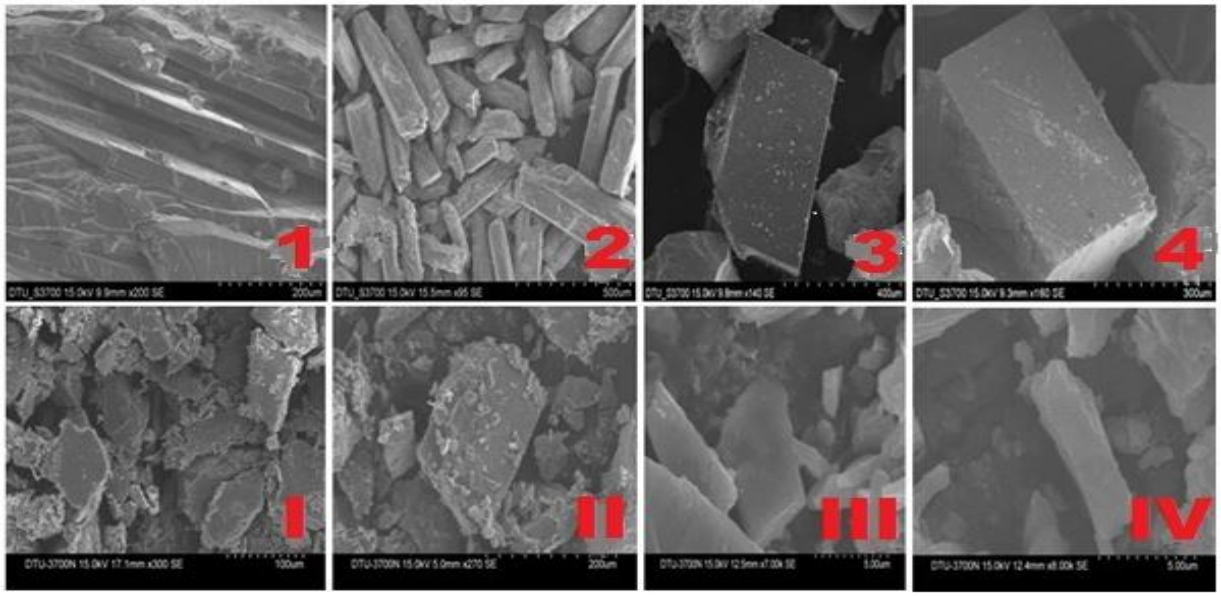

Figure4.14 SEM images of Multi Metal-Citrate complex 1-4 synthesized using Citric Acid & complex I-IV synthesized using Lime Juice

4.6 Energy dispersive X-ray spectroscopy (EDS) of Multi Metal-Citrate complexes

Energy-dispersive X-ray spectroscopy is an attractive tool for qualitative as well as quantitative X-ray microanalysis for a rapid evaluation of specimen which relies on the ability to detect X-rays generated and separate them with different energy levels when a specimen is bombarded with high-energy electrons in an electron microscope.

Transition metals such as iron, copper and nickel tend to have high count rates and thus form well-defined isolated peaks against a low background which enables system to detect extremely low concentrations of these elements, whereas low energy X-rays produced by carbon, nitrogen & oxygen atoms generate much lower count rates and makes it difficult to detect these atoms at low concentrations **[22]**.

Energy-dispersive X-ray spectroscopy (EDS) was performed for elemental analysis of synthesized complexes, which confirms the presence of metals namely Cu, Fe, Ni & Zn as targeted. However no chemical formula could be assigned to complexes because Electron Dispersive Spectroscopy was not able to detect carbon, as analysis of lighter elements such as Be, B, C, N, O & F is difficult with standard EDS technique **[23]**. Energy dispersive X-ray spectrograms of complexes **1 - 4** synthesized using citric acid and complexes **I - IV** synthesized using lime juice are depicted in **Figure 4.15 - Figure 4.18** and **Figure 4.19 - Figure 4.22** respectively. **Tables XI - XVIII** reveals the quantitative results for elemental composition of these complexes.

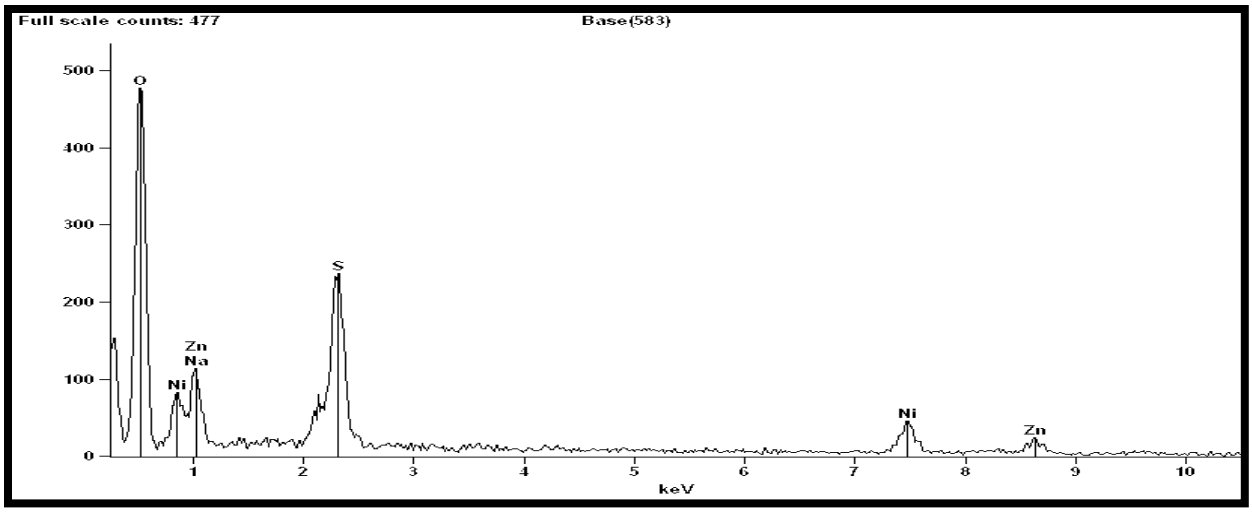

Figure4.15 Energy dispersive X-ray spectroscopy of Complex 1 synthesized using Citric Acid

Table 11 Quantitative Results of EDS for Complex 1

Element	Net Counts	Weight (%)	Weight (%) Error	Atom (%)	Atom (%) Error	Formula
O K	4629	40.55	+/- 0.63	68.20	+/- 1.06	O
Na K	73	0.63	+/- 0.46	0.73	+/- 0.53	Na
S K	2728	13.41	+/- 0.46	11.25	+/- 0.38	S
S L	0	---	---	---	---	
Ni K	632	24.07	+/- 1.60	11.03	+/- 0.73	Ni
Ni L	567	---	---	---	---	
Zn K	282	21.35	+/- 2.50	8.78	+/- 1.03	Zn
Zn L	758	---	---	---	---	
Total		100.00		100.00		

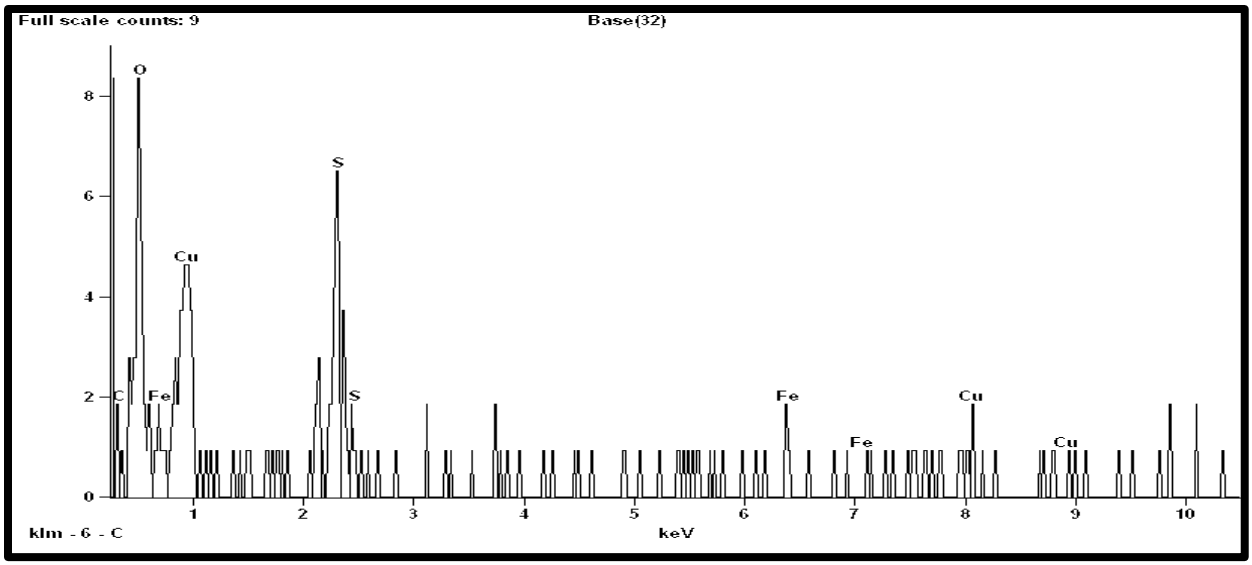

Figure4.16 Energy dispersive X-ray spectroscopy of Complex 2 synthesized using Citric Acid

Table 12 Quantitative Results of EDS for Complex 2

Element	Net Counts	Weight (%)	Weight (%) Error	Atom (%)	Atom (%) Error	Formula
O K	26	30.04	+/- 5.78	56.18	+/-10.80	O
S K	38	22.22	+/- 4.09	20.74	+/- 3.82	S
S L	697	---	---	---	---	
Fe K	3	9.38	+/- 9.38	5.03	+/- 5.03	Fe
Fe L	0	---	---	---	---	
Cu K	6	38.35	+/-31.96	18.06	+/-15.05	Cu
Cu L	31	---	---	---	---	
Total		100.00		100.00		

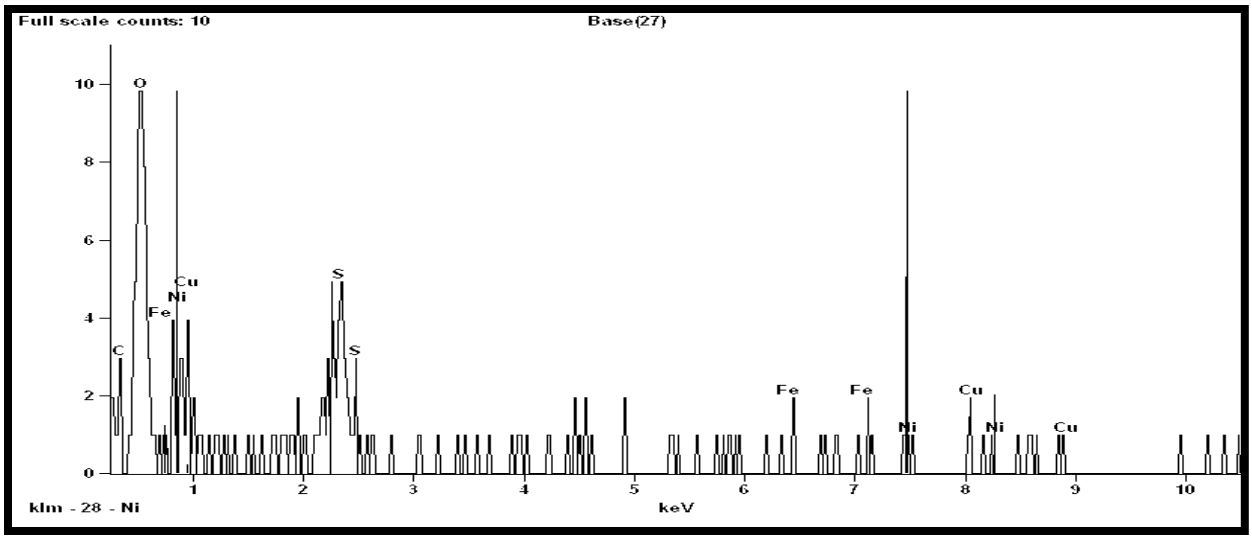

Figure4.17 Energy dispersive X-ray spectroscopy of Complex 3 synthesized using Citric Acid

Table 13 Quantitative Results of EDS for Complex 3

Element	Net Counts	Weight (%)	Weight (%) Error	Atom (%)	Atom (%) Error	Formula
O K	56	33.75	+/- 4.82	62.18	+/- 8.88	O
S K	35	12.16	+/- 3.13	11.18	+/- 2.87	S
S L	1875	---	---	---	---	
Fe K	5	8.42	+/- 6.73	4.44	+/- 3.55	Fe
Fe L	0	---	---	---	---	
Ni K	9	26.57	+/- 8.86	13.34	+/- 4.45	Ni
Ni L	0	---	---	---	---	
Cu K	5	19.10	+/-11.46	8.86	+/- 5.32	Cu
Cu L	13	---	---	---	---	
Total		100.00		100.00		

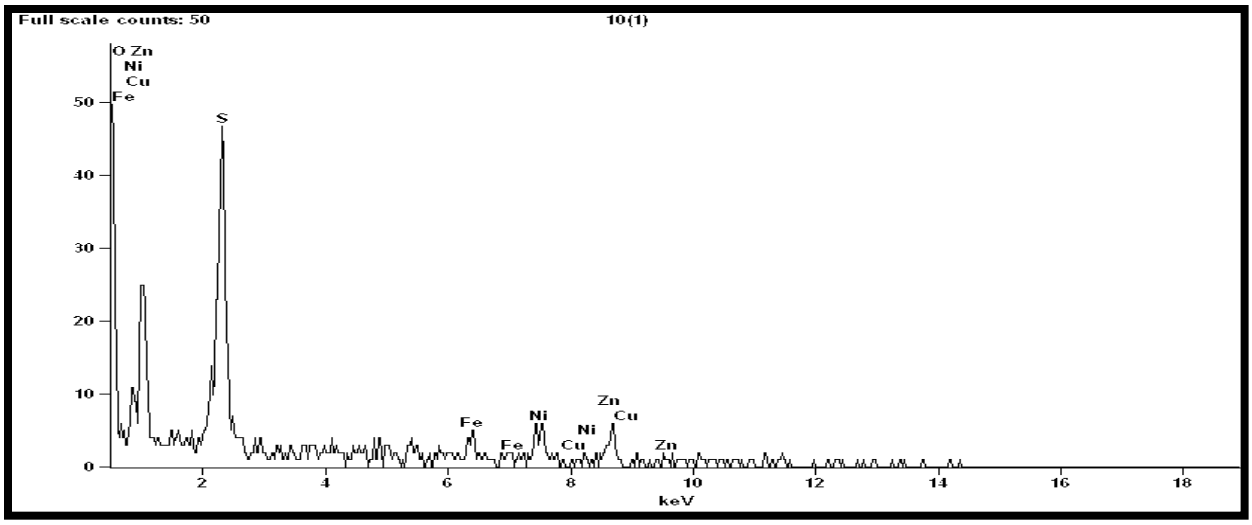

Figure4.18 Energy dispersive X-ray spectroscopy of Complex 4 synthesized using Citric Acid

Table 14 Quantitative Results of EDS for Complex 4

Element	Net Counts	Weight (%)	Weight (%) Error	Atom (%)	Atom (%) Error	Formula
S K	474	25.98	+/- 1.59	40.20	+/- 2.46	S
S L	8631	---	---	---	---	
Fe K	59	13.87	+/- 3.06	12.32	+/- 2.7s2	Fe
Fe L	0	---	---	---	---	
Ni K	57	21.09	+/- 5.18	17.82	+/- 4.38	Ni
Ni L	0	---	---	---	---	
Cu K	3	1.39	+/- 2.78	1.09	+/- 2.17	Cu
Cu L	0	---	---	---	---	
Zn K	51	37.66	+/-10.34	28.57	+/- 7.84	Zn
Zn L	207	---	---	---	---	
Total		100.00		100.00		

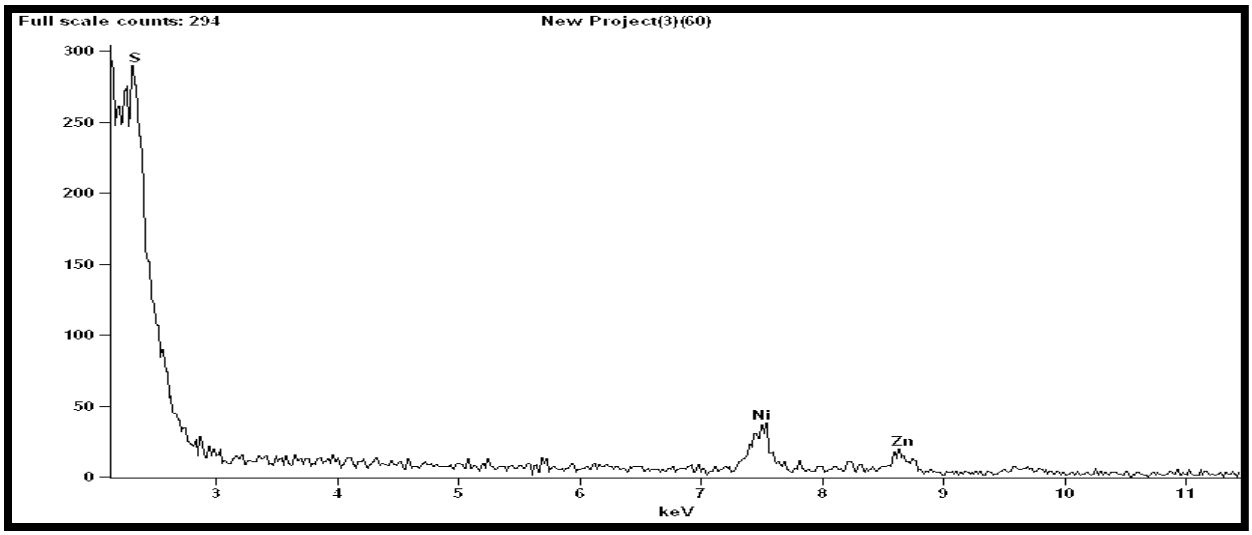

Figure4.19 Energy dispersive X-ray spectroscopy of Complex I synthesized using Lime Juice

Table 15 Quantitative Results of EDS for Complex I

Element	Net Counts	Weight (%)	Weight (%) Error	Atom (%)	Atom (%) Error	Formula
O K	9325	56.59	+/- 4.29	80.57	+/- 6.11	O
S K	2658	10.04	+/- 0.66	7.13	+/- 0.47	S
S L	1220323	---	---	---	---	
Ni K	563	16.88	+/- 2.85	6.55	+/- 1.11	Ni
Ni L	0	---	---	---	---	
Zn K	277	16.49	+/- 2.86	5.74	+/- 1.00	Zn
Zn L	0	---	---	---	---	
Total		100.00		100.00		

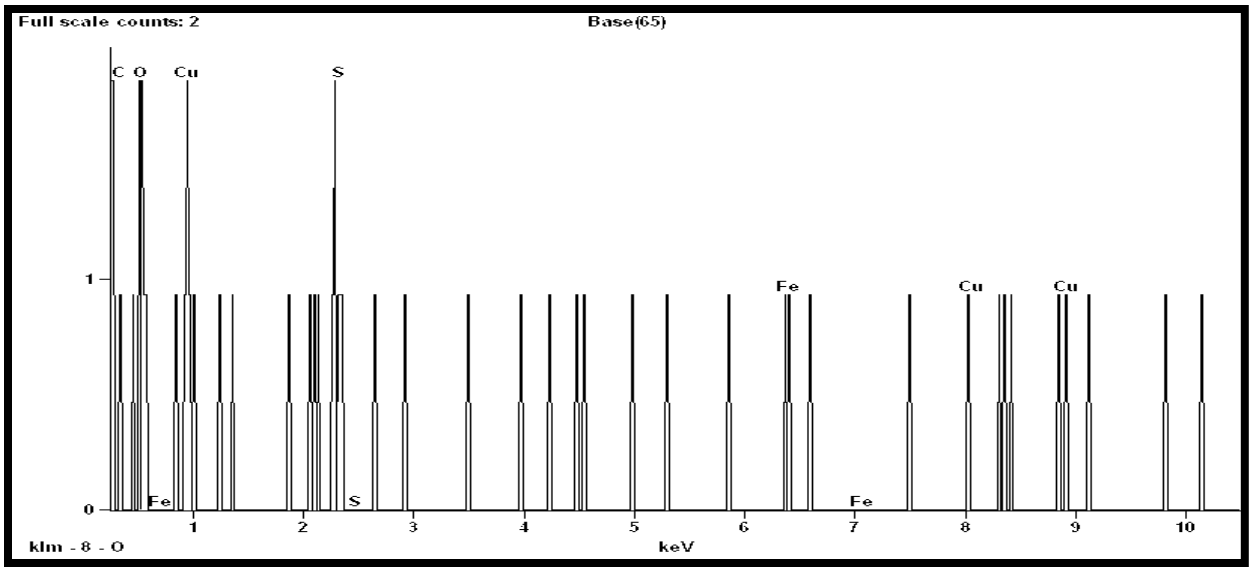

Figure4.20 Energy dispersive X-ray spectroscopy of Complex II synthesized using Lime Juice

Table 16 Quantitative Results of EDS for Complex II

Element	Net Counts	Weight (%)	Weight (%) Error	Atom (%)	Atom (%) Error	Formula
O K	6	17.37	+/- 5.79	41.61	+/-13.87	O
S K	8	12.17	+/- 4.56	14.54	+/- 5.45	S
S L	0	---	---	---	---	
Fe K	2	16.45	+/-16.45	11.29	+/-11.29	Fe
Fe L	0	---	---	---	---	
Cu K	3	54.01	+/-36.00	32.56	+/-21.71	Cu
Cu L	5	---	---	---	---	
Total		100.00		100.00		

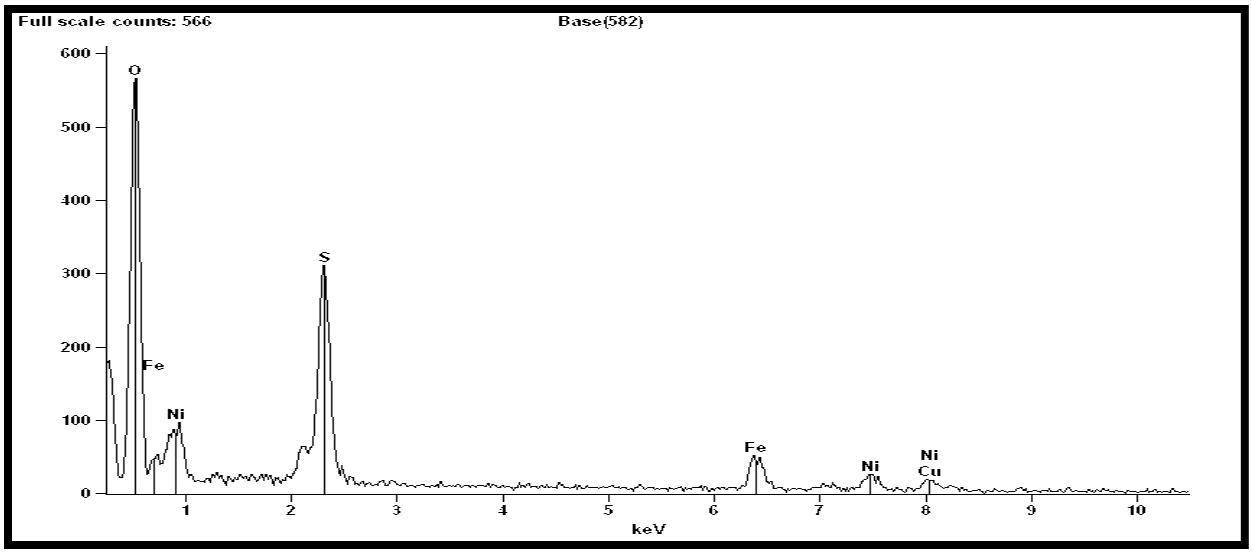

Figure4.21 Energy dispersive X-ray spectroscopy of complex III synthesized using Lime Juice

Table 17 Quantitative Results of EDS for Complex III

Element	Net Counts	Weight (%)	Weight (%) Error	Atom (%)	Atom (%) Error	Formula
O K	4820	38.79	+/- 0.70	65.82	+/- 1.19	O
S K	3502	15.62	+/- 0.45	13.22	+/- 0.38	S
Fe K	741	16.57	+/- 0.94	8.06	+/- 0.46	Fe
Fe L	69	---	---	---	---	
Ni K	377	14.12	+/- 1.31	6.53	+/- 0.61	Ni
Ni L	332	---	---	---	---	
Cu K	289	14.91	+/- 1.70	6.37	+/- 0.73	Cu
Cu L	486	---	---	---	---	
Total		100.00		100.00		

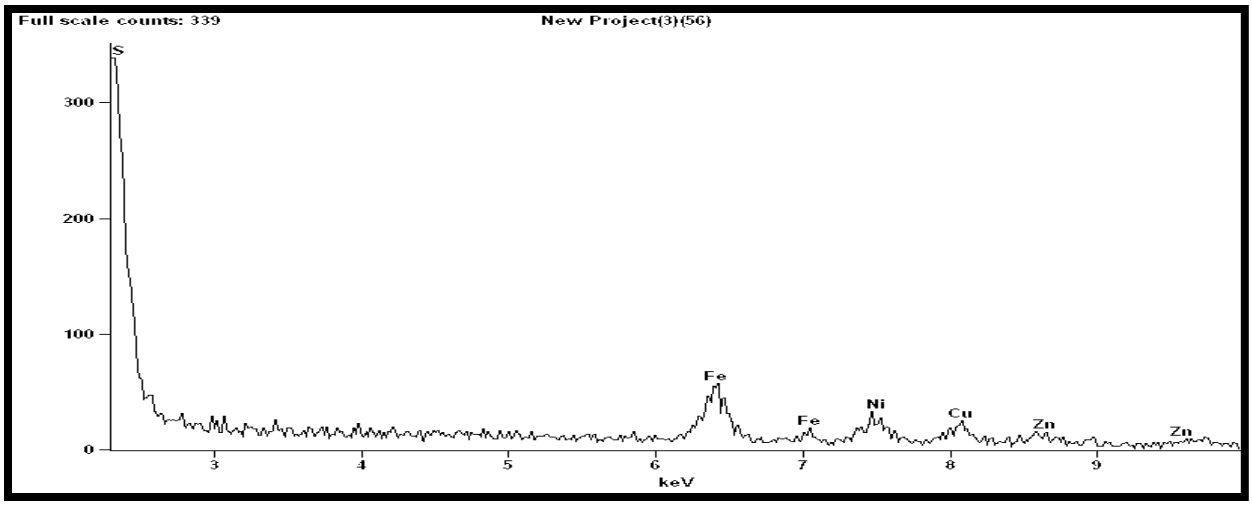

Figure4.22 Energy dispersive X-ray spectroscopy of complex IV synthesized using Lime Juice

Table 18 Quantitative Results of EDS for Complex IV

Element	Net Counts	Weight (%)	Weight (%) Error	Atom (%)	Atom (%) Error	Formula
O K	6524	26.20	+/- 1.83	37.42	+/- 2.61	O
S K	5703	23.26	+/- 1.16	29.11	+/- 1.45	S
S L	1207716	---	---	---	---	
Fe K	796	14.04	+/- 2.05	10.09	+/- 1.47	Fe
Fe L	0	---	---	---	---	
Ni K	369	10.44	+/- 1.70	7.13	+/- 1.16	Ni
Ni L	0	---	---	---	---	
Cu K	372	14.67	+/- 2.17	9.26	+/- 1.37	Cu
Cu L	0	---	---	---	---	
Zn K	212	11.39	+/- 2.63	6.99	+/- 1.62	Zn
Zn L	0	---	---	---	---	
Total		100.00		100.00		

4.7 Thermogravimetric analysis of Multi Metal-Citrate complexes

Thermogravimetry deals with variation of mass of the sample being monitored continuously with change of temperature, when it is heated or cooled at a specified rate in an atmosphere which may be inert or oxidative. Chemical changes which take place in an oxidative atmosphere reveal very important information for characterization of material. It provides valuable information on thermal stability of sample and various chemical reactions such as oxidation, decomposition, decarboxylation and fusion besides crystallization or phase transitions which occur as the sample is being heated at different temperatures under controlled conditions. The thermogram is analyzed to obtain information about percentage weight loss at different temperatures. The 1st derivative of TGA curve, DTG, provides decomposition rate and is helpful for evaluating mass loss steps accurately. Peak of first derivative indicates point of greatest rate of change on weight loss curve. This is also known as inflection point.

The variation in mass of the complexes synthesized through green route was studied by heating the samples under controlled conditions, up to 1500 ºC for complexes **1-4** synthesized using citric acid and up to 900 ºC for complexes **I-IV** synthesized using lime juice. The samples were heated at a rate of 10 ºC min^{-1}. The thermogravimetric curves of complexes **1-4** & complexes **I-IV** have been depicted in **Figure 4.23 - Figure 4.25** & **Figure 4.26, Figure 4.27** respectively. Thermogravimetric curves of complexes **1**, **3** and **4** show four stage decomposition patterns, while thermal decomposition of complex **2** occurs in three stages. Major weight loss in temperature range 120 ºC- 150 ºC in the first stage can be attributed to vaporization of lattice water in all the complexes **[24]**. The second stage reveals a small weight loss corresponding to coordinated water in all complexes, followed by gradual weight loss in temperature range 300 ºC - 700 ºC. A large weight loss in third stage may be attributed to decarboxylation of carboxylic acid groups of citrate moiety. The dehydration takes place at relatively higher temperatures during thermal analysis of multi metal-citrate complexes due to an extensive array of hydrogen bonds in these complexes and probably due to "*resistance of crystal lattice*" to water escaping as described by Rogan and Poleti **[25]**.

Hydrogen bonding occurs between lattice water & coordinated water molecules and between coordinated water molecules & carboxyl oxygen atoms of citrate moiety to form a rigid three dimensional supramolecular structure with great stability **[26]**. Moreover decarboxylation of citrate ligand occurs at higher temperature as thermal stability of citrate ligand increases on complexation with metal ions **[27]**. The residue contains mixed metal oxides as a result of decomposition of complexes in air. Pyrolysis of these complexes in an atmosphere of nitrogen leaves more residues as compared to their thermal decomposition in air due to carbon black formed from pyrolysis of citrate moiety. Thermal stability of multi metal-citrate complexes **I-IV** was established based on their thermogravimetric analysis carried out in an inert atmosphere of nitrogen by scanning these complexes under controlled heating between 30 ºC − 900 ºC. Thermogravimetric curves for these complexes exhibit four step thermal decomposition pattern except complex **II** in which thermal decomposition occurs in five stages. The first stage involves major weight loss to a temperature range of 120 - 130 ºC due to vaporization of lattice water in all complexes. A small weight loss in second stage may be attributed to loss of coordinated water followed by weight loss at around 350 ºC due to onset of decomposition process involving decarboxylation of carboxylic acid groups of citric acid linker and crystallization of oxides of different metals at higher temperature around 700 ºC in all complexes. The thermal treatment of complex **2** reveals a five step process due to formation of carbonate and oxy carbonate intermediates which is lacking in complexes **I, III and IV** due to the presence of nickel ions which decompose to form oxides at higher temperature without forming intermediates **[28]**.

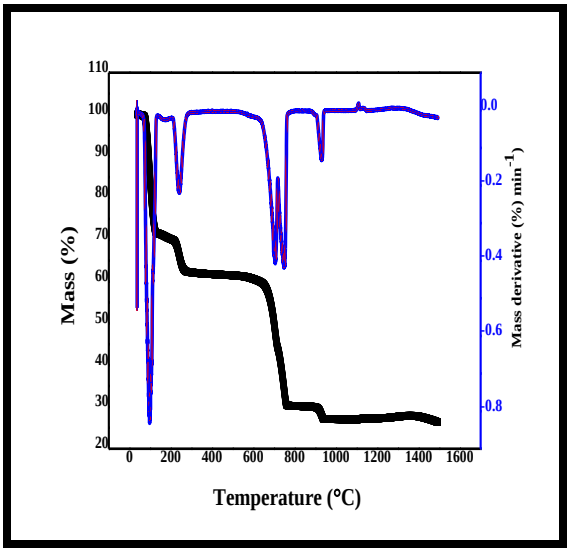

Complex 1

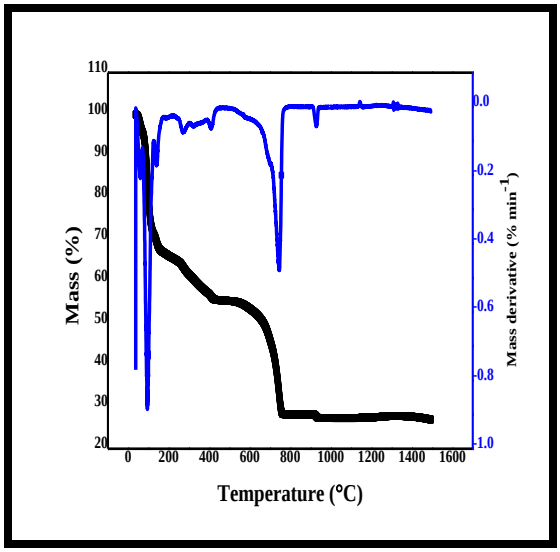

Complex 2

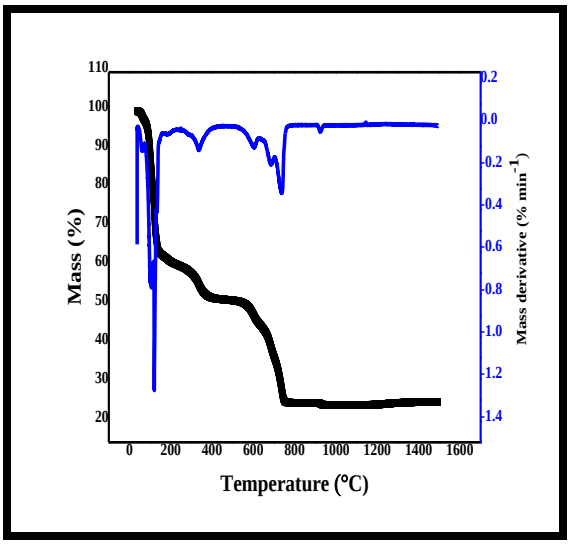

Complex 3

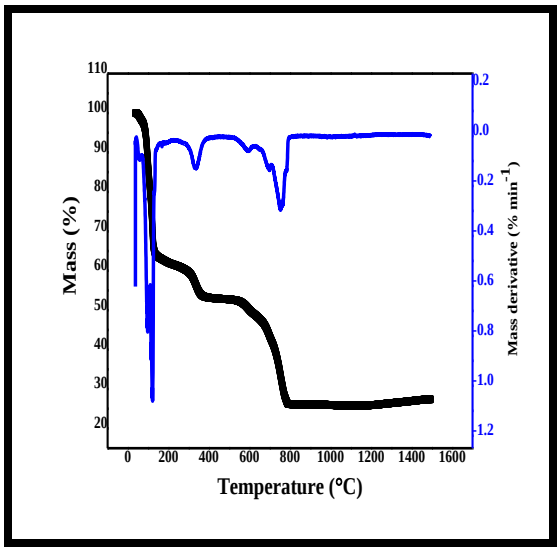

Complex 4

Figure4.23 TGA/DTG curve for Complexes 1-4 synthesized using Citric Acid

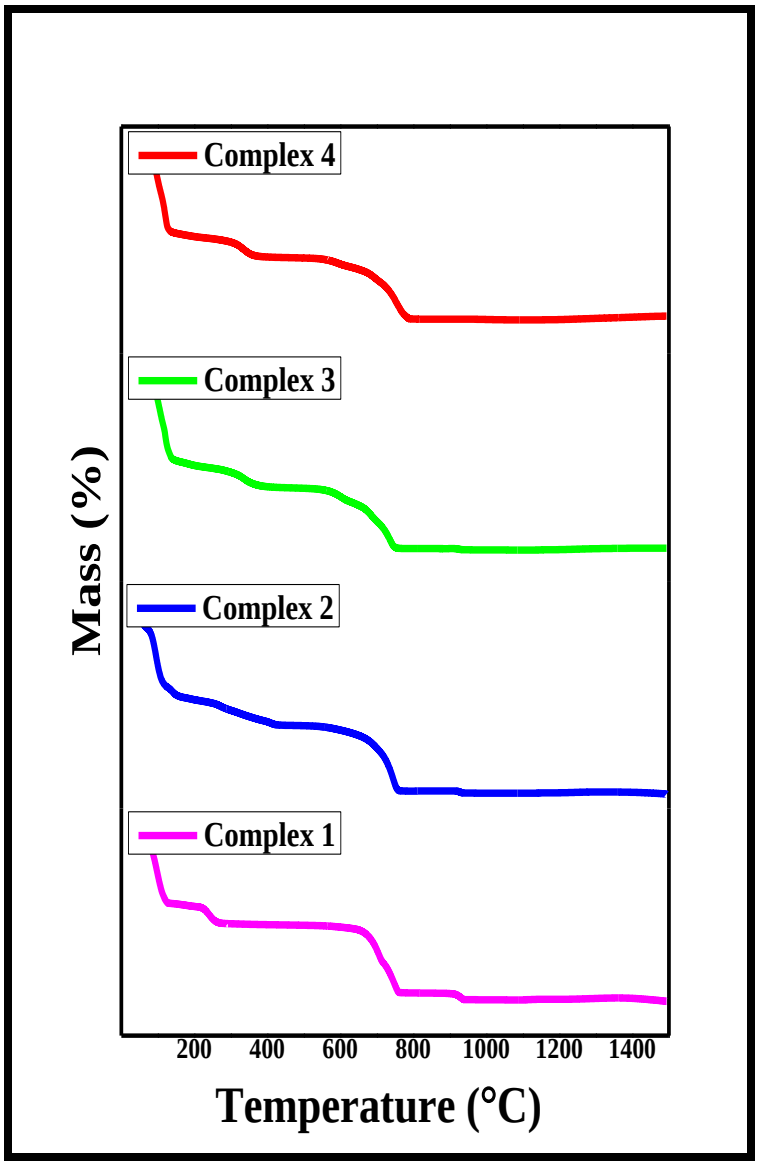

Figure4.24 Thermogravimetric curve in air: combined graph for Complexes 1- 4

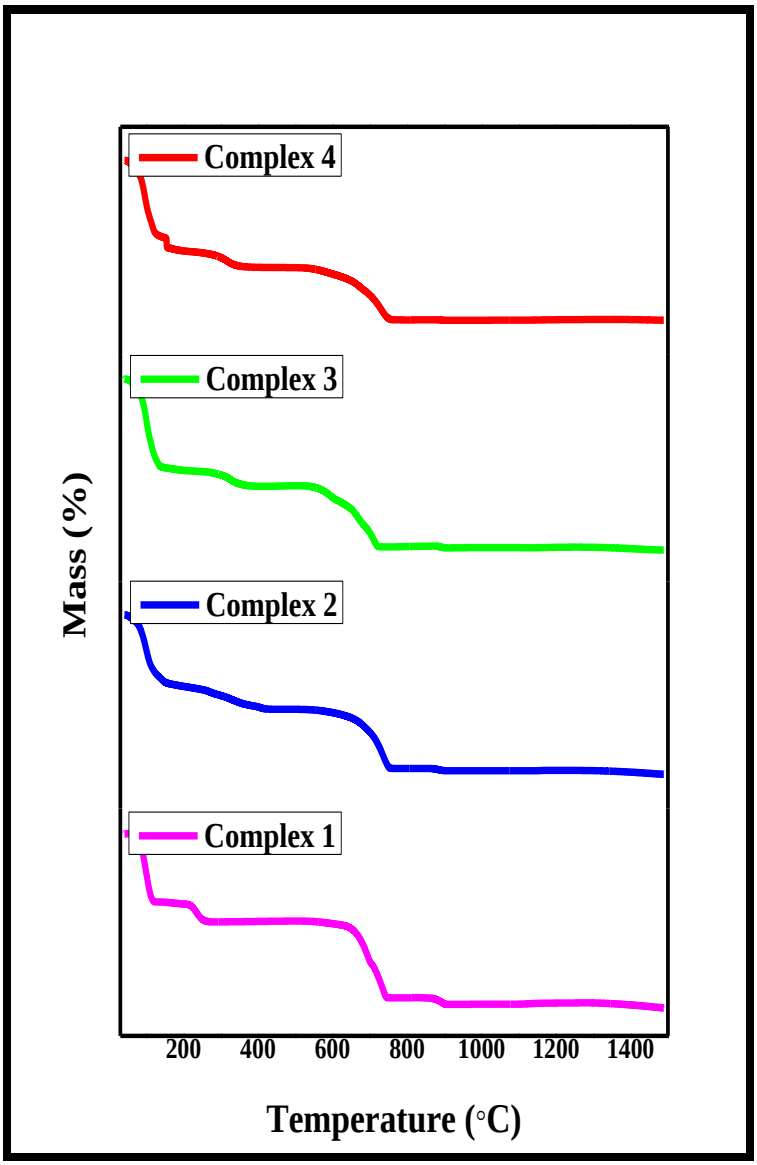

Figure4.25 Thermogravimetric curve in nitrogen: combined graph for Complexes 1- 4

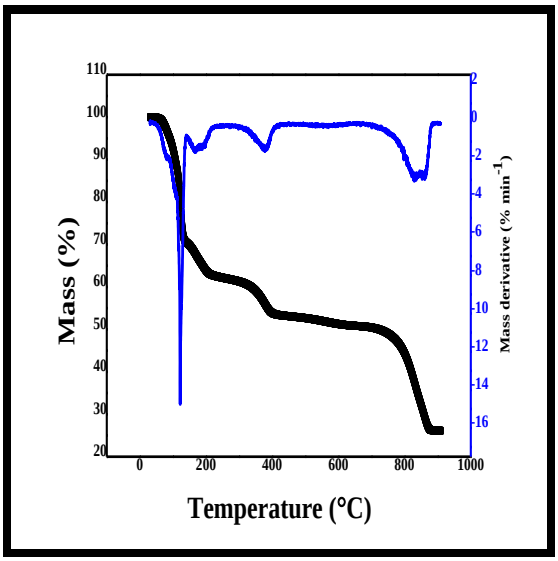

Complex I

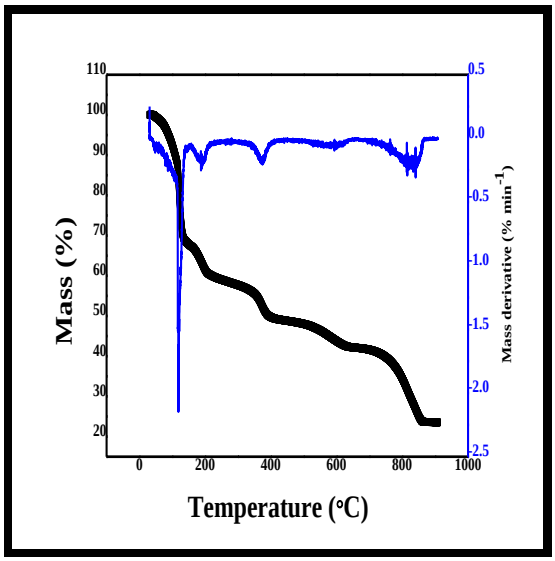

Complex II

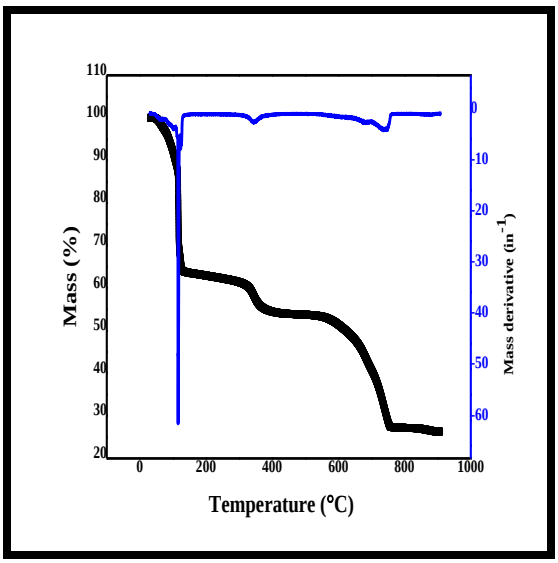

Complex III

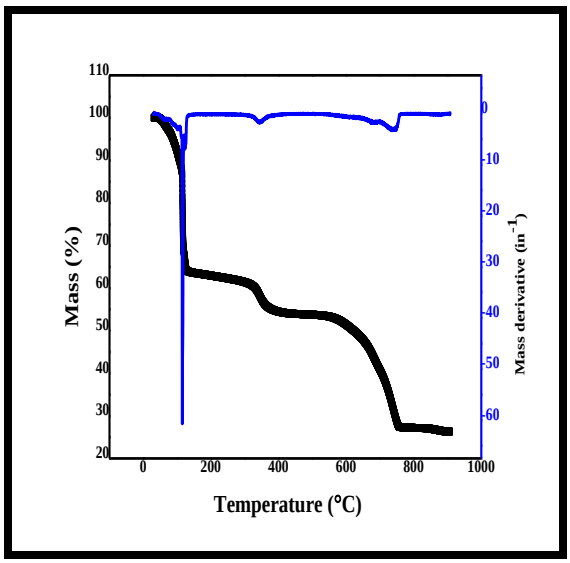

Complex IV

Figure4.26 TGA/DTG curve for complexes I - IV synthesized using Lime Juice

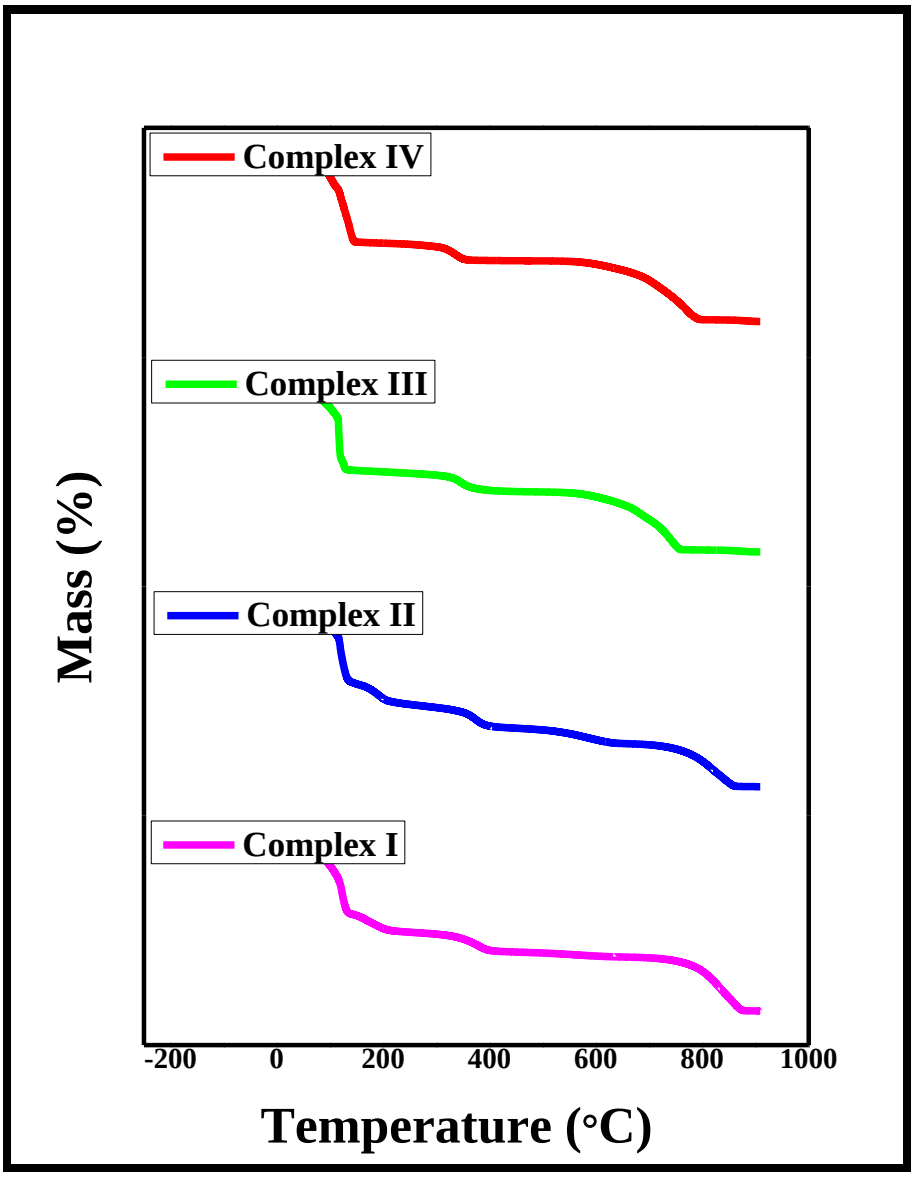

Figure4.27 Thermogravimetric curve in air: combined graph for Complexes I - IV

4.8 Differential Scanning Calorimetry of Multi Metal-Citrate complexes

DSC curve for the samples exhibit a broad endothermic start up hook and sloping base line at the commencement which is primarily based on difference in heat capacity of the sample and the reference. Broad endothermic peak in the beginning refers to dehydration of surface water. No melting peak could be visualized due to dissolution of metal citrate complexes in water of crystallization associated with the samples. A sharp endothermic peak between 100 ºC & 118 ºC followed by an exothermic peak at around 130 ºC are indicative of dehydration involving escape of lattice water followed by precipitation of metals **[29, 30]**. The melting peak for complexes was not observed, which is attributed to dissolution of complex in water of hydration followed by crystallization and precipitate formation which melts at higher range of temperature around 30 350 ºC as reported in literature. DSC curves for complexes **I-IV** have been represented in **Figure 4.28 & Figure 4.29.**

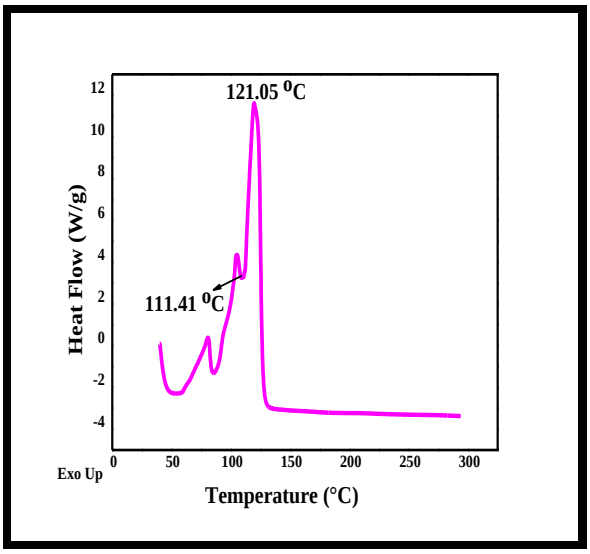

Complex I

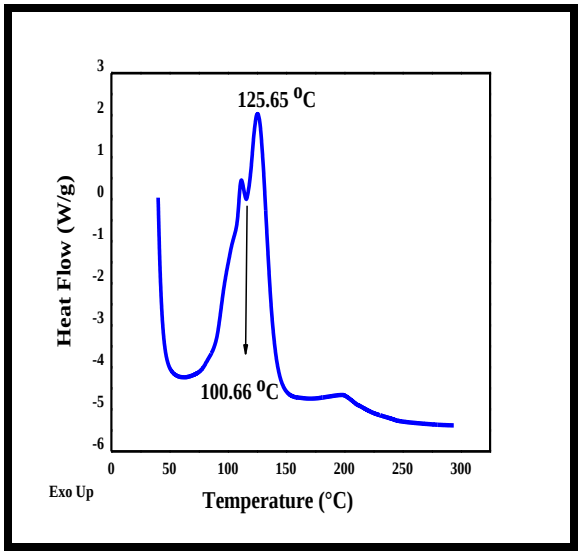

Complex II

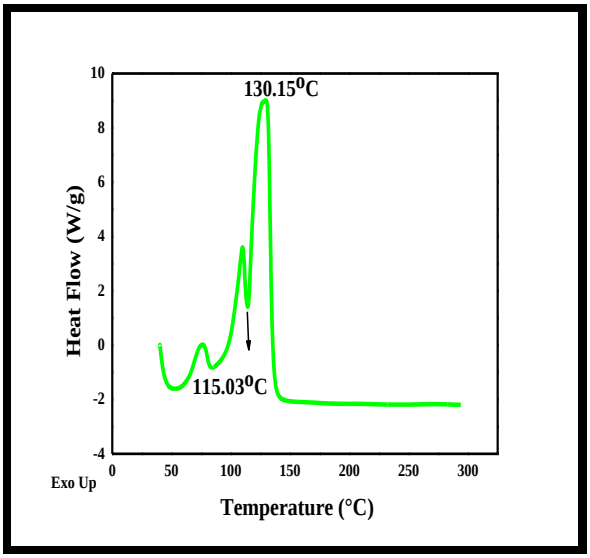

Complex III

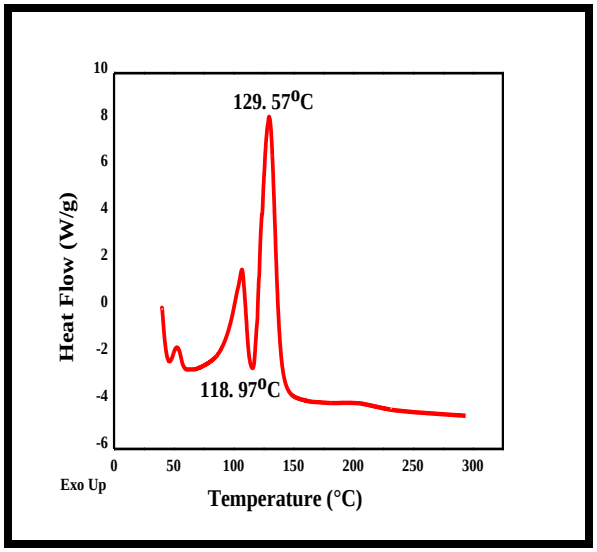

Complex IV

Figure4.28 DSC curve for complexes I - IV synthesized using Lime Juice

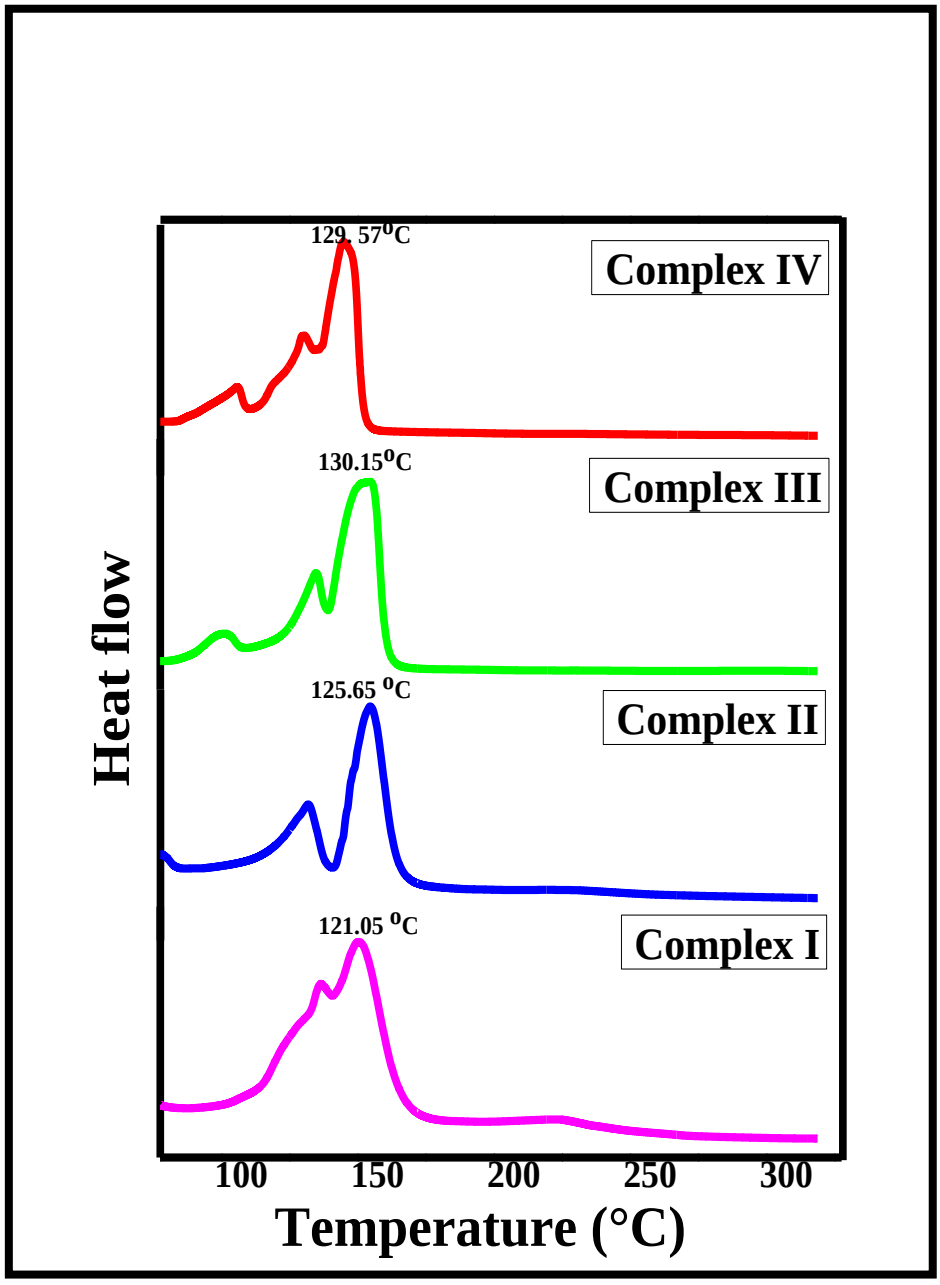

Figure4.29 DSC: combined graph for complexes I - IV

4.9 UV-Vis spectroscopy of Multi Metal-Citrate complexes

UV-Vis Spectroscopy is a powerful tool for characterization of crystals. It is a type of absorption spectroscopy in which a beam of light propagates through a sample which has ability to interact with electromagnetic radiation. When a monochromatic beam of light in Ultraviolet Visible region of electromagnetic spectrum is passed through the material, some of it is absorbed by the material and remaining gets transmitted through the sample. The one absorbed by material causes excitation of outermost electrons of molecule from ground state to higher energy states. As a result of absorption of energy the electrons in sample undergo various transitions. The amount of energy absorbed depends on difference in energy of ground state and higher energy excited state to which electron gets promoted. A typical UV-Vis spectrophotometer generates a spectrum of absorbance against wavelength. The absorbance is generated as a ratio of transmitted light to the incident light represented by the equation **(4)** which is known as Beer-Lambert law.

$$A = log_{10} I_0 / I = \varepsilon c\, l \qquad \textbf{(4)}$$

Where, A = absorbance, I_0 = intensity of light incident upon sample cell, I = intensity of light leaving sample cell, c = molar concentration of solute, l = length of sample cell (cm.), ε = A constant called molar absorptivity or molar extinction coefficient and is a measure of probability of electronic transition.

The extent to which a sample absorbs light depends upon wavelength of light. The wavelength at which a substance shows maximum absorption is designated as absorption maximum or λ_{max} which can be determined by plotting absorbance versus wavelength graph. λ_{max} is very important as it is characteristic for a compound and provides information about electronic structure of material.

UV- Visible spectroscopy is particularly useful for characterization of metal–ligand complexes because of distinct d–d transitions, charge transfer and ligand-based transitions for different metal ions, ligands, and complexes.

If ligand molecular orbital are full of electrons, charge transfer may occur from ligand molecular orbital to empty or partially filled metal d-orbital. These transitions are selection rule allowed, called ligand-to-metal charge-transfer bands (LMCT). In transition metal complexes selection rule allowed charge transfer transitions result in intense colored complexes because of high probability of these transitions **[31]**.

The electronic spectra of multi metal-citrate complexes **1- 4** synthesized using citric acid & complexes **I - IV** synthesized using lime juice were recorded in water at room temperature, are shown in **Figure 4.30 - Figure 4.31** and **Figure 4.32 - Figure 4.33** respectively. All complexes exhibit a high intensity peak in region 392 nm - 385 nm owing to good optical quality of multi metal-citrate crystals. Peak near 390 nm in all complexes is observed due to transfer of charge mainly from oxygen lone pair of carbonyl group of carboxylate ligands belonging to citric acid moiety to metal centre in these complexes **[32]**. The carboxylate ligands being rich in electrons lead to easy charge transfer to partially filled d- orbital's of coordinating metals. Band near 390 nm is distinctly sharp in complexes **1, 2** and **I, II** as ligand-to-metal electronic transitions are localized to single or two atomic centers, particularly in these complexes **[33].** In addition to high energy intense band a very broad and less intense band gets displayed in visible region and beyond in all complexes due to spin allowed d-d transitions of metal ions which remain Laporte - forbidden.

A broad band is observed because numbers of vibrational energy levels are available for electrons to jump. This results in peak broadening. The simultaneous determination of all four metal ions by traditional absorption spectroscopy is difficult because absorption spectra overlap in visible region and superimposed curves are not suitable for quantitative evaluation. Peaks resulting from $n \rightarrow \pi^*$ transitions of >C=O group are not observed as these are shifted to shorter wavelengths (blue shift) because of increased solvation of lone pairs of oxygen, in ground state by polar solvent water which lowers energy of n orbital. As >C=O group participates in the hydrogen bond formation with water of crystallization present in the complex as proto acceptor, shows blue shift owing to hydrogen bonding **[34, 35]**.

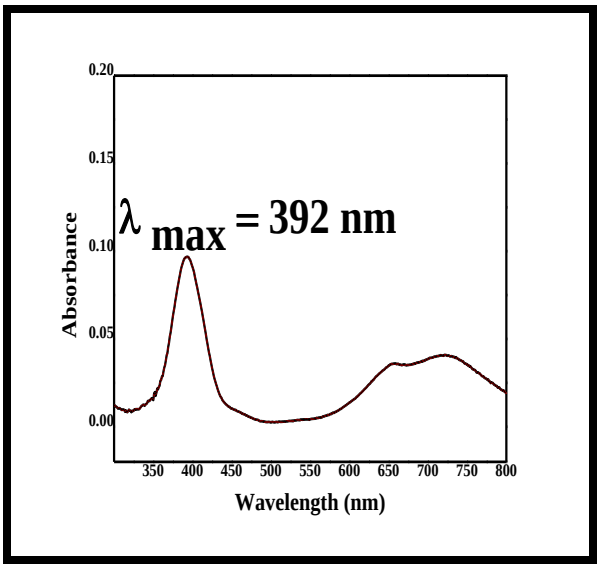

Complex 1

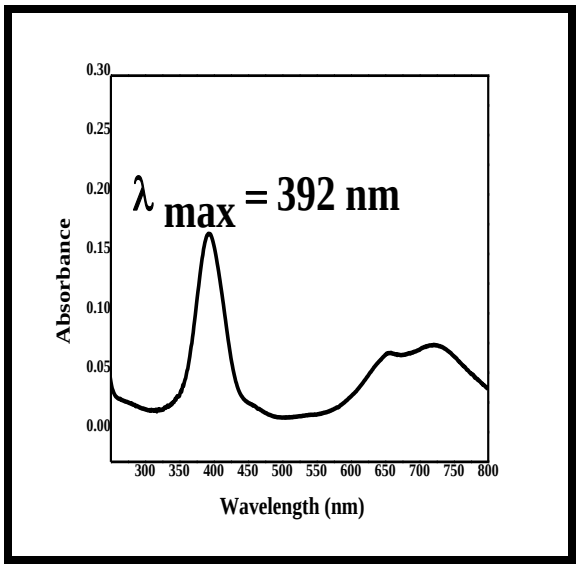

Complex 2

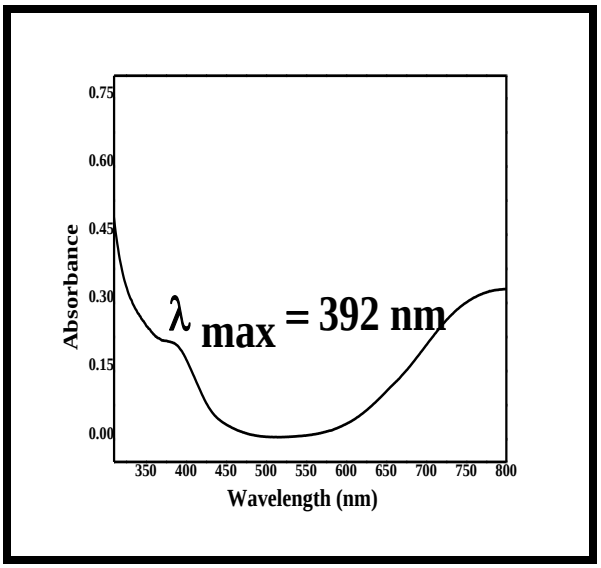

Complex 3

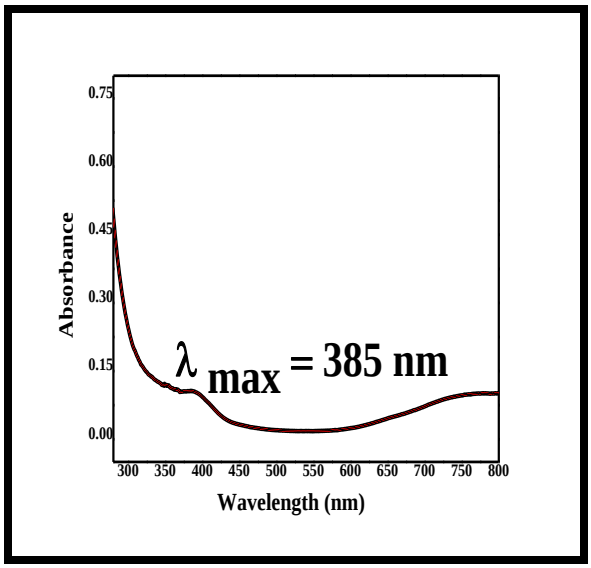

Complex 4

Figure4.30 UV-VIS spectroscopy of Complex 1-4 synthesized using Citric Acid

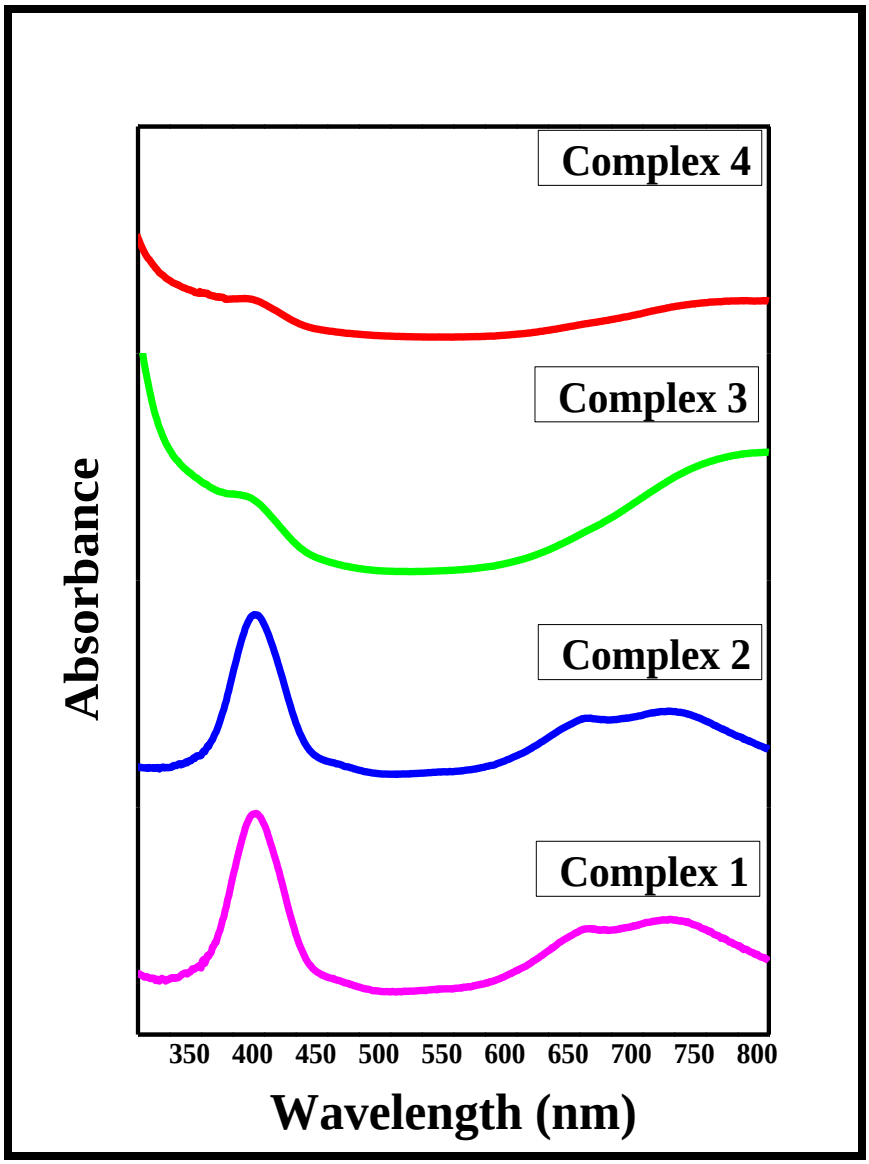

Figure4.31 UV-VIS spectroscopy: combined graph for Complexes 1- 4

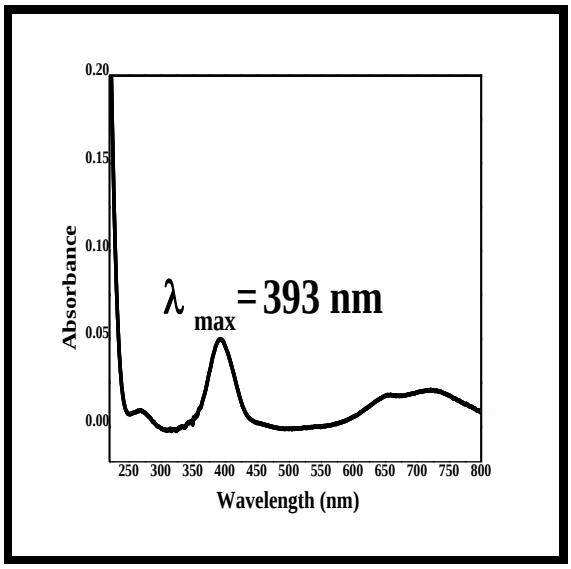

Complex I

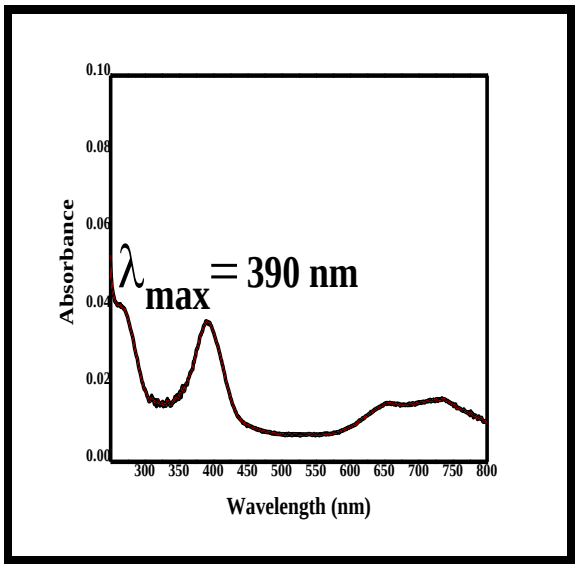

Complex II

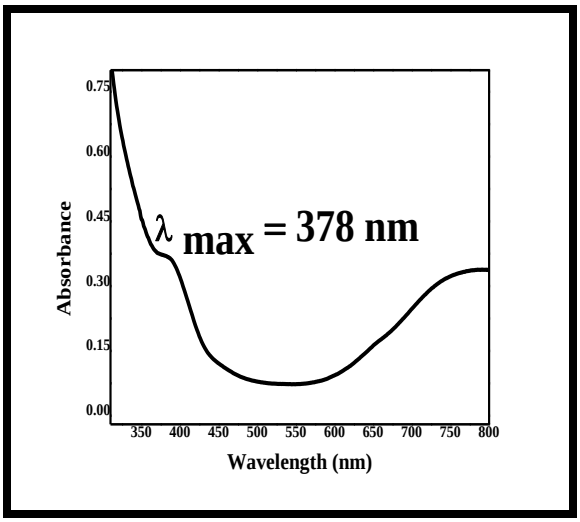

Complex III

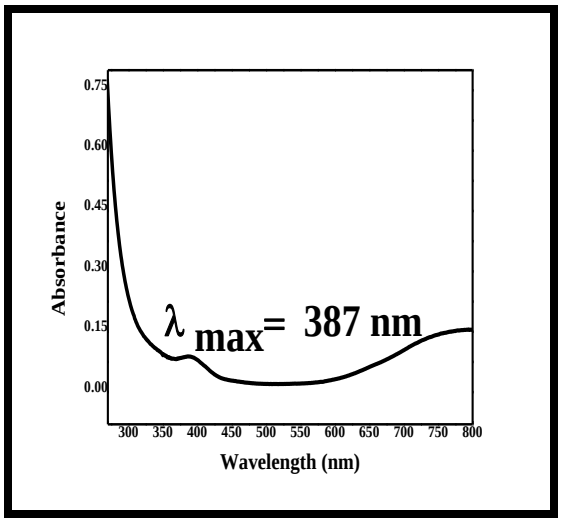

Complex IV

Figure4.32 UV-VIS spectroscopy of Complex I - IV synthesized using Lime Juice

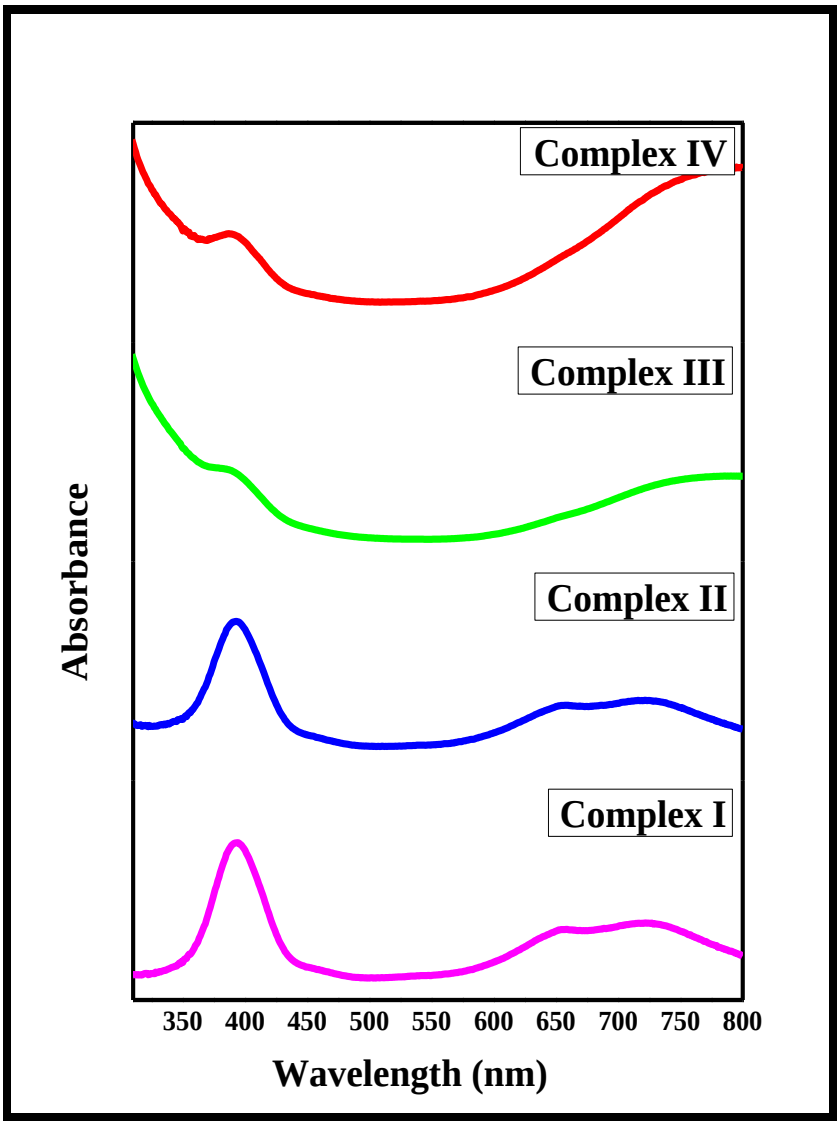

Figure4.33 UV-VIS spectroscopy: combined graph for Complex I - IV

4.10 Multi Metal-Citrate complexes as Photo luminescent materials

Many of transition metal complexes are colored & colors are determined by electronic structure of complex. When irradiated with UV radiations, the Multi metal-citrate complexes reveal luminescence. Photo luminescent properties of complexes may be exploited for their optical & electronics applications. Enhancement of fluorescence of ligands upon complexation with metal ions is of great interest as it discloses an opportunity for a variety of photochemical applications **[36]**. Upon complexation with ligand, the luminescent properties of Cu^{2+} & Zn^{2+} ions get enhanced due to their ability to bind strongly to ligands & show strong UV absorption **[37].**

The excitation spectra of multi metal-citrate complexes were analyzed in the range from 350 nm - 700 nm to observe transfer of electrons among 3d orbital's of metals. Each complex shows one absorption band at 392 nm. Emission spectra were recorded for **I - IV** upon excitation at 310 nm and emission was observed in between 400 nm - 422 nm, that indicates promotion of electrons to d orbital of metal having lowest energy **[38]**. All complexes except complex **II** exhibit intense fluorescence emission with maxima at 347 nm due to coordination effects of citrate ligand to Zinc(II) ions involving charge transfer caused by antenna effect of citrate ligand and ligand-to-metal intra molecular photo induced energy transfer process **[39]**. A similar narrow comparatively less intense peak observed in complex **II** is due to optical excitation caused by spin flip intra configurational transition taking place in unpaired electrons of Fe **[40]**. Ultraviolet photoluminescence spectroscopy of multi metal-citrate complexes display a wide emission behavior in the range 350 nm - 520 nm due to characteristic d-d transitions of transition metal ions with emission in blue region. These materials thus have potential as hybrid-inorganic-organic emitting materials for electroluminescent devices and may play a significant role in flat panel display applications **[41]**.

Intense luminescence in complexes is observed due to the phenomenon involving capture of UV radiation by citrate linker and passing it on to the metal ions coordinated to the citrate ligand **[42]**. Photoluminescence graphs of Complexes **I - IV** are depicted in **Figure 4.34 & Figure 4.35.**

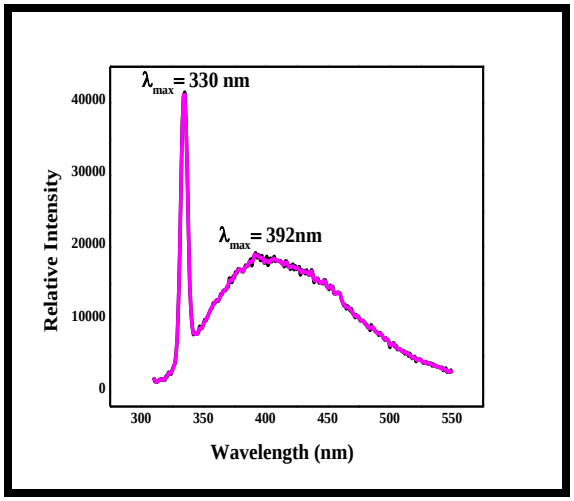

Complex I

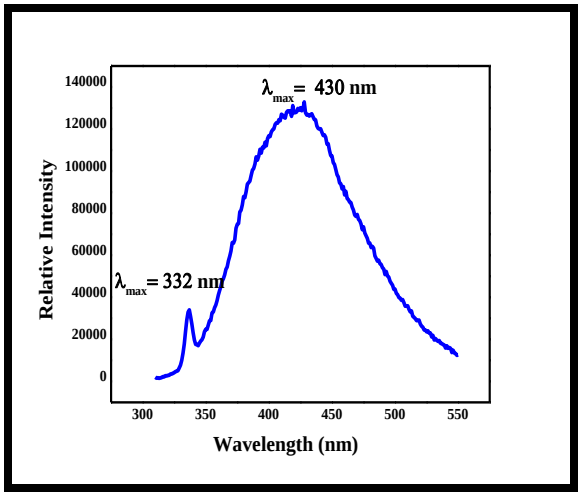

Complex II

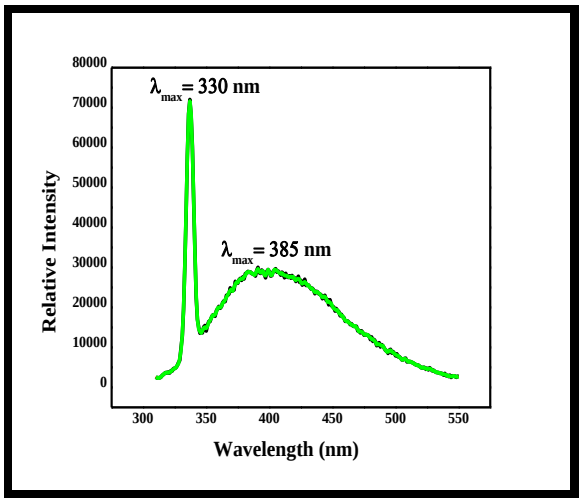

Complex III

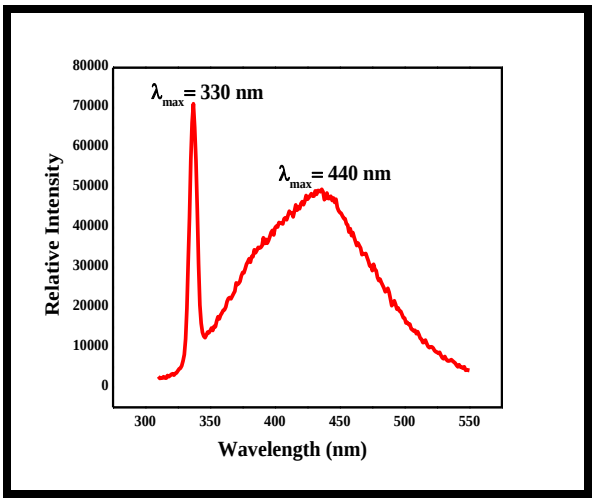

Complex IV

Figure4.34 Photoluminescence graph of Complex I - IV synthesized using Lime juice

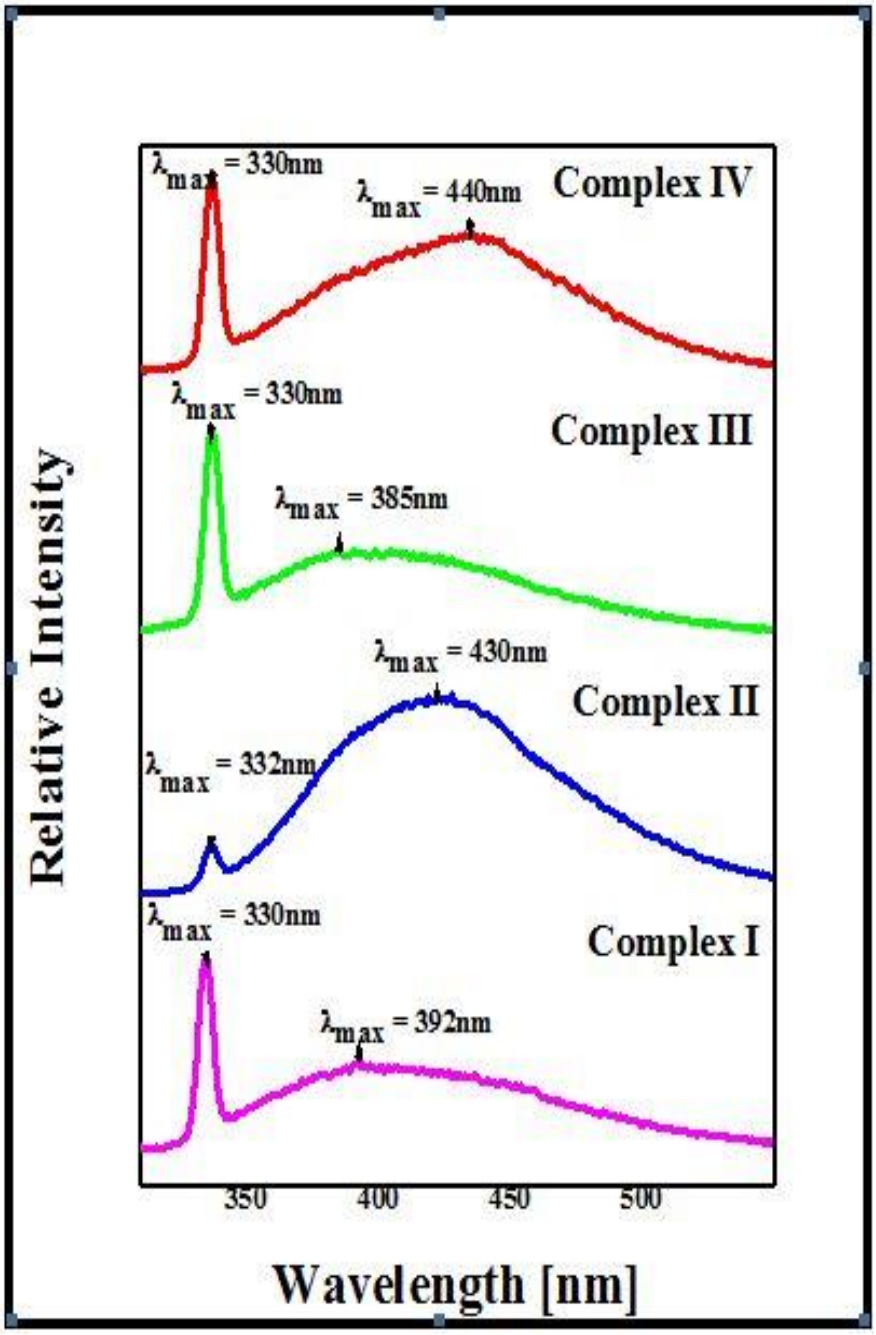

Figure4.35 Photoluminescence: combined graph for Complex I - IV (λex= 310 nm)

4.11 Multi Metal-Citrate complexes for storage and separation of gases

4.11.1 BET Surface area of Multi Metal-Citrate complexes

Threatening level of polluting gases in the Atmosphere caused by automobile exhaust arouse interest of scientific community in use of an alternative fuel for mobile applications. Hydrogen due to its clean combustion, easy availability from water and high mass energy density may serve as future generation fuel for vehicular applications once problems concerning its safe and efficient storage are overcome **[43]**. Low cost, light weight Metal-organic framework material which can efficiently store hydrogen in a reversible manner under ambient conditions may prove to be a magical tool to control carbon emission and further degradation of environment **[44].** Hydrogen gas may bind to a surface either by physisorption through weaker interactive forces or by chemisorptions involving true chemical linkages. Physisorption of a gas on surface of a solid material is directly related to its surface area. Surface area is one of most important characteristic of porous material for adsorption of gases. Specific surface area of a material can be determined by BET method by measuring the physisorption of adsorbate gas on the surface of solid adsorbent **[45]**. BET theory is based on multimolecular layer adsorption of adsorbate on to the surface of an adsorbent, an infinite number of layers can build up on adsorbent and Langmuir model is applicable to all such layers. Metal-organic frameworks are novel materials known to exhibit large BET surface area.

BET theory can be represented by the equation **(5)**:

$$\frac{p}{v(p_o - p)} = \frac{1}{v_m C} + \frac{C-1}{v_m C}\frac{p}{p_o} \qquad \textbf{(5)}$$

Where p = equilibrium pressure of absorbate gas, p_o = saturation pressure of adsorbate gas, v = volume of gas adsorbed, v_m = Volume of adsorbate gas forming complete monolayer on surface of adsorbent.

C = BET constant representing extent of interaction between adsorbate and adsorbent surface. Equation **6** represents expression for constant C.

$$C \approx e^{\left(\frac{E1-E2}{RT}\right)} \quad \textbf{(6)}$$

E_1 = Enthalpy for adsorption of first layer, E_2 = Enthalpy of adsorption of second layer.

A plot of $\frac{p}{v(p_o-p)}$ versus $\frac{p}{p_o}$ gives a straight line whose intercept is $\frac{1}{v_m C}$ and slope $\frac{C-1}{v_m C}$.

Constants V_m & C can be evaluated from slope & intercept of adsorption isotherm respectively.

Nitrogen adsorption technique has been used in to determine surface area of multi metal-citrate complexes synthesized by using citric acid as well as using lime juice. **Figure 4.36** represents Adsorption-desorption isotherm for multi metal-citrate complexes. Multi metal-citrate complexes exhibit Type V adsorption isotherm which explains multimolecular layers formation on the surface. **Table XIX- XXII** depicts BET N_2 adsorption data for multi metal-citrate complexes **1 - 4**. BET plot for complexes **1 - 4** are presented in **Figure 4.37 – Figure 4.40.** The quantity of gas adsorbed by a solid depends on equilibrium pressure of gas, temperature and nature of adsorbate-adsorbent interaction. Constant C is related to affinity of solid with adsorbate and thus to heat of adsorption: $C_{(BET)} < 20$ & $C_{(BET)} > 100$ represent low & high interaction strength respectively **[46]**. Despite low value of specific surface area, multi metal-citrate complexes exhibit high values of C, which indicates strong adsorbate-adsorbent interaction due to open metal sites and active functionalities at the surface. BET equation is generally used to give an apparent surface area related to adsorption capacity of solid.

But if material contains micro pores, value of S_{BET} has no physical meaning because no pure multilayer adsorption of nitrogen is ensured. Hudec *et al.* has demonstrated that value of C-constant in classical BET-isotherm is very sensitive even with very small content of microporous materials in mesoporous matrix.

Pure zeolites exhibit negative values of C_{BET} constant **[47]**. The isotherms obtained for microporous materials are composite.

Rouquerol *et al.* have examined the suitability of this method through comparison of surface area of microporous materials and mesoporous materials **[48]**.

De Lange *et al.* have reported that these methods may yield highly inaccurate results as N_2 might had adsorbed earlier at lower pressure **[49]**. Therefore there is significant deviation between BET surface areas and nitrogen accessible surface areas when there are both Mesopores and large micro pores in a given pore structure as demonstrated in present research **[50]**. Low value of surface area may be attributed to the fact that chain-based MOFs generally exhibit one dimensional channel that lead to low surface areas and reduced micro pore volumes despite exhibiting a relatively high adsorption enthalpy **[51]**.

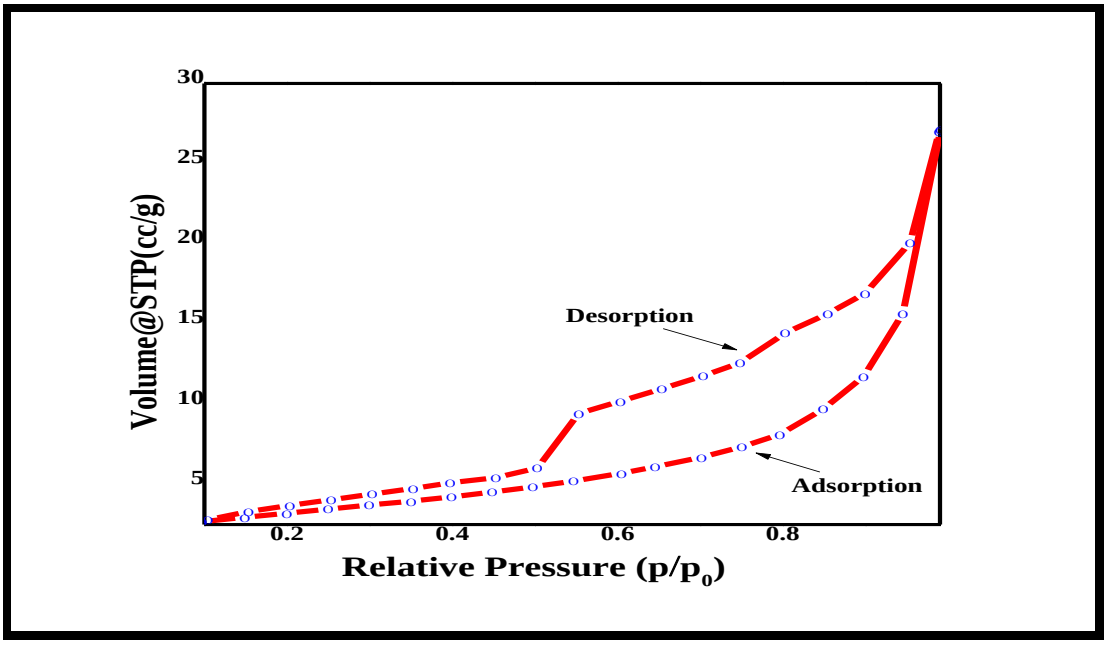

Figure4.36 Nitrogen Adsorption-desorption isotherm for Multi Metal-Citrate Complexes

Table 19 Multi-Point BET Data for Complex 1 synthesized using Citric Acid

Relative Pressure [P/Po]	Volume at STP / [cc/g]	1 / [W((Po/P) - 1)]
5.26510e-02	3.6658	1.2131e+01
8.06059e-02	3.8783	1.8087e+01
1.05772e-01	4.0673	2.3269e+01
1.54545e-01	4.3787	3.3402e+01
2.04665e-01	4.6797	4.3998e+01
2.54434e-01	5.0137	5.4461e+01
3.04526e-01	5.3360	6.5658e+01

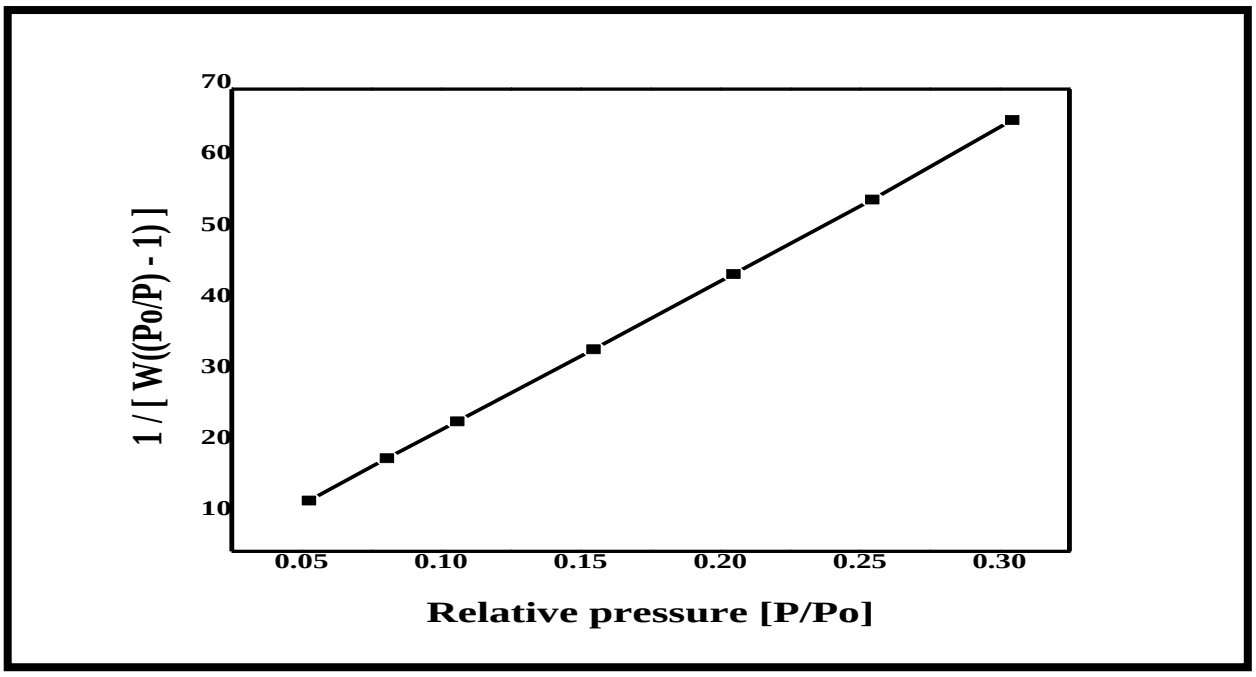

Figure4.37 BET plot for Multi Metal-Citrate complex 1 synthesized using Citric Acid

Table 20 Multi-Point BET Data for Complex 2 synthesized using Citric Acid

Relative Pressure [P/Po]	Volume at STP [cc/g]	1 / [W((Po/P) - 1)]
4.88780e-02	2.8582	1.4386e+01
8.11299e-02	3.1683	2.2298e+01
1.06398e-01	3.3522	2.8419e+01
1.55774e-01	3.6641	4.0293e+01
2.05861e-01	3.9489	5.2524e+01
2.55999e-01	4.2097	6.5398e+01
3.05969e-01	4.4809	7.8721e+01

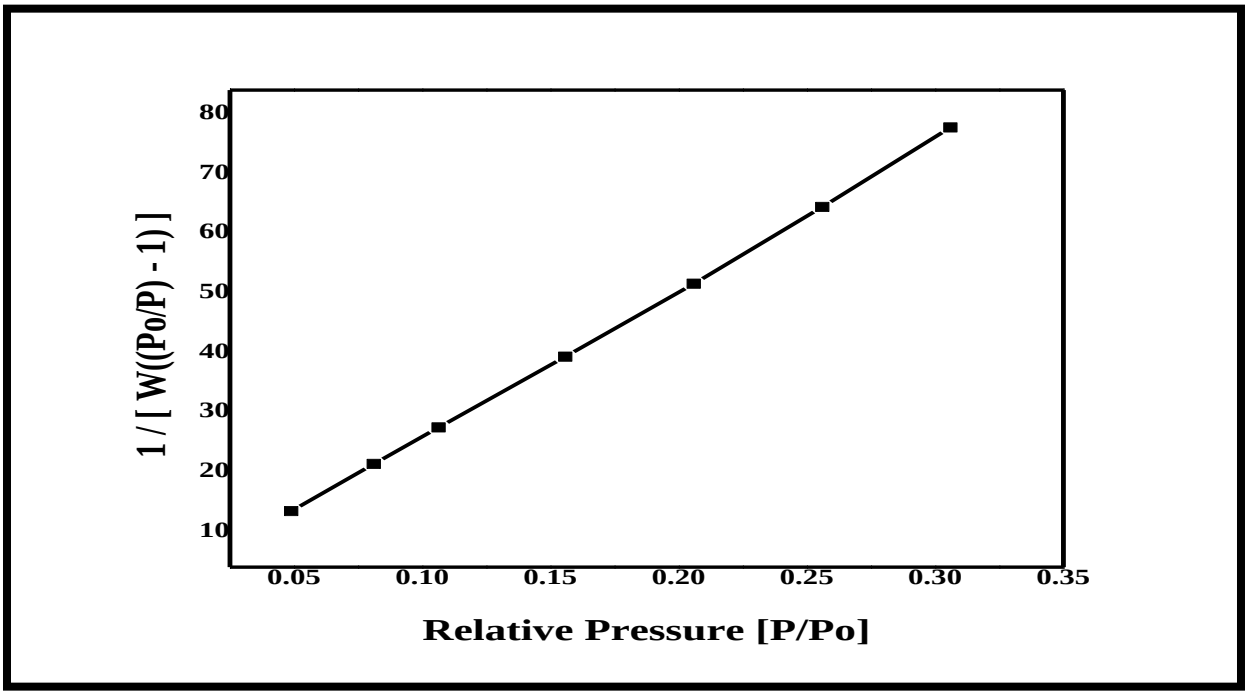

Figure4.38 BET plot for Multi Metal-Citrate complex 2 synthesized using Citric Acid

Table 21 Multi-Point BET Data for Complex 3 synthesized using Citric Acid

Relative Pressure [P/Po]	Volume at STP [cc/g]	1 / [W((Po/P) - 1)]
5.14878e-02	1.7276	2.5141e+01
8.13782e-02	1.8874	3.7554e+01
1.06486e-01	1.9786	4.8193e+01
1.56036e-01	2.1222	6.9705e+01
2.06015e-01	2.2397	9.2695e+01
2.56114e-01	2.3250	1.1848e+02
3.06374e-01	2.4157	1.4630e+02

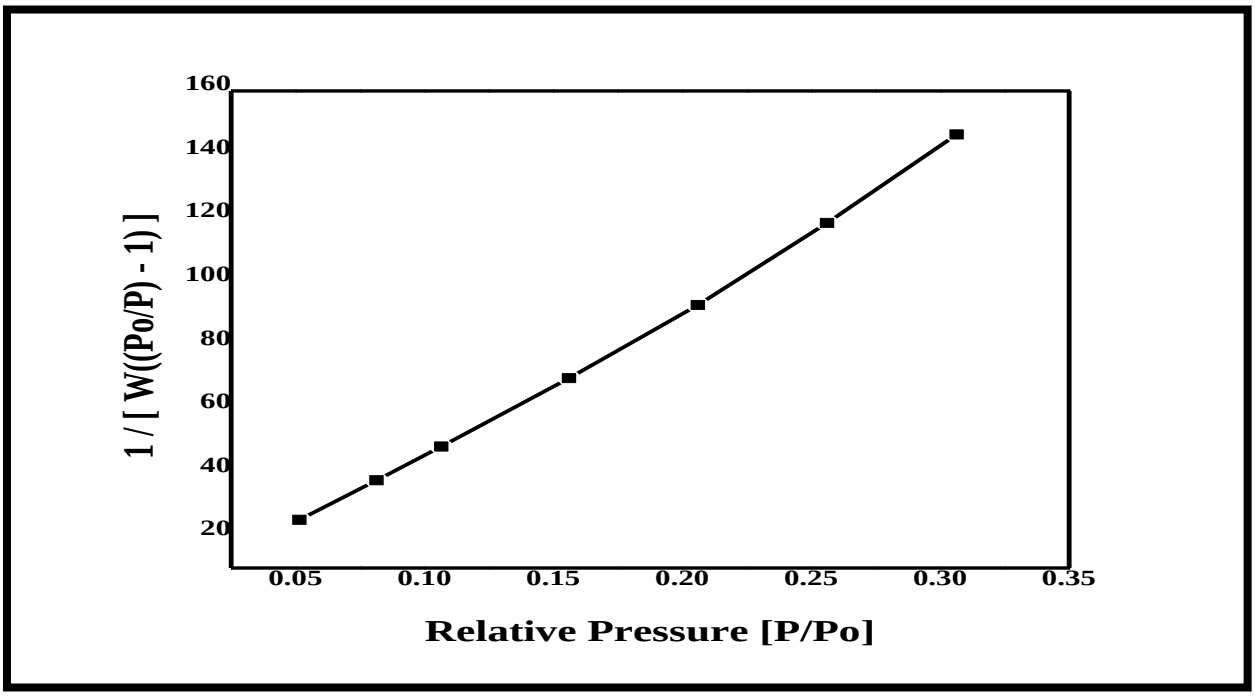

Figure4.39 BET plot for Multi Metal-Citrate complex 3 synthesized using Citric Acid

Table 22 Multi-Point BET Data for Complex 4 synthesized using Citric Acid

Relative Pressure [P/Po]	Volume at STP [cc/g]	1 / [W((Po/P) - 1)]
5.07289e-02	1.1713	3.6504e+01
8.12591e-02	1.3295	5.3229e+01
1.06691e-01	1.4394	6.6391e+01
1.55769e-01	1.6128	9.1539e+01
2.05868e-01	1.7649	1.1753e+02
2.55838e-01	1.9145	1.4368e+02
3.05774e-01	2.0586	1.7119e+02

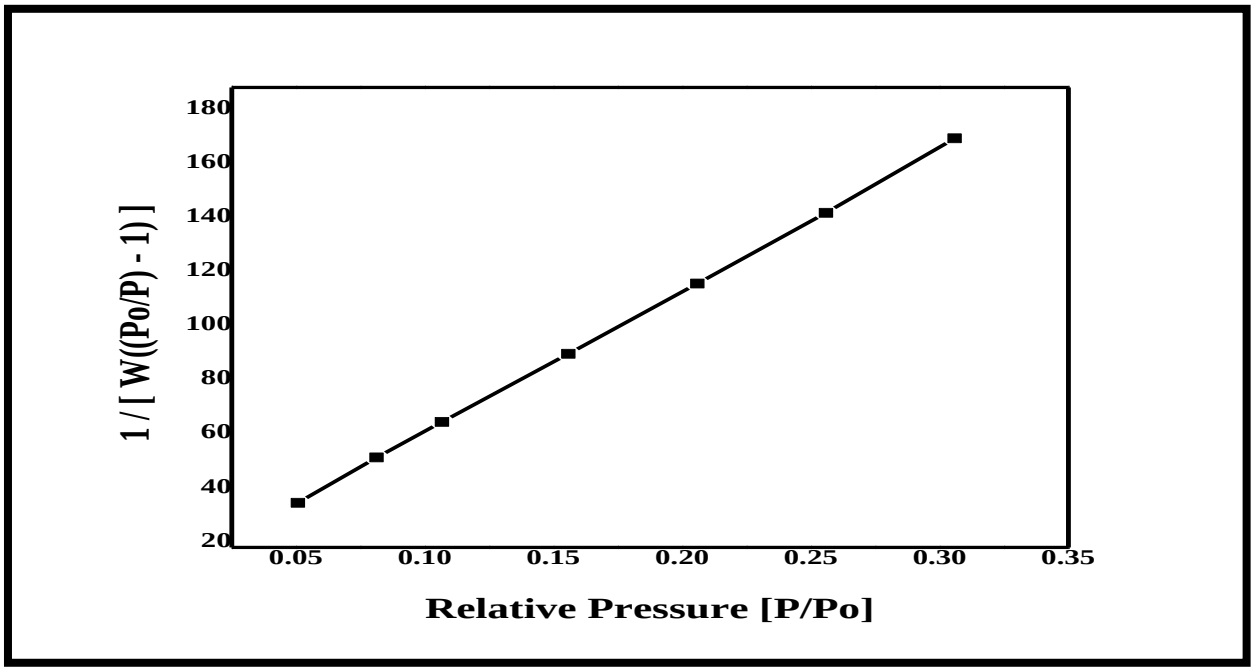

Figure4.40 BET plot for Multi Metal-Citrate complex 4 synthesized using Citric Acid

4.11.2 Pore volume & pore size distribution in Multi Metal-Citrate complexes

BJH method (Barrett, Joyner and Halenda method introduced in 1951) was employed to examine pore size of complexes synthesized through green synthetic pathways **[52]**. This method is based on assumptions that; a pore contains a surface on which gas molecules can adsorb and adsorbed molecules undergo condensation to fill the interior radius of the pore. At a given relative pressure amount of gas adsorbed includes adsorbate gas condensed in all pores and adsorbed on interior walls of pores **[53]. Table XXIII** depicts the pore size, total pore volume and corresponding surface area of multi metal-citrate complex **1**. The complex exhibits a surface area 50.967 m^2/g with pore volume 0.106 cc/g and pore diameter 3.855 nm measured upon desorption of N_2. **Figure 4.41** & **Figure 4.42** represent volume histogram & area histogram for data obtained from Density Functional Theory model applied to physical adsorption of nitrogen. BJH pore diameter & pore volume values confirmed that complex **2 - 4** contain Cu–O & Fe–O which are non-porous materials and explains their low surface area, whereas complex **1**, a mesoporous material has relatively higher values of surface area. Such mesoporous materials having narrow distribution of pore size, having high stability are widely used as electro catalyst support, electrode in electric double layer capacitors (EDLC) and as an ultra capacitor. Extra large pore size in these complexes may be attributed to various metal ions coordinated to citrate ligands in different modes, hydrogen interactions involving hydroxyl group and water molecules forming a network of hydrogen bonds between the layers. Consequently large number of oxygen atoms constitutes the circumference of the pore and result in large size of pores suitable for capture of bigger molecules **[54]**. Because of their biocompatibility & non toxicity these Mesoporous materials are ideal for diagnostics applications due to increased image contrast & chemical stability. As most biological molecules & pharmaceuticals are of order of a few nanometers, synthesized multi metal-citrate complexes may be used for encapsulation of pharmaceutical drugs, proteins & other biological molecules.

Table 23 Nitrogen adsorption data for Multi Metal-Citrate complex 1 synthesized using Citric Acid

Pore width / nm	Pore Volume / cc g^{-1}	Surface Area / cc g^{-1}
5.00 - 9.00	3.2190e-02	1.8355e+01
9.00 - 13.00	1.6306e-02	4.8990e+00
13.00 - 17.00	6.9849e-03	1.2751e+00
17.00 - 21.00	5.9539e-03	7.8170e-01
21.00 - 25.00	4.3580e-03	4.5507e-01
25.00 - 29.00	2.7355e-03	2.3469e-01
29.00 - 33.00	1.8328e-03	1.3194e-01

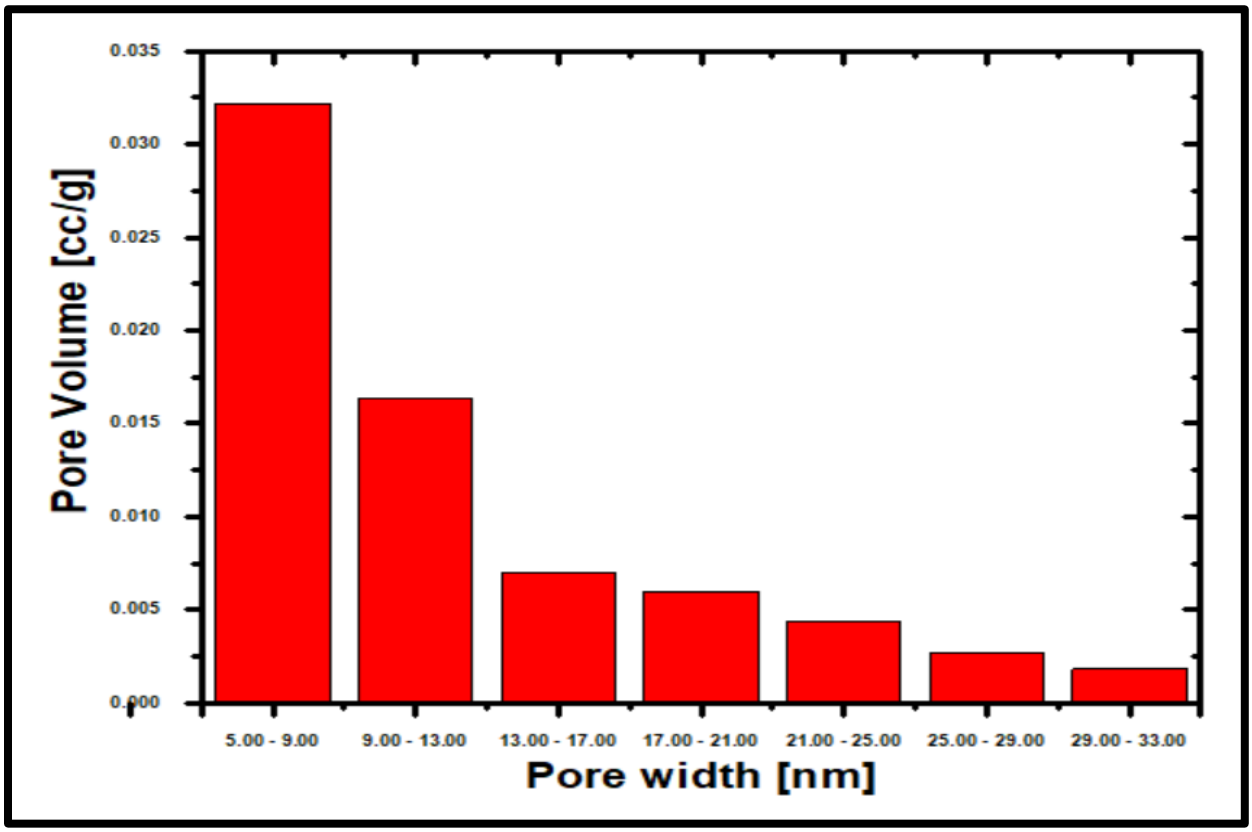

Figure4.41 Volume Histogram; data based on Density Functional Theory

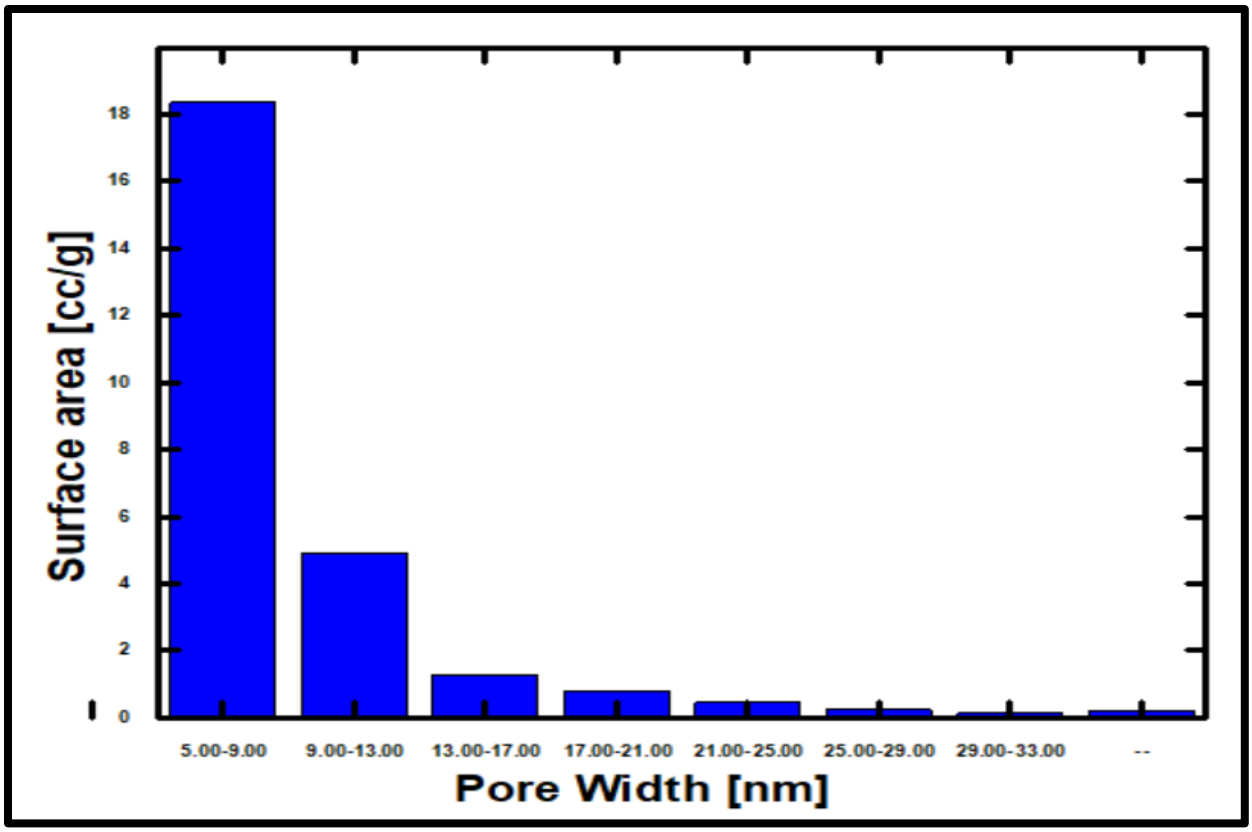

Figure4.42 Area Histogram; data based on Density Functional Theory

4.11.3 Multi Metal-Citrate complexes for separation of CO_2/CH_4

CO_2 gas produced as a result of combustion of carbon fuels is the major cause of green house effect. Most commonly employed methods for separation of CO_2/CH_4 mixture include zeolites and expensive carbon adsorbents. The multi metal-citrate complexes are Mesoporous materials with large pore diameter (≈ 4 nm) & pore volume **Figure 4.43**. These complexes may thus serve as strong candidate for CO_2 /CH_4 separation. Pore size plays an important role in concluding gas adsorption and gas separation properties of materials.

CO_2 has effective diameter of the order of 0.33 nm while CH_4 molecule has about 0.38 nm, thus it becomes impossible for microporous materials to capture and hold methane molecules in their porous structure through the adsorption process.

Mesoporous materials (pore size 2 - 50 nm) show great prospective in separation of CO_2/CH_4 gaseous mixture under high pressure. Methane molecules adsorption is strongly affected by surface area and pore volume as compared to adsorption of carbon dioxide molecules. Adsorption capacity of materials strongly depends on pore structure at elevated pressure than at atmospheric pressure **[55]**.

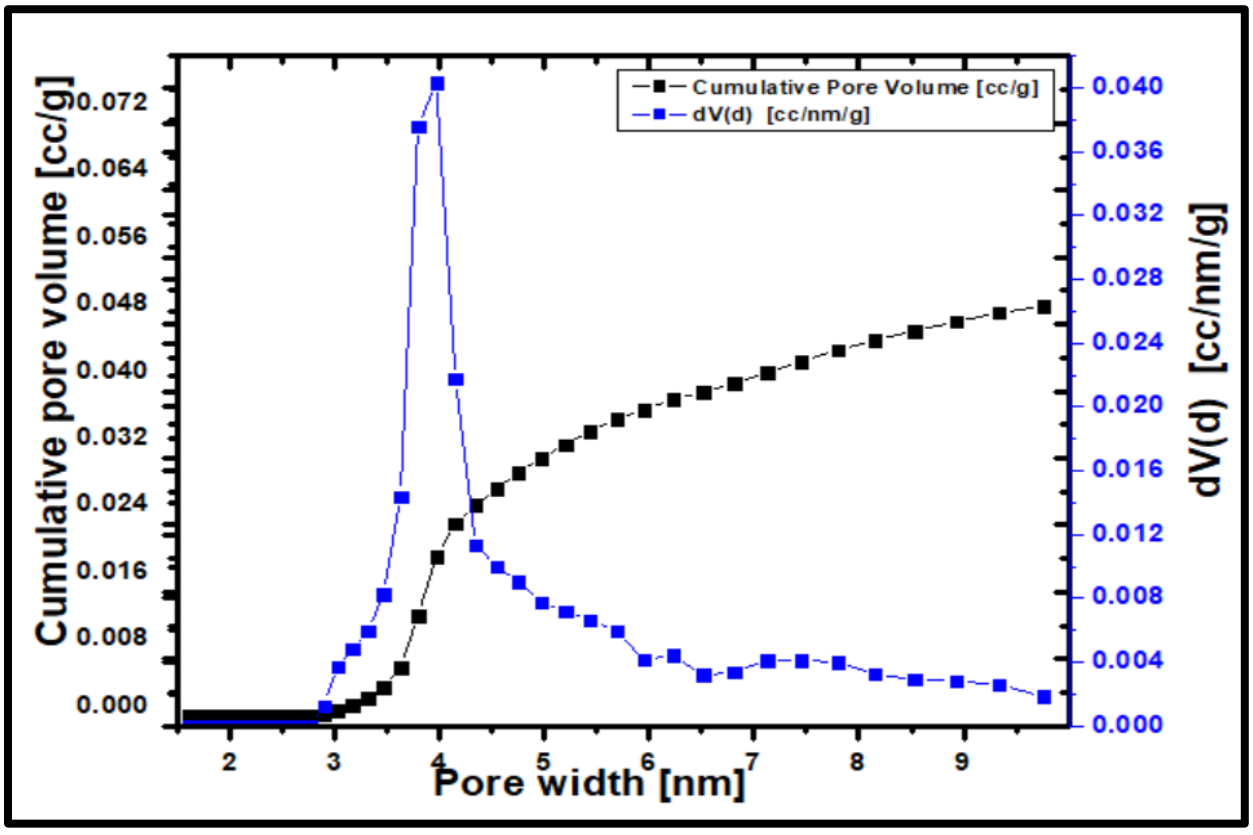

Figure4.43 Pore size distribution graph: data derived from Density Functional Theory

4.12 Mesoporous Multi-Metal Citrates as Scavengers for Organic Dyes

Adsorption-desorption N_2 isotherm for Multi Metal-Citrate complexes exhibit hysteresis loop due to capillary condensation, characteristic of mesoporous materials. These mesoporous materials have narrow pore size distribution & high stability. Large pore size in these complexes attributed to mixed-metal ion coordination and terminal hydroxyl groups. Extra-large pores of these materials can be exploited in utilization of these materials for specific applications where microporous materials become unsuitable.

Multi metal-citrate complexes exhibit adsorption affinity for large molecules of dyes. Activated crystals when soaked in solutions of Eriochrome Black T (EBT, pH ≈ 7), Indigo blue dye (In B, pH ≈ 11) and Methyl orange dye (MO, pH ≈ 5), result in adsorption of dye molecules. **Figure 4.44** depicts structures of organic dyes namely Methyl Orange, Eriochrome Black T & Indigo Blue dyes for which complexes display high affinity. Adsorption of anionic azo dyes; MO & EBT can be attributed to electrostatic & hydrogen bond interactions between adsorbent & dye molecules. At lower pH, surface of adsorbent is positively charged due to protonation & strong electrostatic interactions exist between adsorbent surface & anionic dye molecules. In case of In B, di-ionic form exists in equilibrium with mono-ionic form in alkaline region (pH ≈ 11) and undergoes extensive hydrogen bonding with adsorbent surface. Color change of crystals was uniform and clearly observed with naked eyes (**Figure 4.45**). Uniform distribution of colors in crystals suggests that dye molecules not only get adsorbed on external surface, but penetrate into large pores and get adsorbed throughout the crystal structure.

UV-Vis spectra of loaded multi metal-citrate complexes reveal absorption peaks corresponding to adsorbed dye molecules by these complexes, which occurs due to $\pi \rightarrow \pi^*$ & $n \rightarrow \pi^*$ transitions usually taking place in visible region **[56].** λ_{max} at 548 - 530 nm characteristic of bluish violet dyes was observed for In B adsorbed by complexes **[57].**Similar absorption peaks between 520 nm - 500 nm were observed for EBT & MO dyes adsorbed **(Figure 4.46).**

FTIR spectra of crystals loaded with MO & EBT reveal peak at 1639.0 cm^{-1} & 1640.5 cm^{-1} respectively corresponding to N = N stretching vibrations of azo group (**Figure 4.47**). These complexes may replace high cost carbon adsorbents to curb water pollution & resultant toxic, carcinogenic & mutagenic effects of dye stuff on living beings

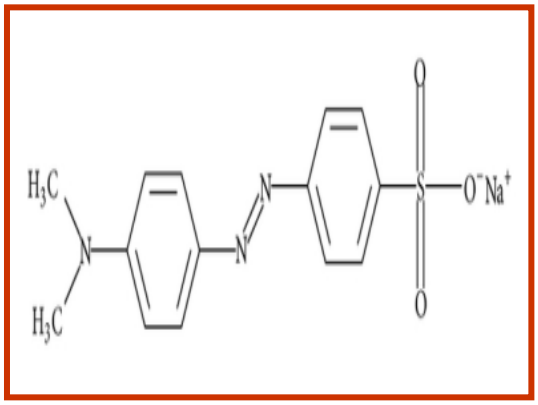

(1)

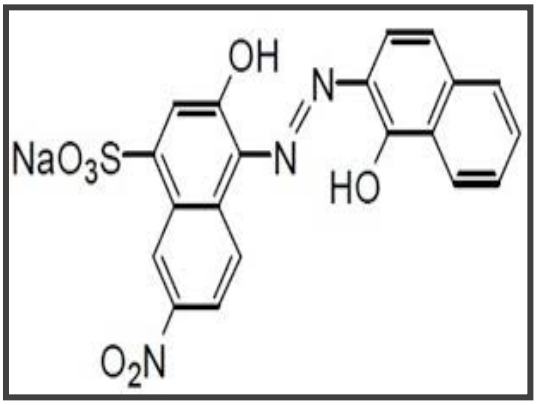

(2)

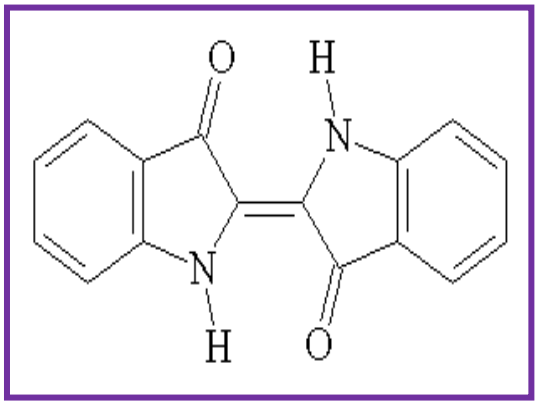

(3)

Figure4.44 Structure of Organic dyes;(1) Methyl Orange (2) Eriochrome Black T (3) Indigo Blue dye

Figure4.45 Adsorption of dyes by Multi-metal citrate complex (1) Crystals as synthesized (2) Activated crystals (3) Adsorption of Eriochrome Black T (4) Adsorption of Indigo Blue dye (5) Adsorption of Methyl Orange dye by activated crystals

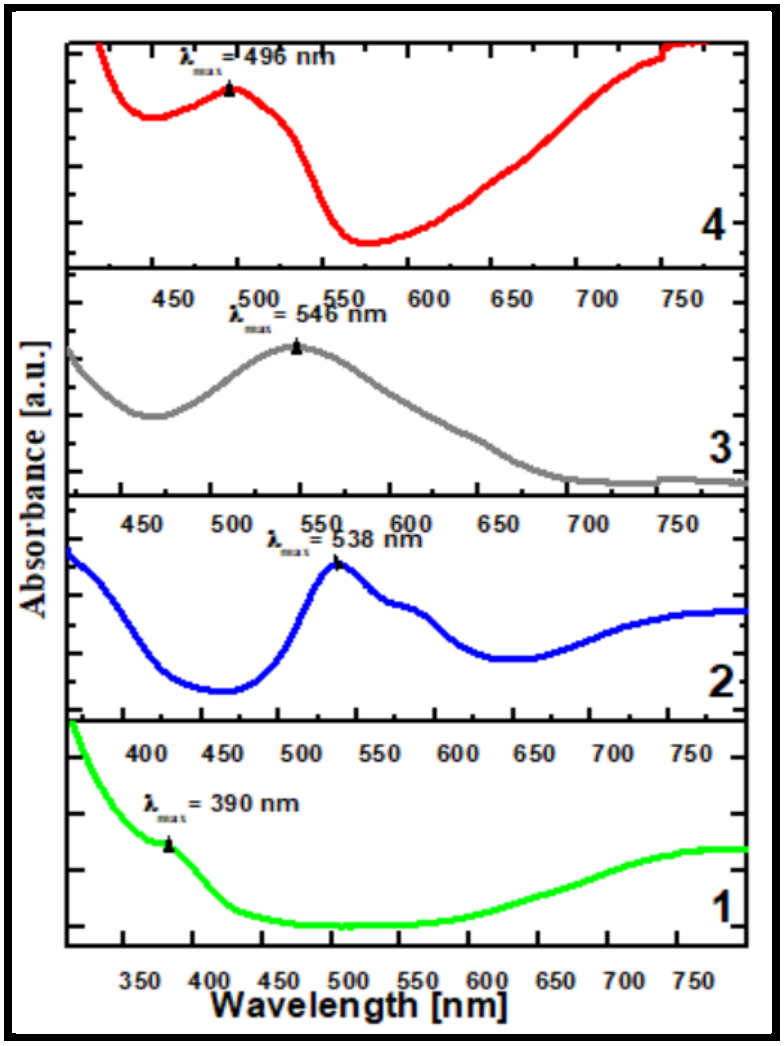

Figure4.46 UV-Vis spectra of (1) Multi metal-Citrate complex (2) Loaded with Indigo blue dye (3) Loaded with Methyl orange dye (4) Loaded with Eriochrome black T dye

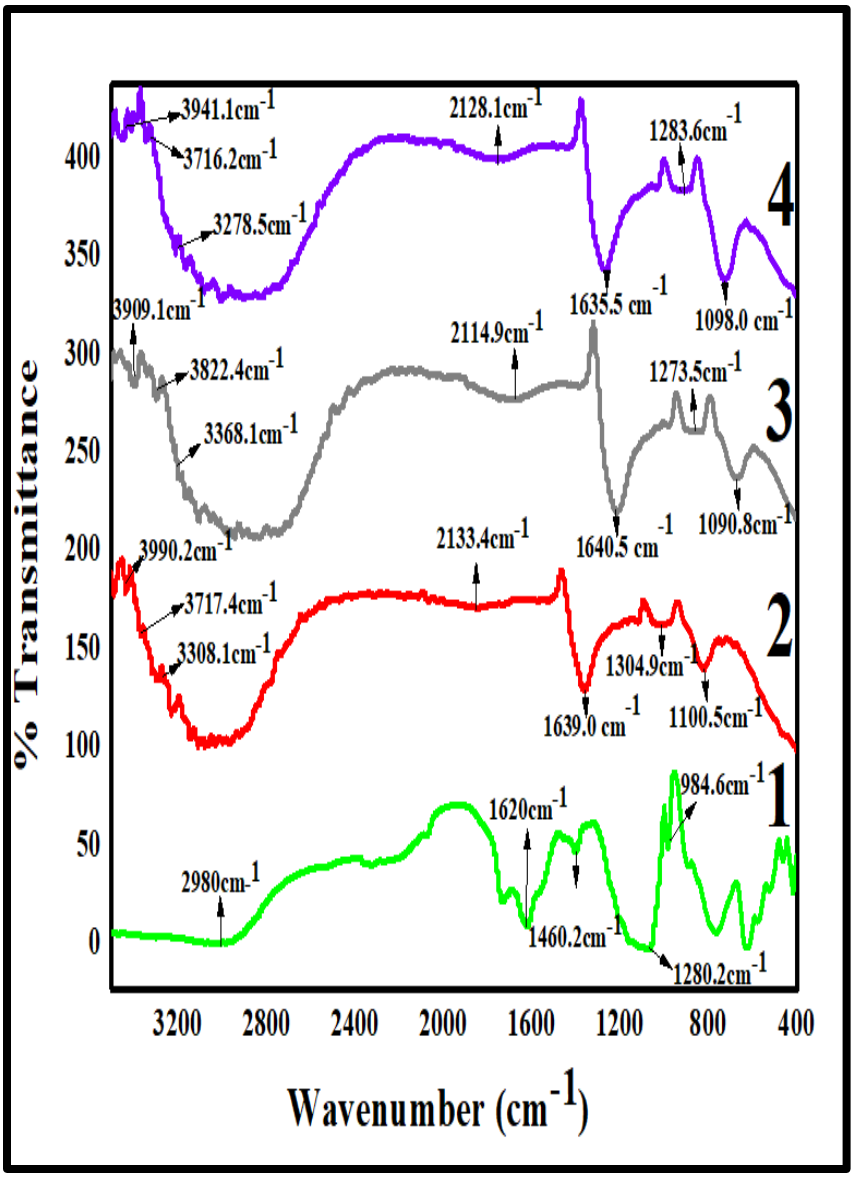

Figure4.47 FTIR spectra of (1) Multi Metal-Citrate complex (2) Loaded with Methyl Orange dye (3) Loaded with Eriochrome Black T dye (4) Loaded with Indigo Blue dye

The efficiency of multi metal-citrate complexes for removal of Eriochrome black T, an azo dye has been examined quantitatively by UV-Vis spectrophotometer. Dye samples of concentration ranging from 20 - 60 mg L^{-1} were prepared separately and adsorbed on fixed weight of activated complex 4, synthesized using citric acid. The percent efficiency for dye removal by the complex was calculated using initial dye concentration and after adsorption by complex 4. UV-Vis spectra were recorded before and after adsorption of dye by complex **(Figure 4.48 & Figure 4.49).** The measured absorbance was converted to concentration by using equation **4**. Percent removal of Eriochrome black T by Multi metal-citrate complex **4** has been depicted in **Table XXIV.**

Table 24 Removal of EBT Dye by Multi metal-citrate complex 4

S. No	Initial Dye concentration Mol L^{-1}	Final Dye Concentration Mol L^{-1}	Percent dye removal
1	1.300×10^{-4}	0.217×10^{-4}	83.30
2	1.084×10^{-4}	0.240×10^{-4}	77.86
3	0.867×10^{-4}	0.217×10^{-4}	74.97
4	0.650×10^{-4}	0.163×10^{-4}	74.92
5	0.433×10^{-4}	0.193×10^{-4}	55.42

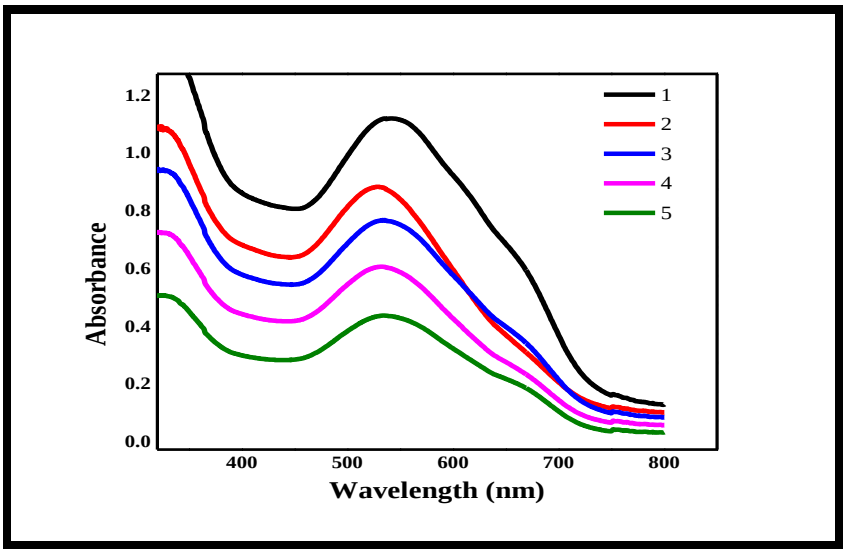

Figure 4.48 UV-Vis graph at different concentrations of EBT Dye (1) 0.060 g L^{-1}(2) 0.050 g L^{-1}(3) 0.040 g L^{-1}(4)0.030 g L^{-1}(5) 0.020 g L^{-1}

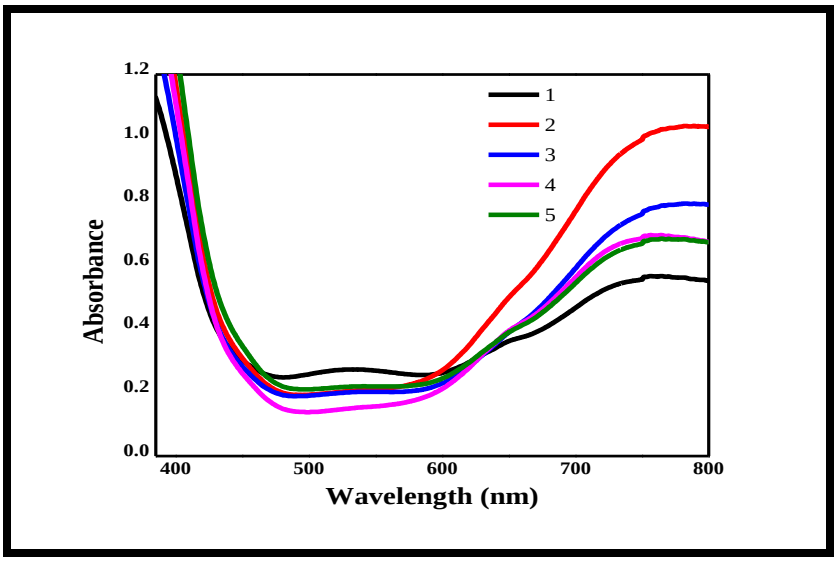

Figure 4.49 UV-Vis graph for different concentrations of EBT Dye after adsorption by Multi-metal citrate complex 4: (1) 0.060 g L^{-1} (2) 0.050 g L^{-1} (3) 0.040 g L^{-1} (4) 0.030 g L^{-1} (5) 0.020 g L^{-1}

4.13 Porous Multi Metal-Citrates for sensing & recognition of ions in Industrial effluent water

Some of transition metal cations such as mercury (II) & lead (II) are highly toxic for living beings and a serious threat to the environment. Anions like CrO_4^{2-} and $Cr_2O_7^{2-}$ can cause crucial gene mutations, deformity and life threatening diseases like cancer **[58].**

Metal-organic frameworks due to their porous nature, presence of active metal sites & hydrogen bonding interactions function as host for a variety of guest molecules. Molecules entrapped in voids of synthesized materials may induce two visible changes either by alteration of emission spectrum or change of fluorescence intensity. Luminescence enhancement is termed "turn-on" and luminescence quenching is known as "turn off" **[59]**. A major portion of MOFs for sensing &detection of analyte make use of “turn off” mechanism by quenching fluorescence of parent MOF by guest ion. Whereas “turn on” mechanism involving luminescence enhancement or shift of emission peaks which enable quick conspicuous color change visible to naked eye & exhibit better selectivity based on host-guest chemistry **[60, 61].** Luminescent MOFs can selectively detect molecules/ ions of various sizes due to adjustable porosity in their structures.

Real time detection / sensing of toxic cations & anions present even in trace amount through a straight forward technique is much desired. Though luminescent properties of MOFs have widely been exploited, yet controlling their size & morphology with desired optical properties is still a challenge. Multi metal-Citrates due to their porous nature, active metal sites & hydrogen bonding interactions serve as host for a variety of guest ions.

Multi metal-Citrates serve as promising luminescent probe for sensing & recognition of NH_4^+, $Fe(CN)_6^{4-}$, I^- by “turn on” mechanism and CrO_4^{2-} & $Cr_2O_7^{2-}$ ions by “turn off” mechanism **(Figure 4.50)**. Present technique is decorated with features of being a simple & straight forward method involving conspicuous visual display of color change upon introduction of guest ions in their framework **(Figure 4.51)**. They exhibit high sensitivity with regard to iodide ions.

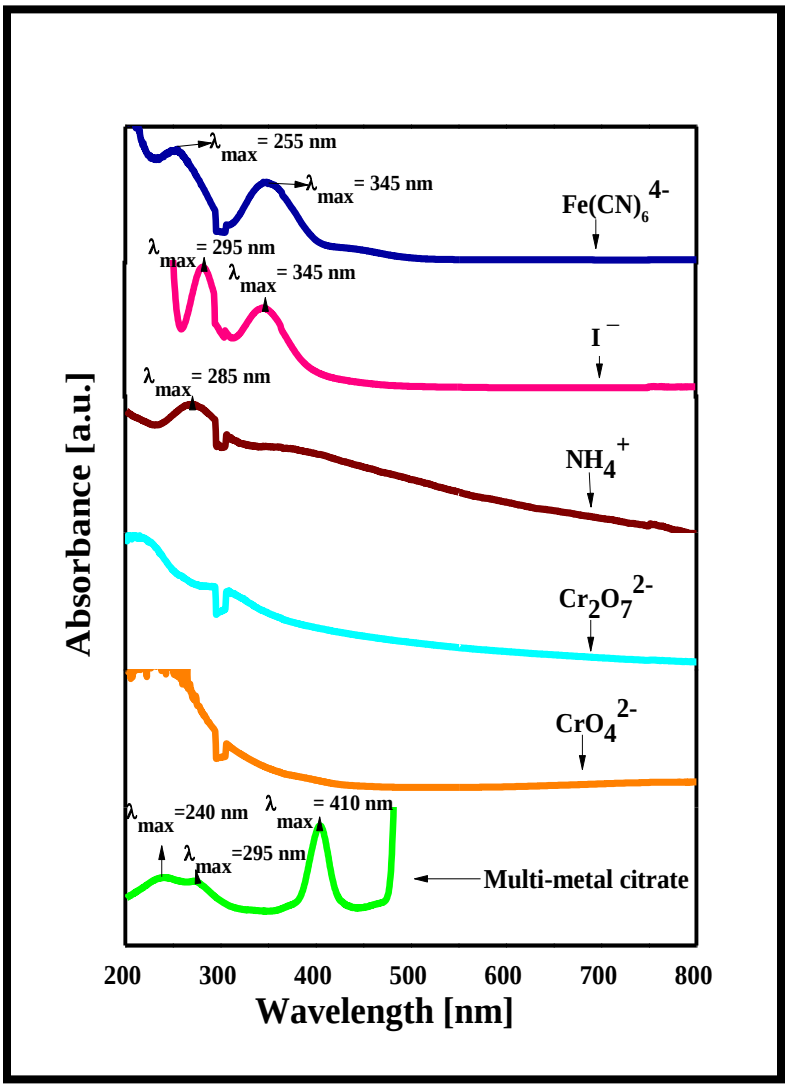

Figure 4.50 UV-Vis graph for Luminescent Multi Metal-Citrates

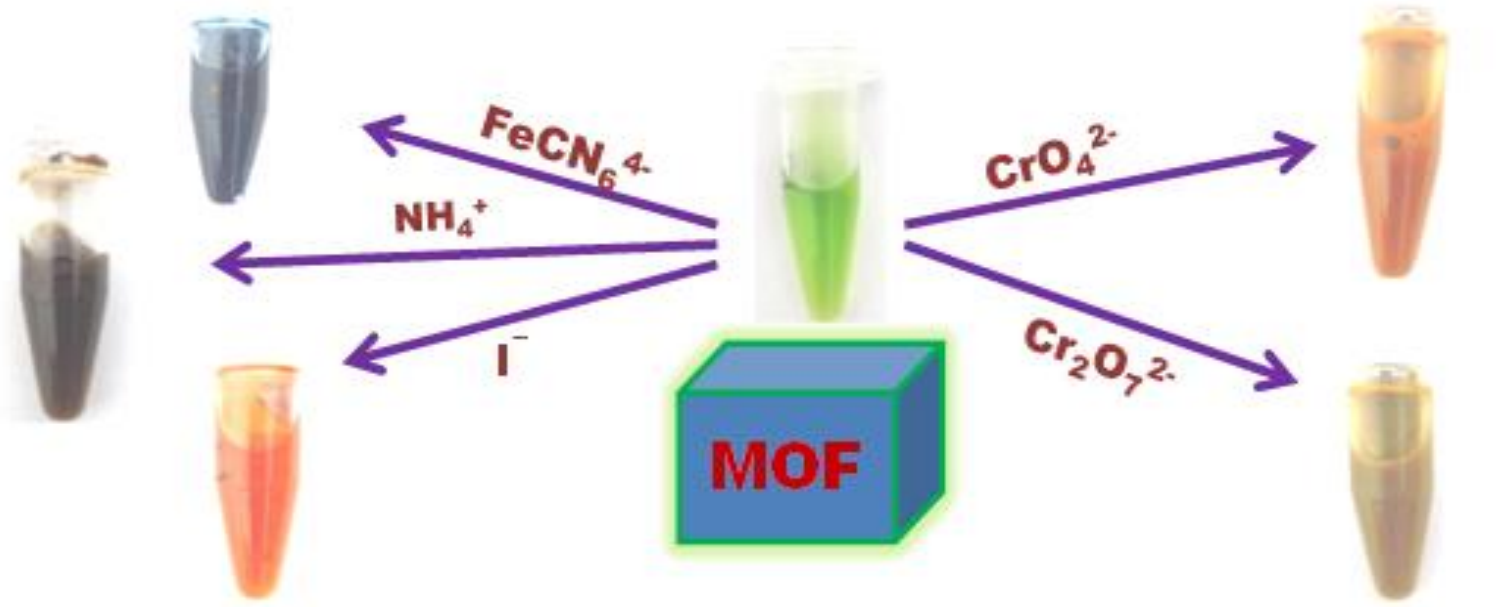

Figure4.48 Conspicuous visual display of color change upon introduction of guest species in Multi Metal-Citrates

4.14 Mixed-metal oxides customized from Multi Metal-Citrates and their applications

Magnetic materials find a host of applications in fields like electromagnetism, electronic and medical appliances, magnetic sweepers, credit cards, conveyer belts *etc*. The porous nature of multi metal-citrate complexes synthesized in present research due to their magnetic properties could find various applications in porous molecular magnets **[62]**. The multi metal-citrate complex **4** and **IV** when heated to 300 ºC yield copper doped nickel-zinc-ferrite like materials and Complex **2** and II on strong heating yield nickel doped Zinc oxide as revealed by their Fourier transform Infrared spectroscopy **(Figure 4.52)**. ZnO is a very versatile and important semiconducting oxide due to its piezoelectric and transparent conducting properties. It exhibits many potential applications in various fields such as laser diodes, solar cells, gas sensors, optoelectronic devices and photo catalysts **[63 - 66].**

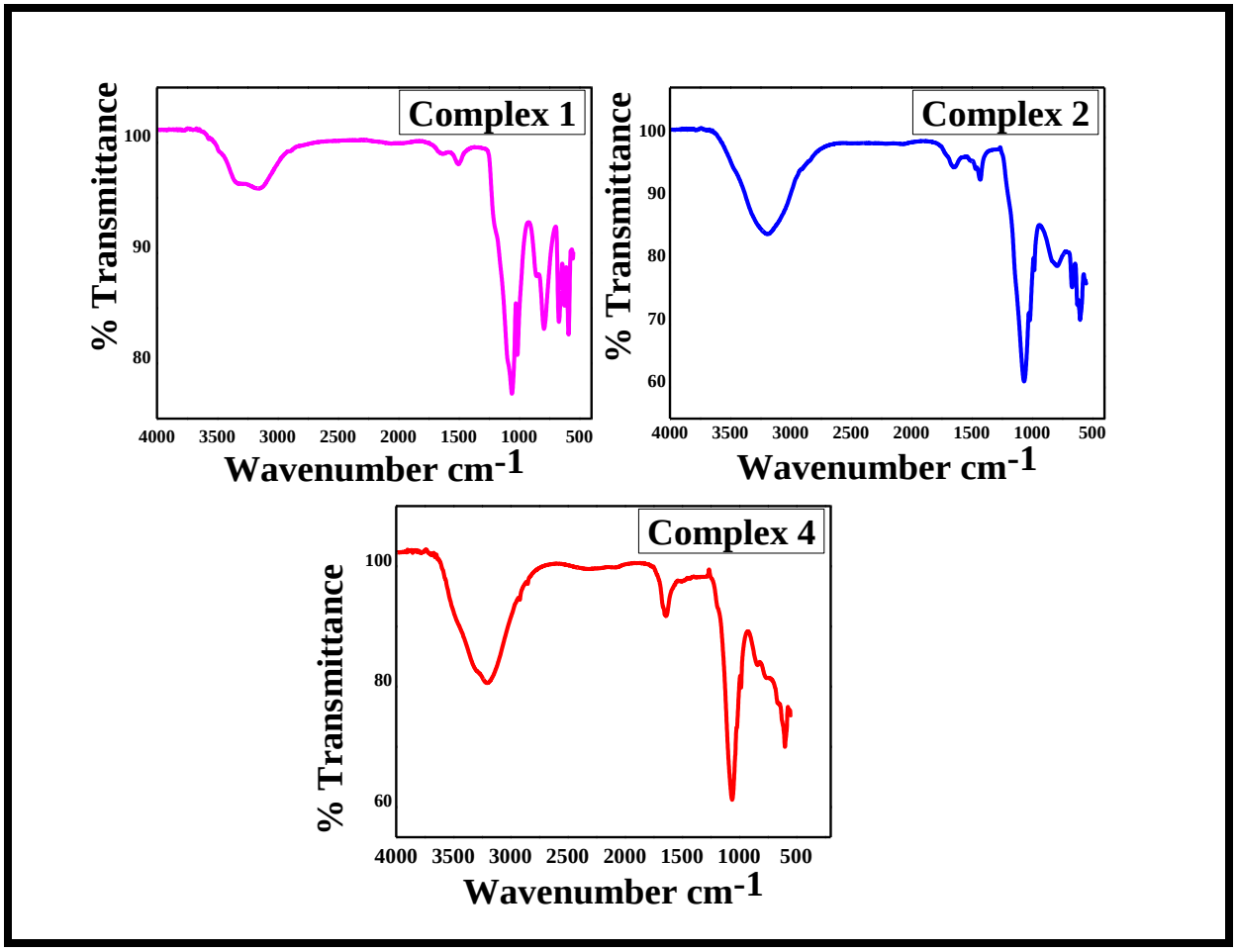

Figure 4.52 FTIR spectra for mixed metal oxides obtained from Multi Metal-Citrates

4.15 Mesoporous Multi Metal-Citrate complexes for Bio medical Applications

The mesoporous Copper, Iron, Nickel & Zinc multi metal-citrate complexes with different combinations of metal ions and citric acid linker, owing to their non toxicity may prove ideal for diagnostics applications due to increased image contrast. Most biological molecules and pharmaceuticals are of order of a few nanometers, thus synthesized complexes may be used for encapsulation of pharmaceutical drugs, proteins and other biological molecules **[67]**. Such mesoporous materials are widely used as electro catalyst support, electrode in electric double layer capacitors (EDLC) and ultra capacitor **[68 - 70]**.

REFERENCES

1. J. Lewis, R. G. Wilkins (Eds.), Modern coordination chemistry, Interscience Publishers, New York **1960**.

2. G. B. Deacon, R. J. Phillips, Relationships between the carbon-oxygen stretching frequencies of carboxylate complexes and the type of carboxylate coordination, *Coord. Chem. Rev*., **1980**, 33, 227-250.

3. K. Nakamoto, Infrared and Raman spectra of inorganic and coordination compounds, Wiley, New York **1978**.

4. Z. Nickolov, G. Georgiev, D. Stoilova, I. Ivanov, Raman and IR study of cobalt acetate dihydrate, *J. Mol. Struct*., **1995**, 354, 119-125.

5. R. C. Mehrotra, R. Bohra, Metal carboxylates, Academic press, New York **1983**.

6. S. M. Tsimbler, L. L. Shevchenko, V. V. Grigoreva, IR absorption spectra of the tartrate and citrate complexes of nickel, cobalt, and iron, *J. Appl. Spectrosc*., **1969**, 11, 1096- 1101.

7. B. Stuart, Infrared spectroscopy, fundamentals and applications, John Wiley & Sons Ltd, United Kingdom **2004**.

8. G. R. Hedwig, J. R. Liddle, R. D. Reeves, Complex formation of nickel (II) ions with citric acid in aqueous solution: a potentiometric and spectroscopic study, *Aust. J. Chem*., **1980**, 33, 1685-1693.

9. O. M. Yaghi, Crystalline metal-organic microporous materials**,** *US Patent No. 5648508 A*, **1997**.

10. K. Nakamoto, Infrared and Raman spectra of inorganic and co-ordination compounds, 4th edition, Wiley-Interscience, New York **1986**.

11. Y. X. Zhang, M. Huang, F. Li, Z. Q. Wen, Controlled synthesis of hierarchical CuO nanostructures for electrochemical capacitor electrodes, *Int. J. Electrochem. Sci.*, **2013**, 8, 8645-8661.

12. R. S. Periathai, K. Rajagopal, FTIR and Raman vibrational investigations on the complex of pyridine with tartaric acid, *IOSR J. App. Physics*, **2014**, 6(4), 09-12.

13. P. Tarakeshwar, S. Manogaran S, Ground state vibrations of citric acid and citrate trianion-an ab initio study, *Spectrochim. Acta Mol. Biomol. Spectrosc.*, **1994**, 50(14), 2327-2343.

14. P. Mani, FTIR, FTR spectra and vibrational analysis of some alicyclic and aromatic compounds, Ph D Thesis, Pondicherry University, Puducherry, India **2002**.

15. D. Mastropaolo, D. A. Powers, J. A. Potenza, H. J. Schugar, Crystal structure and magnetic properties of copper citrate dihydrate, $Cu_2C_6H_4O_7$.cntdot.$2H_2O$, *Inorg. Chem.*, **1976**, 15 (6), 1444-1449.

16. N. Kallay (Ed.), Interfacial Dynamics, Surfactant Science Series V 88 Marcel Dekker Inc, New York **2000**.

17. R. D. Shannon, C. T. Prewitt, Revised values of effective ionic radii, *Acta Cryst.*, **1970**, 26, 1046-1048.

18. B. D. Cullity, Elements of X-ray diffraction, Second Edition, Addison-Wesley Publishing Company Inc., USA **1978**.

19. B. D. Cullity, S. R. Stock, Elements of X-Ray diffraction, 3rd Edition, Prentice Hall, New York **2001**.

20. A. L. Patterson, The Scherrer Formula For X-Ray Particle Size Determination**,** *Phys. Rev.*, **1939,** 56, 978-982**.**

21. F. Liu, J. Wu, K. Chen, D. Xue, Morphology study by using Scanning Electron Microscopy: In Microscopy: Science, Technology, Applications and Education, A. Mendez-Vilas, J. Diaz (Eds.) Microscopy Series No 4, Volume 3, Formatex, Spain **2010**.

22. J. Heath (Ed.), Energy Dispersive Spectroscopy, 2nd Edition, Essential Knowledge Briefings - New Original Science Guides From Wiley, John Wiley & Sons Ltd, USA **2015**.

23. F. C. Miguens, M. L. de Oliveira, R. V. Marins, L. D. de Lacerda, A new protocol to detect light elements in estuarine sediments by X-ray microanalysis (SEM/EDS), *J. Electron Microsc*., **2010**, 59, 437-446.

24. C. Duval, Inorganic thermogravimetric analysis. Elsevier, Amsterdam **1953**.

25. J. Rogan, D. Poleti, Thermal behavior of mixed ligand Co(II), Ni(II) and Cu(II) complexes containing terephthalate ligands, *Thermochim. Acta*, **2004**, 413, 227-234.

26. G. R. Desiraju, The supramolecular concept as a bridge between organic, inorganic and organometallic crystal chemistry, *J. Mol. Struct.*, **1996**, 374, 191-198.

27. B. Mathew, S. Jacob, Thermogravimetric studies of the metal complexes of polystyrene-supported ethanolamine, *Polym. Degrad. Stab*., **1996**, 54, 107-111.

28. P. Duran, F. Cape, D. Gutierrez, J. Tartaj, M. A. Banares, C. Moure, Metal citrate polymerized complex thermal decomposition leading to the synthesis of $BaTiO_3$: effects of the precursor structure on the $BaTiO_3$ formation mechanism, *J. Mater. Chem*, **2001**, 11**,** 1828-1836.

29. L. L. Chaves, L. A. Rolim, M. L. C. M. Goncalves, A. C. C. Vieira, L. D. S. Alves, M. F. R. Soares, J. L. S. Sobrinho, M. C. A. Lima, P. J. Rolim-Neto, Study of stability and drug-excipient compatibility of diethylcarbamazine citrate, *J Therm. Anal. Calorim*., **2013**, 111, 2179-2186.

30. J. Osten, B. Milkereit , C. Schick, O. Kessler, Dissolution and precipitation behavior during continuous heating of Al–Mg–Si alloys in a wide range of heating rates, *Materials*, **2015**, 8, 2830-2848.

31. A. K. Brisdon, Inorganic Spectroscopic Methods, Oxford University Press, UK **1998**.

32. C. E. Housecroft, A. G. Sharpe, Inorganic Chemistry, 3rd edition, Pearson Prentice Hall, United States **2008**.

33. A. K. Zak, R. Razali, W. H. Majid, M. Darroudi, Synthesis and characterization of a narrow size distribution of zinc oxide nanoparticles, *Int. J. Nanomedicine*, **2011**, 6, 1399-1403.

34. S. Nagakura, M. Gouterman, Effect of hydrogen bonding on the near ultraviolet absorption of naphthol, *J. Chem. Phys.*, **1957**, 26, 881-886.

35. G. J. Brealey, M. Kasha, The Role of hydrogen bonding in the $n \rightarrow \pi^*$ blue-shift phenomenon, *J. Am. Chem. Soc.*, **1955**, 77 (17), 4462-4468.

36. N. Chattopadhyay, A. Mallick, S. Sengupta, Photo physical studies of 7-hydroxy-4-methyl-8-(4 -methylpiperazin-1 -yl) methylcoumarin: A new fluorescent chemo sensor for zinc and nickel ions in water, *J. Photochem. Photobiol. A. Chem*., **2006,** 177, 55-60.

37. Z. Onal, H. Zengin, M. Sonmez, Synthesis, characterization, and photoluminescence properties of Cu(II), Co(II), Ni(II), and Zn(II) complexes of N-aminopyrimidine-2-thione, *Turk. J. Chem.*, **2011**, 35, 905-914.

38. S. F. Weng, Y. H. Wang, C. S. Lee, New metal-organic frameworks of [M $(C_6H_5O_7)(C_6H_6O_7)(C_6H_7O_7)(H_2O)]$. H_2O (M = La, Ce) and $[Ce_2 (C_2O_4)(C_6H_6O_7)_2]$. $4H_2O$, *J. Solid State Chem*., **2012**, 188, 77-83.

39. G. H. Wang, Z. G. Li, H. Q. Jia, N. H. Hu, J. W. Xu, Metal–organic frameworks based on the pyridine-2, 3-dicarboxylate and a flexible bispyridyl ligand: syntheses, structures, and photoluminescence. *Cryst. Eng. Comm*., **2009**, 11, 292-297.

40. J. K. Grey, Vibronic luminescence properties of tetragonal transition metal complexes, A Ph. D thesis, McGill University, Montreal, Canada **2004**.

41. T. R. Chen, J. D. Chen, T. C. Keng, J. C. Wang, A new pyridylamine for blue light electroluminescent devices, *Tetrahedron Lett*., **2001**, 42, 7915-7917.

42. M. H. Keefe, K. D. Benkstein, J. T. Hupp, Luminescent sensor molecules based on coordinated metals: a review of recent developments, *Coordin. Chem. Rev.*, **2000,** 205 201-228.

43. A. W. C. van den Berg, C. O. Arean, Materials for hydrogen storage: current research trends and perspectives, *Chem. Commun*., **2008**, 668-681.

44. L. J. Murray, M. Dinca, J. R. Long, Hydrogen storage in metal–organic frameworks, *Chem. Soc. Rev*., **2009**, 38, 1294-1314.

45. S. Brunauer, P. H. Emmett, E. Teller, Adsorption of gases in multimolecular layers, *J. Am. Chem. Soc*., **1938**, 60(2), 309-319.

46. F. Schuth, K. S. W. Sing, J. Weitkamp (Eds.), Handbook of Porous Solids, vol. 1, Wiley-VCH, Berlin, Germany **2002**.

47. P. Hudec, A. Smieskova, V. Jorik, Sensitivity of the C-constant of BET-isotherm to the content of micropore volume in mesoporous matrix, *Stud. Surf. Sci. Catal*., **2008**, 174, 981-984.

48. J. Rouquerol, P. Llewellyn, F. Rouquerol, Is the BET equation applicable to microporous adsorbents? , In Characterization of porous solids VII*"*, Studies in surface science and catalysis, P. Llewellyn, F. Rodriguez-Reinoso, J. Rouquerol, N. Seaton (Eds.), Vol. 160, Elsevier, USA **2007**.

49. M. F. De Lange, T. J. H. Vlugt, J. Gascon, F. Kapteijn, Adsorptive characterization of porous solids: Error analysis guides the way, *Microporous Mesoporous Mater.*, **2014,** 200, 199-215.

50. D. A. Gomez-Gualdro, P. Z. Moghadam, J. T. Hupp, O. K. Farha, R. Q. Snurr, Application of consistency criteria to calculate BET areas of micro and mesoporous metal−organic frameworks, *J. Am. Chem. Soc*. **2016**, 138, 215-224**.**

51. M. Dinca, J. R. Long, Hydrogen storage in microporous metal–organic frameworks with exposed metal sites, *Angew. Chem. Int. Ed.*, **2008**, 47, 6766-6779.

52. E. P. Barrett, L. G. Joyner, P. P. Halenda, The determination of pore volume and area distributions in porous substances. I. Computations from nitrogen isotherms, *J. Am. Chem. Soc.*, **1951,** 73, 373-380.

53. F. De Lange, T. J. H. Vlugt, J. Gascon, F. Kapteijn, Adsorptive characterization of porous solids: Error analysis guides the way, *Microporous Mesoporous Mater.*, **2014,** 200, 199-215.

54. M. E. Davis, Ordered porous materials for emerging applications, *Nature*, **2002**, 417(689), 813-821.

55. H. Yi, Yu. Li, X. Tang, F. Li, K. Li, Q. Yuan, X. Sun, Effect of the adsorbent pore structure on the separation of carbon dioxide and methane gas mixtures, *J. Chem. Eng. Data*, **2015**, 60(5), 1388-1395.

56. S. Wahyuningsih, A. H. Ramelan, D. K. Wardani, F. N. Aini, P. L. Sari, B. P. N. Tamtama, Y. R. Kristiawan, 'Indigo Dye Derived from Indigofera Tinctoria as Natural Food Colorant, *IOP Conf. Ser.: Mater. Sci. Eng.*, **2017,** 193, 012048.

57. D. Thetford, Triphenylmethane and Related Dyes, Kirk-Othmer Encyclopedia of Chemical Technology, John Wiley & Sons **2013**.

58. Q. Tang, S. Liu, Y. Liu, J. Miao, S. Li, L. Zhang, Z. Shi, Z. Zheng, Cation sensing by a luminescent metal-organic framework with multiple lewis basic sites, *Inorg. Chem.*, **2013**, 52, 2799-2801.

59. R. Gao, F. Wang, Y. Zhu, G. Li, A luminescent dimer as a turn-off sensor for both nitrite anion and ferric Cation, *Supramol. Chem*., **2016**, 28(3-4), 204-211.

60. M. Wang, L. Guo, D. Cao, Metal-organic framework as luminescence turn-on sensor for selective detection of metal ions: Absorbance caused enhancement mechanism, *Sens Actuators B Chem.*, **2018**, 256, 839-845.

61. R. W. Huang, Y. S. Wei, X.Y. Dong, X. H. Wu, C. X. Du, S. Q. Zang, T. C. W. Mak, Hypersensitive dual-function luminescence switching of a silver-chalcogenolate cluster-based metal–organic framework, *Nat. Chem*., **2017**, 9, 689-697.

62. C. Dey, T. Kundu, B. P. Biswal, A. Mallick, R. Banerjee, Crystalline metal-organic frameworks (MOFs): synthesis, structure and function, *Acta Cryst.*, **2014**, B 70, 3-10.

63. O. Lupan, S. Shishiyanu, V. Ursaki, H. Khallaf, L. Chow, T. Shishiyanu, V. Sontea, E. Monaico, S. Railean, Synthesis of Nanostructured Al-doped zinc oxide films on Si for solar cells applications, *Sol. Energ. Mat. Sol. Cells*, **2009**, 93, 1417-1422.

64. K. G. Kanade, B. B. Kale, J. O. Baeg, S. M. Lee, C. W. Lee, S. J. Moon, H. Chang, Self-assembled aligned Cu doped ZnO nanoparticles for photocatalytic hydrogen production under visible light irradiation, *Mater. Chem. Phys.*, **2007**, 102(1), 98-104

65. J. J. Freedsman, L. J. Kennedy, R. T. Kumar, G. Sekaran, J. J. Vijaya, Studies on the structural and optical properties of zinc oxide nanobushes and Co-doped ZnO self-aggregated nanorods synthesized by simple thermal decomposition route, *Mater. Res. Bull.*, **2010**, 45(10), 1481-1486.

66. K. Rekha, M. Nirmala, M. G. Nair, A. Anukaliani, Structural, optical, photocatalytic and antibacterial activity of zinc oxide and manganese doped zinc oxide nanoparticles, *Physica B: Condens Matter*, **2010**, 405(15), 3180-3185.

67. M. Moritz, M. Geszke-Moritz, Mesoporous materials as multifunctional tools in biosciences: Principles and applications, *Mater Sci Eng C Mater Biol Appl.* **2015**, 49, 114-151.

68. B. Fang, L. Binder, A novel carbon electrode material for highly improved EDLC performance, *J. Phys. Chem. B*, **2006**, 110(15), 7877-7882.

69. L. Wang, W. Ding, Y. Sun, The preparation and application of mesoporous materials for energy storage, *Mater. Res. Bull.*, **2016**, 83, 230-249.

70. A. B. Fuertes, G. Lota, T. A. Centeno, E. Frackowiak, Templated mesoporous carbons for super capacitor application, *Electrochim. Acta*, **2005**, 50(14), 2799-2805.

CHAPTER 5

CONCLUSIONS AND FUTURE SCOPE

Conclusions

Multi Metal-Citrate complexes synthesized using Citric acid / Lime juice through green synthetic pathways are polynuclear complexes with cubic geometry. All complexes are brightly colored, well defined crystalline solid, stable up to 300 ºC and decompose at higher temperature. Based on analytical, spectral and thermal analysis, the multi metal-citrate complexes synthesized using citric acid / lime juice in present research are assigned a layered structure bearing a strong network of hydrogen bonds formed by ─OH of coordinated water, lying between tetrahedral & octahedral sheets in complexes and occupying the pores. The carboxylate groups of citrate ligand in complexes **1** & **2** are coordinated to metal ions in a mono dentate fashion, while in complex **3** & **4** by bidentate bridging mode, the most preferred co-ordination of carboxylate groups of citrate ligand in these complexes.

Multi metal-citrate complexes exhibit Type V adsorption isotherm which explains formation of multilayer. Despite low value of specific surface area, these complexes exhibit high values of C, due to strong adsorbate-adsorbent interaction owing to open metal sites and active functionalities at the surface. Low value of surface area attributed to the fact that chain-based MOFs generally exhibit one dimensional channel and lead to low surface areas & reduced micro pore volumes despite exhibiting high adsorption enthalpy.

Multi metal-citrate complexes are mesoporous materials having narrow pore size distribution and high stability. Owing to excellent adsorption properties and mesoporous nature, Multi metal-citrate complexes exhibit exorbitant adsorption affinity for large molecules of dyes.

Activated crystals of multi metal-citrates soaked in solutions of Eriochrome Black T, Indigo blue dye and Methyl orange dye result in adsorption of dye molecules.

Adsorption of anionic azo dyes; MO & EBT can be attributed to electrostatic & hydrogen bond interactions between adsorbent & dye molecules. In case of Indigo blue dye di-ionic form of the dye undergoes extensive hydrogen bonding with adsorbent surface. Color change of crystals was uniform and clearly observed with naked eyes Uniform distribution of colors in crystals suggests that dye molecules not only get adsorbed on external surface, but penetrate into large pores and get adsorbed throughout the crystal structure. These complexes may thus replace high cost carbon adsorbents to curb water pollution & resultant toxic, carcinogenic & mutagenic effects of dye stuff on living beings.

Multi Metal-Citrates serve as promising luminescent probe for sensing & recognition of NH_4^+, CO_3^{2-}, I^- by "turn on" mechanism and CrO_4^{2-} & $Cr_2O_7^{2-}$ ions by "turn off" mechanism. Present technique is decorated with features of being a simple & straight forward method involving conspicuous visual display of color change upon introduction of guest ions in their framework They exhibit high sensitivity with regard to iodide ions.

The porous nature of multi metal-citrate complexes synthesized in present research owing to their magnetic nature can be explored for use as porous molecular magnets. The multi metal-citrate complex **4** and **IV** when heated to 300 ºC yield copper doped nickel-zinc-ferrite like materials.

Biocompatibility and non toxicity of Multi metal-Citrates makes these Mesoporous materials ideal for diagnostics applications due to increased image contrast. Luminescent Multi Metal-Citrates may serve as perfect candidates for photovoltaic devices, bio sensors, electro luminescent devices and laser systems.

Established protocol has merits of being; A simple one pot synthesis, cost effectiveness, easy to scale up for industrial production, environmentally benign as it eliminates use and recovery of potentially harmful organic solvents particularly DMF & DEF usually employed in the synthesis of Metal-organic framework complexes. Lime juice substituted for Citric acid makes method appreciably economical in terms of time and energy.

Future Scope

Increasing surface area of Multi Metal-Citrate complexes by post synthetic modifications and super critical drying can enhance their hydrogen adsorption properties. These biocompatible luminescent complexes may be reduced to nano size suitable for biological applications. Besides reducing carbon content in air owing to their green synthesis, the multi-metal oxides obtained upon thermal treatment of these complexes may be exploited for use in devices like microwave, magnetic memories, isolators, noise filters *etc.* as low cost alternative to traditional magnetic materials commonly used in industry.

LIST OF PUBLICATIONS

RESEARCH PAPERS

1. **Usha Raju**, Anil Kumar*, Storage of hydrogen: a future generation fuel, by metal-organic frameworks, Der Chemica Sinica, **2015**, 6(9), 25-29.

2. **Usha Raju**, Sudhir G. Warkar, Anil Kumar*, Green synthesis of Multi metal-Citrate complexes and their characterization, J Mol Struct, **2017**, 1133, 994.

3. **Usha Raju**, Anil Kumar*, Multi metal-Citrate complex: Green synthesis using lime juice for hydrogen storage applications, Int J Pharma Bio Sci, **2018**, 9(2), 19198.

4. **Usha Raju**, Atul Varshney, Anil Kumar*, Mesoporous multi metal-Citrates as scavengers for organic dyes, J Surface Sci Technol, 34(1-2), June **2018** DOI: 10.18311/jsst/2018/18112, ISSN (Online): 0976-9420.

CONFERENCE CONTRIBUTIONS

1. **Usha Raju**, Chansi Gupta, Anil Kumar*, Structural and morphological characterization of CdSe/PVA film prepared by solvothermal method, ICAPIE 2016 International Conference on Advanced Production and Industrial Engineering, 9-10 December, **2016**.

2. **Usha Raju**, Anil Kumar,* Porous multi metal-Citrates for sensing and recognition of ions in industrial effluent water, International conference on Sustainable Initiatives in Water Management, 6th March **2018**.